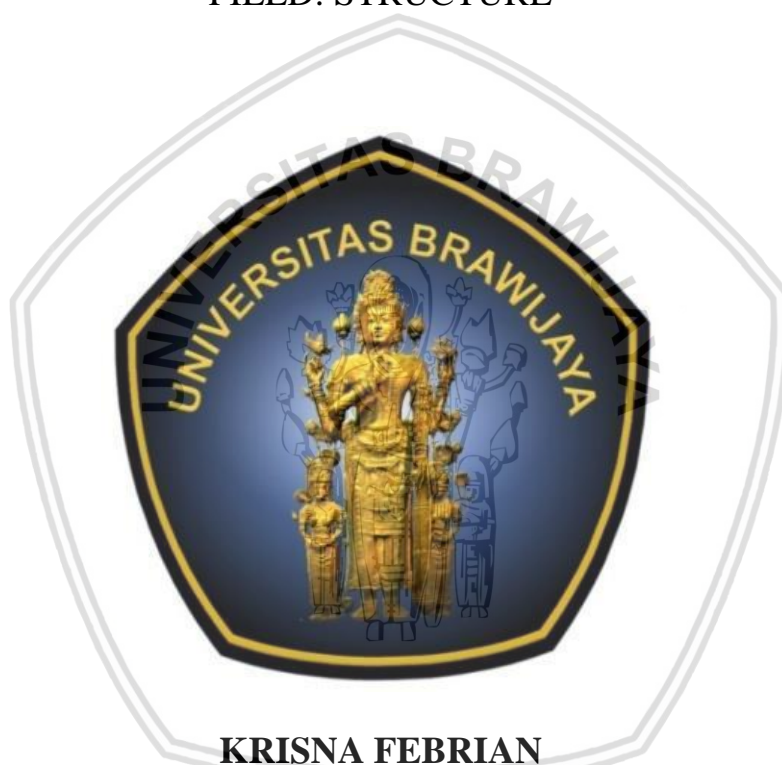


**DYNAMIC ANALYSIS OF IRREGULAR BRIDGES
WITH POLYNOMIAL ROCKING BEARINGS**

THESIS

**MASTER PROGRAM OF CIVIL ENGINEERING
FIELD: STRUCTURE**



**KRISNA FEBRIAN
NIM. 136060112011002**

**UNIVERSITY OF BRAWIJAYA
FACULTY OF ENGINEERING
MALANG**

2017

ACKNOWLEDGEMENT

Praise to the Lord. I express my highest gratitude to Lord Jesus for His blessing, love, opportunity, and mercy in completing my master thesis. Thank you for always protect and strengthen me through the whole things. This master thesis entitled “Dynamic Analysis of Irregular Bridges with Polynomial Rocking Bearings” is submitted as the final requirement in accomplishing master degree in Civil Engineering at University of Brawijaya, Indonesia and National Central University, Taiwan.

In arranging this thesis, a lot of people have provided motivation, advice, and support for me. In this valuable chance, I intended to express my gratitude and appreciation to all of them. First, my deepest appreciation goes to my beloved parents, my father Ir. Soerojo and my mother Welasih Soesilowati for their endless love, pray, support, and always remind me to keep going up and never giving up. My gratitude also goes to my beloved brother Devian for every support in any form.

This thesis would not have been possible without the help and support of my advisors Prof. Lee Tzu-Ying and Ari Wibowo, Ph.D for their supervision, advice, and guidance from the preliminary stage of this research as well as giving me extraordinary experiences throughout the past few years. My greatest appreciation also goes to Prof. Juang Der-Shin and Prof. Hsu Hsieh-Lung as my examiners for their advices, supervisions, and crucial contributions in the improvement of this master thesis.

I also want to express my great appreciation to my lab-mates Ragil, Fita, Raiza, Lingga, 鍾昆潤, 張顥, 曹哲瑋, 林耿億, 劉修愿, 陳重瑞, 蘇宇, 王俊清, 朱浚邦, Kartika, Vy, Alfin, 林玠亨, 張展嘉, 沈世涵, 呂捷宏, 陳坤生, 李孟嶸, 許誌斌, 洪文孝 for ingenuity discussion that helped me unravel the problems in my research. I am very grateful to have some close friends, Nancy, Albert, Desy, Vicky, Abdul, Tomas, Ellsa, Feisal, and Yoga, you all are always a good listener for every problem I faced, especially when I had to revise this thesis and re-start over and over again. I would like to thank all of the members of Indonesian Student Association in NCU.

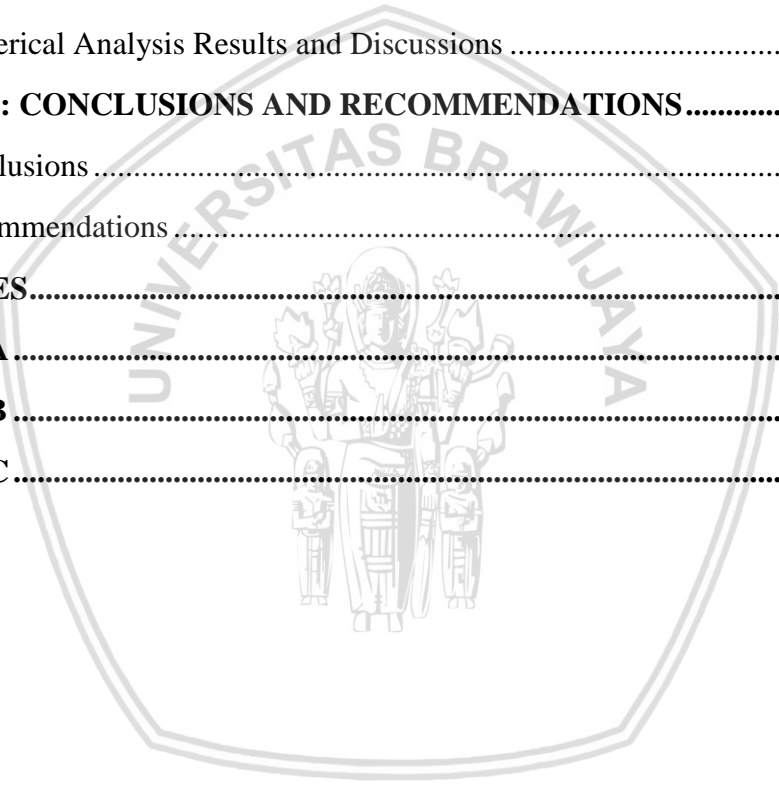
Finally, I would like to thank everybody who was important to the successful realization of this master thesis. This master thesis is far from perfect, but it is expected that it will be useful not only for the researcher, but also for the readers. For this reason, constructive thoughtful suggestion and critics are welcomed.

TABLE OF CONTENTS

ACKNOWLEDGEMENT	i
TABLE OF CONTENTS	ii
LIST OF TABLES	iv
LIST OF FIGURES	v
RINGKASAN	vii
SUMMARY	viii
CHAPTER I: INTRODUCTION	1
1.1. Background	1
1.2 Literature Review	2
1.2.1 Seismic Control System	2
1.2.2 Structure Response with Seismic Isolation System	4
1.3 Research Objectives	7
1.4 Outline	7
CHAPTER II: POLYNOMIAL ROCKING BEARINGS	10
2.1 Configuration of a General Polynomial Rocking Bearing	10
2.2 Horizontal Restoring Force of a Polynomial Rocking Bearing	10
2.3 Isolation Stiffness and Frequency of a Polynomial Rocking Bearing	12
2.4 Horizontal Friction Force of a Polynomial Rocking Bearing	13
2.5 Equivalent Horizontal Friction Coefficient	15
CHAPTER III: NUMERICAL ANALYSIS MODEL AND ANALYSIS METHOD	19
3.1 Design of Target of Bridge	19
3.2 Equation of Motion Derivation	19
3.3 Horizontal Friction Force of PRB	21
3.3.1 Sticking State	23
3.3.2 Rocking State	23
3.3.3 Partial Rocking State	23
CHAPTER IV: OPTIMAL DESIGN OF POLYNOMIAL ROCKING BEARINGS USING PSO-SA METHOD	28

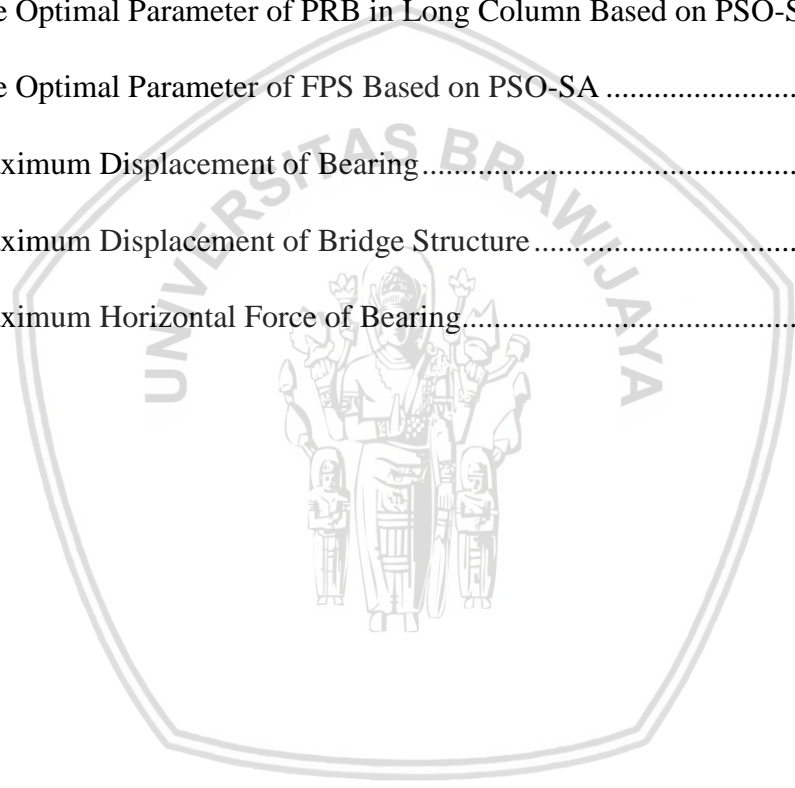


4.1	PSO-SA Hybrid Searching Method	28
4.1.1	Mathematical Model of Optimization Problem	28
4.1.2	Particle Swarm Optimization (PSO).....	29
4.1.3	Simulated Annealing (SA).....	30
4.1.4	Particle Swarm Optimization-Simulated Annealing (PSO-SA)	31
4.2	Bearing's Objective Function.....	33
4.3	PRB Parameter Setting.....	34
4.4	FPS Parameter Setting.....	34
4.5	Ground Motion Input	35
4.6	Numerical Analysis Results and Discussions	37
CHAPTER V: CONCLUSIONS AND RECOMMENDATIONS.....		63
5.1	Conclusions	63
5.2	Recommendations	63
REFERENCES.....		65
APPENDIX A.....		73
APPENDIX B.....		78
APPENDIX C.....		84



LIST OF TABLES

Table 3.1 Parameter of Irregular Bridges	24
Table 4.1 Parameter of PSO-SA Hybrid Searching Algorithm	39
Table 4.2 PRB Parameter Setting in PSO-SA Hybrid Searching Method.....	39
Table 4.3 FPS Parameter Setting in PSO-SA Hybrid Searching Method.....	39
Table 4.4 The Optimal Parameter of PRB in Short Column Based on PSO-SA.....	40
Table 4.5 The Optimal Parameter of PRB in Long Column Based on PSO-SA.....	40
Table 4.6 The Optimal Parameter of FPS Based on PSO-SA	40
Table 4.7 Maximum Displacement of Bearing.....	41
Table 4.8 Maximum Displacement of Bridge Structure	41
Table 4.9 Maximum Horizontal Force of Bearing.....	41



LIST OF FIGURES

Figure 1.1 Seismic Isolation Systems on Building	9
Figure 1.2 Seismic Isolation Systems on Bridge	9
Figure 1.3 Experimental Test (a) PRBs Installed on Building; (b) PRBs Installed on Regular Bridge	9
Figure 2.1 Polynomial Rocking Bearings Installed under Bridge's Deck.....	17
Figure 2.2 Polynomial Rocking Bearings.....	17
Figure 2.3 Free Body Diagram of Polynomial Rocking Bearings.....	18
Figure 2.4 Equivalent Force Systems at Spherical Head of PRBs	18
Figure 3.1 Model of Irregular Bridges	25
Figure 3.2 Mathematical Model of Irregular Bridges	26
Figure 3.3 Free Body Diagram of Irregular Bridges: (a) Upper Part (b) Lower Part ..	26
Figure 3.4 Analysis Process	27
Figure 4.1 Time History of Near-Fault Ground Motions, PGA = 250 gal	42
Figure 4.2 Time History of Far-Fault Ground Motions, PGA = 250 gal.....	43
Figure 4.3 PRB Convergence Characteristics by PSO-SA.....	44
Figure 4.4 PRB Curvature by PSO-SA Subjected to Northridge Ground Motion	45
Figure 4.5 PRB Curvature by PSO-SA Subjected to Hachinohe Ground Motion	45
Figure 4.6 PRB Curvature by PSO-SA Subjected to TCU068 Ground Motion.....	45
Figure 4.7 PRB Curvature by PSO-SA Subjected to Imperial Ground Motion	46
Figure 4.8 PRB Curvature by PSO-SA Subjected to Sylmar Ground Motion	46
Figure 4.9 PRB Curvature by PSO-SA Subjected to JMA Kobe Ground Motion	46
Figure 4.10 PRB Curvature by PSO-SA Subjected to El Centro Ground Motion	47
Figure 4.11 FPS Convergence Characteristics by PSO-SA.....	48

Figure 4.12 Bridge’s Time History Displacement Subjected to Northridge Earthquake	49
Figure 4.13 Bridge’s Hysteretic Loop Subjected to Northridge Earthquake.....	50
Figure 4.14 Bridge’s Time History Displacement Subjected to Hachinohe Earthquake	51
Figure 4.15 Bridge’s Hysteretic Loop Subjected to Hachinohe Earthquake.....	52
Figure 4.16 Bridge’s Time History Displacement Subjected to TCU068 Earthquake	53
Figure 4.17 Bridge’s Hysteretic Loop Subjected to TCU068 Earthquake	54
Figure 4.18 Bridge’s Time History Displacement Subjected to Imperial Earthquake	55
Figure 4.19 Bridge’s Hysteretic Loop Subjected to Imperial Earthquake.....	56
Figure 4.20 Bridge’s Time History Displacement Subjected to Sylmar Earthquake ..	57
Figure 4.21 Bridge’s Hysteretic Loop Subjected to Sylmar Earthquake.....	58
Figure 4.22 Bridge’s Time History Displacement Subjected to JMA Kobe Earthquake	59
Figure 4.23 Bridge’s Hysteretic Loop Subjected to JMA Kobe Earthquake.....	60
Figure 4.24 Bridge’s Time History Displacement Subjected to El Centro Earthquake	61
Figure 4.25 Bridge’s Hysteretic Loop Subjected to El Centro Earthquake.....	62
Figure A. 1 Transformation Coordinates Diagram	77
Figure C. 1 Bridge’s Hysteretic Loop Subjected to Imperial Earthquake in Short Column.....	84
Figure C. 2 Bridge’s Hysteretic Loop Subjected to JMA Kobe Earthquake in Long Column.....	84
Figure C. 3 Bridge’s Hysteretic Loop Subjected to El Centro Earthquake in Long Column.....	85



RINGKASAN

Krisna Febrian, Magister Teknik Sipil, Jurusan Teknik Sipil, Fakultas Teknik Universitas Brawijaya, Oktober 2017, *Dynamic Analysis of Irregular Bridges with Polynomial Rocking Bearings*, Dosen Pembimbing: Ari Wibowo, S.T., M.T., Ph.D dan Professor Tzu-Ying Lee.

Friction Pendulum System (FPS) adalah salah satu dari sistem penahan gempa konvensional yang sudah banyak digunakan dan terbukti secara efektif dapat mengurangi bahaya akibat gempa dalam. Namun, teknologi ini mungkin tidak efektif ketika struktur terkena gempa dangkal, karena periode dari gempa dangkal biasanya akan mendekati periode dari struktur tersebut. Pada studi ini, *Polynomial Rocking Bearing* (PRB) yang mempunyai kekakuan isolasi yang dapat berubah-ubah, digunakan untuk meningkatkan performa dari sistem penahan gempa pada gempa dangkal. PRB tersusun atas *articular joint* dan *concave rocking surface*. Kelengkungan dari *rocking surface* ini didefinisikan dengan menggunakan fungsi pangkat enam.

Berdasarkan penelitian terdahulu pada struktur bangunan dan jembatan dengan kolom beraturan (kolom dengan tinggi yang sama), PRB telah terbukti secara efektif dapat mengurangi perpindahan isolator pada gempa dangkal. Namun teknologi ini belum pernah diterapkan pada struktur jembatan dengan kolom tidak beraturan (kolom dengan tinggi yang berbeda). Studi ini bertujuan untuk menganalisis perilaku dari PRB yang akan diterapkan pada jembatan dengan kolom tidak beraturan. Pada studi ini juga dilakukan optimisasi pada desain parameter dari PRB dengan menggunakan metode *Particle Swarm Optimization-Simulated Annealing* (PSO-SA). Jika dibandingkan dengan *Friction Pendulum Systems* (FPS), performa dari PRB jauh lebih baik dalam mengurangi perpindahan dari dek jembatan pada jenis gempa dangkal maupun gempa dalam.

Kata kunci: kekakuan isolasi yang berubah-ubah, *polynomial rocking bearing*, *irregular bridges*, gempa dangkal.

SUMMARY

Krisna Febrian, Department of Civil Engineering, Faculty of Engineering, University of Brawijaya, October 2017, *Dynamic Analysis of Irregular Bridges with Polynomial Rocking Bearings*, Supervisors: Ari Wibowo, S.T., M.T., Ph.D and Professor Tzu-Ying Lee.

Conventional sliding isolators such as Friction Pendulum System (FPS) are widely used and effectively proved to mitigate seismic hazard in far-fault earthquakes. However, it may not be effective when the structures are subjected to near-fault earthquakes because the earthquake's period is usually close to the isolation period. In this study a Polynomial Rocking Bearing (PRB) which has variable isolation stiffness is used to improve the performance of seismic isolation systems under near-fault earthquakes. A PRB is composed of an articular joint and concave rocking surface. The rocking surface is defined by a sixth-order polynomial function.

According to previous studies, the PRB has been verified to effectively suppress the large isolator displacement induced by near-fault earthquakes on building and regular bridges. However it has not been used yet in the irregular bridges. This study aims to analyze the behavior of Polynomial Rocking Bearing installed on an irregular bridge. Also the optimal design parameters of PRBs are found out by using the Particle Swarm Optimization-Simulated Annealing (PSO-SA) hybrid searching algorithm. As compared with conventional Friction Pendulum Systems (FPS), the performance of PRBs is superior to effectively suppress the displacement of the bridge deck in both near and far-fault earthquakes.

Keywords: variable isolation stiffness, polynomial rocking bearing, irregular bridges, near-fault earthquakes.

CHAPTER I: INTRODUCTION

1.1. Background

Nowadays, a transportation system becomes very important in human life. People need a well-ordered transportation system to help them to move from one place to another conveniently, and to support their economic, social, politic activity, and so forth. Besides, the facilities and infrastructures, such as highways and railways are important to construct the transportation system. Bridges are the most vital and vulnerable components in the transportation system. Bridges are designed based on its function, ground condition, material construction, and the available funds. No matter what kinds of bridges will be constructed, in order to provide the users safety and comfort, they must be able to carry any loads especially seismic loading.

In the past extreme earthquakes, a number of bridges suffered serious damage even collapse. Once bridges failure or collapse during an earthquake, it will impede recovery and rehabilitation such as the 1994 Northridge Earthquake in California, the 1995 Kobe Earthquake in Japan, the 1999 Chi-Chi Earthquake in Taiwan, and the 2010 Haiti Earthquake in Haiti (e.g., Basoz and Kiremidjian, 1998; Basoz *et al*, 1999; Bruneau *et al*, 1999; Ghobarah and Ali, 1988; Kawashima, 2002; Kosa *et al*, 2002; Lee and Loh, 1999; Otsuka, 1997). Hence, it becomes very important to understand about how to design the bridges for mitigating the seismic risks by developing a good method.

To protect bridges from seismic damage, bridges must be designed based on the bridge seismic design codes. However, a modern technique of mitigating seismic induced forces of structures is structural control. Structural control can be classified into passive, active, and semi-active control. More than 20 years, most of the previous researchers use passive control, especially base isolation systems or seismic isolation systems as shown in Figures 1.1-1.2 (e.g., Asher *et al*, 1995; Bozorgnia *et al*, 1998; Çelebi, 1996; Fujita, 1998; Kelly, 1998; Martelli and Forni, 1998).

Seismic isolators are usually placed between structure and foundation on buildings. The main concept of seismic isolation is to increase the fundamental period of structures and/or dissipate the seismic energy transmitted directly onto the structure systems (Matsagar and Jangid, 2006). Thus, such systems can protect the structural and non-structural systems from earthquakes. Generally, a seismic isolation system

has five characteristics. First, it has a soft isolation layer to mitigate the seismic force transmitted to the main structure. Second, it should have the ability to recover into initial position in order to reduce the residual displacement of structure after earthquakes. Third, it has an energy dissipation mechanism to avoid an excessive isolator displacement. Fourth, it should have a sufficient vertical stiffness to retain the stability of structures. The last, it should have the appropriate stiffness to resist small vibration (Bukle and Mayes, 1990). Seismic isolators can be divided into two groups, namely, sliding bearings and elastomeric bearings (e.g., Kelly, 1986; Koh and Kelly, 1988; Naeim and Kelly, 1999). A Friction Pendulum System (FPS) is commonly-used sliding bearings. Previous research has shown that the FPS has good isolation effect when structures are subjected to far-fault earthquakes. However, it may result in an excessive isolator displacement under near-fault earthquakes.

To overcome such a problem, some researchers suggested the isolation systems with variable mechanical properties, which may be adaptive to a wider range of earthquakes. Polynomial Rocking Bearings (PRBs) proposed by Lu *et al.* (2013) has variable mechanical properties. In the previous study, Polynomial Rocking Bearing has applied on the building by Lu and Hsu (2013) and also it has applied to the regular bridge (bridge with the same dimensions of the pier) by Tzeng (2013). Based on both previous researches above, Polynomial Rocking Bearing is able to effectively suppress the large isolator displacement induced by strong near-fault earthquake. Bridges structure may be irregular in column heights due to complex terrain, route alignment, ramps, interchanges, and so on. In this study, PRBs are employed and installed between the deck and the pier for an irregular bridge. The behavior of the irregular bridge with PRBs is investigated through analysis using MATLAB®. The optimum parameters of PRBs are found out by using the Particle Swarm Optimization-Simulated Annealing (PSO-SA) hybrid searching algorithm.

1.2 Literature Review

1.2.1 Seismic Control System

Generally, there are 3 types of seismic control systems: passive control system, active control system, and hybrid control system. The passive control system does not need any additional energy source to operate and it is activated by the earthquake input motion only. In general, the passive control system has three kinds of

mechanical devices: energy dissipation systems, base isolation systems, and dynamic oscillators.

Energy dissipation systems are typically designed mechanical systems to dissipate a large number of the earthquake in special devices or special details connection which will deform or yield during the earthquake. In general, this device is characterized by its capability to enlarge the energy dissipation in a structural system with a view to resist earthquake-induced forces. For example are friction dampers, metallic-yielding dampers, viscous-elastic dampers, and fluid viscous dampers.

Base isolation systems or seismic isolation systems are applied to increase the structure's natural period lead to decrease its natural frequency of vibration. In this way, the super-structure can be decoupled from earthquake-induced ground motion and its formidable energy. Decreasing on the frequency of vibration will also decrease the pseudo-acceleration of structures thereby reducing the base shears.

Dynamic oscillators are kind of seismic control system includes supplemental oscillators which act as dynamic absorbers. For example of the dynamic oscillator is tuned mass damper. Its frequency of vibration-tuned to the exciting frequency is attached to the main structural system. During the excitation, tuned mass damper simply moves in out of phase of the main structural system thereby imparting opposing inertial forces of the external vibration forces acting on the structure. In this way, the motion of the main structural system almost ceased or highly diminished.

Active control system provides seismic protection by imposing forces on a structure that counterbalance the earthquake-induced forces. This system is active in that it requires an energy source and computer-controlled actuators to operate special braces of tuned-mass dampers located throughout the building. It is more complex than passive control system because it relies on computer control, motion sensors, feedback mechanisms, and moving parts which may require service or maintenance. It also needs an emergency power source to ensure that it will operable during a major earthquake and any immediate aftershocks. This technology is highly sophisticated and expensive one and also may not be feasible for small projects.

Hybrid control system combines features of both passive and active control systems. In general, it has reduced power demands, improved reliability, and reduced cost when compared to fully active seismic control systems. It could be used for civil infrastructures such as cable-stayed bridges, which need large control forces and good controller robustness to apply real structures. This system could relieve some of the

limitations of each system. For example, additional active or semi-active control devices in the LRBs-based hybrid control system could reduce the deformation of LRBs and LRBs could offer some degree of protection in the case of the power failure of the active controller.

1.2.2 Structure Response with Seismic Isolation System

In the past decades, seismic control system has been studied by many researchers to offers a promising solution for protecting structure from seismic hazard. Passive control system is one of the seismic control systems that used to increase the energy dissipation capacity of a structure (Symans and Constantinou, 1999). This system has already reviewed by Soong and Constantinou (1994), ATC (1993 and 1994), Constantinou *et al.* (1998). The energy dissipation capacity can be enhanced by setting passive supplemental devices such as base isolation systems, tuned mass damper, fluid viscous dampers, viscous-elastic dampers, metallic-yielding damper, and friction dampers. Passive control utilized the structural response by the earthquake input motion to generate the control force so it doesn't need any energy source. In practical application of some bridges, passive control system has been implemented worldwide since 1970's [e.g., Robinson and Greenbank, 1976; Kawashima *et al.*, 1991; Priestley *et al.*, 1996; Roberts, 2005; Vaurigaud *et al.*, 2011; Taflanidis, 2011; Chen *et al.*, 2015; Rådestrom *et al.*, 2016; Shi *et al.*, 2016]. Remarkable progress in analytical and experimental research had been established in order to improve the seismically response of bridge. Early work was performed by Kawashima *et al.* (1989, 1991, 1992a, 1992b) to investigate the seismic response control of highway bridges by using mass dampers and variable dampers.

Lu et al (2003) studied the sliding isolated structure subjected to near-fault and far-fault ground motions. In the test, a set of pulse accelerations with various pulse periods were artificially generated on the isolated structure. Several effects of near-fault earthquakes on the response of the isolated structure like the vertical ground motion, the over-turning moment of the structure, and the period of the pulse wave are investigated and discussed. The test results showed that the pulse component in the near-fault earthquake can lead to an isolation motion similar to resonant response. As a result, the isolator displacement of the sliding isolated structure was considerably amplified in the near-fault earthquake as compared with the far-fault earthquake.

Lu et al (2008) presented the stiffness controllable system for near-fault seismic isolation. This system is a kind of sliding base isolation system. Previously, many researchers used conventional passive isolation system, but this system usually had long-period structural system and may result excessive isolator displacement when subjected to near-fault earthquake. To overcome such a problem, stiffness controllable system is proposed in this study. By varying the stiffness of the isolation system, the restoring force provided by the system can be controlled by a proposed semi-active control method that is developed based on active feedback control. The result of numerical simulation has shown that the proposed system is able to effectively mitigate the effect of low frequency resonance induced by a near-fault earthquake. As a result, the base displacement and super-structure acceleration of the isolated structure can be reduced simultaneously.

Lu et al (2011) developed the seismic isolation system using variable mechanical properties called Sliding Isolators with Variable Curvatures (SIVCs). SIVCs are similar to FPS isolator, except its sliding surface has variable curvature rather than being spherical. This research did the simulation and experimental study. The SIVC is put on the steel frame and did the cyclic element test and shaking table test. The result of both tests has verified that SIVC has the hysteretic property of variable stiffness. It was also demonstrated that the proposed SIVC is able to effectively reduce the isolator drift in a near-fault earthquake with strong long period components as compared to FPS with the same friction coefficient.

Lu & Hsu (2013) analyzed the Variable-Frequency Rocking Bearings (VFRBs) as the seismic isolation system that applied to the building. VFRBs have variable mechanical properties. Generally, it has an axially symmetric rocking surface with a variable curvature. This research did the simulation and experimental study. This bearing is installed between the foundation and superstructure. The experimental results have a good agreement with the simulation. The experimental results also show that the VFRB system was able to effectively suppress the excessive isolator displacement induced by a near-fault earthquake while retaining good isolation efficiency for the superstructure.

Lu et al (2013) presented Polynomial Friction Pendulum Isolators (PFPIs) for building floor isolation. This research studied numerically and experimentally. Due to its variable-stiffness behavior, PFPIs was able to achieve multiple design objectives. The shaking table tests verify that the prototype system possesses the desired

hysteretic property with variable stiffness and the measured responses match with the simulation. The simulation results demonstrate that the isolation performance complies with the designated dual performance objectives, which yield either acceleration or displacement control depending on the earthquake intensity and isolator drift.

Tzeng (2013) investigated the regular bridges (bridges with the same size of the column) with the Polynomial Rocking Bearings (PRBs) as the seismic isolation system. Previous research has confirmed that PRBs have good isolation effect on the building structure and it has not been applied to the bridge. This research did the simulation and experimental study. PRB were installed between the column and deck of bridges. The result was a hysteretic property of PRB has softening and hardening section. Both of this section can reduce the structural acceleration and inhibit the excessive isolator displacement, respectively. In order to find the optimum parameters of the PRB, this research also did the optimization using PSO-SA (Particle Swarm Optimization-Simulated Annealing). For the simulation result, PRBs were able to suppress excessive isolator displacement better than FPS.

Wang (2014) investigated the Polynomial Friction Pendulum Isolators (PFPIs) that applied on the regular bridges (bridges with the same size of the column). The sliding surface of PFPIs is defined by a sixth-order polynomial function. The restoring force processes a softening and a hardening section. The restoring stiffness is decreasing in softening section to mitigate the acceleration response, and the restoring stiffness is increasing in hardening section to reduce the displacement response. It has been proven that PFPI can reduce the response of structure efficiently both in a far-field and near-field earthquake. This research also did the optimization using Particle Swarm Optimization-Simulated Annealing (PSO-SA) to find the optimum parameters of PFPI. The results show that the bridges with PFPIs designed by this simple procedure can also reduce the seismic response effectively.

Tsao (2016) studied the Polynomial Friction Pendulum Isolators (PFPIs) that applied on the irregular bridges (bridges with different size of the column). Compare with typically isolated bridges, the isolated bridges with different height of column have the different stiffness of columns, and the characteristic of PFPIs will also different, therefore the numerical analysis is more complicated. This research did the simulation and experimental study. The results show that the analysis method developed in this study has the good agreement with the experimental result. In the

last part of this research, this research also did the optimization using Particle Swarm Optimization-Simulated Annealing (PSO-SA) to find the optimum parameters for PFPI. The results show that the structural response can effectively achieve the goal set by the PSO-SA objective function.

Cheng & Chao (2017) studied the seismic performance of base-isolated structure with the rocking bearing. The rocking bearing is designed to move until moderate earthquakes and the structure will rock in the rigid body motion, so it can isolate the seismic energy under the earthquakes. Based on the force-displacement relations and the effective damping of the systems, the seismic response may be estimated through the modified elastic response spectrum. To verify this idea, the shaking table tests did for one story spaced structure with rocking bearing isolation. The results showed that structures with a lower aspect ratio of bearing or a rocking toe with polynomial curve vibrated in a higher natural frequency.

1.3 Research Objectives

This research is aimed to analyze the behavior of Polynomial Rocking Bearing installed on an irregular bridge subjected to the seismic loading. The optimum parameters of PRBs are found out using PSO-SA hybrid searching algorithm. The seismic performances of the irregular bridge with PRBs and FPS are compared to verify the superiority of PRBs.

1.4 Outline

The outline of this research is as follows:

Chapter 1 presents general introduction and background of this study. In this part also explain about the previous study related to this study, brief literature review, and research objectives.

Chapter 2 explains the theory of Polynomial Rocking Bearings (PRBs).

Chapter 3 presents the main idea of this study and do the modeling of the irregular bridges with Polynomial Rocking Bearing. In this chapter also explain more about the discrete time state space as the method to simulate the bridge's model.

Chapter 4 explains about the optimization of Polynomial Rocking Bearing using Particle Swarm Optimization-Simulated Annealing (PSO-SA) hybrid searching method and shows the results of optimization. In this chapter will

also explain about the conventional system Friction Pendulum System (FPS) that will be compared with Polynomial Rocking Bearing.

Chapter 5 will be the conclusion of this study and gives some recommendations for future work.



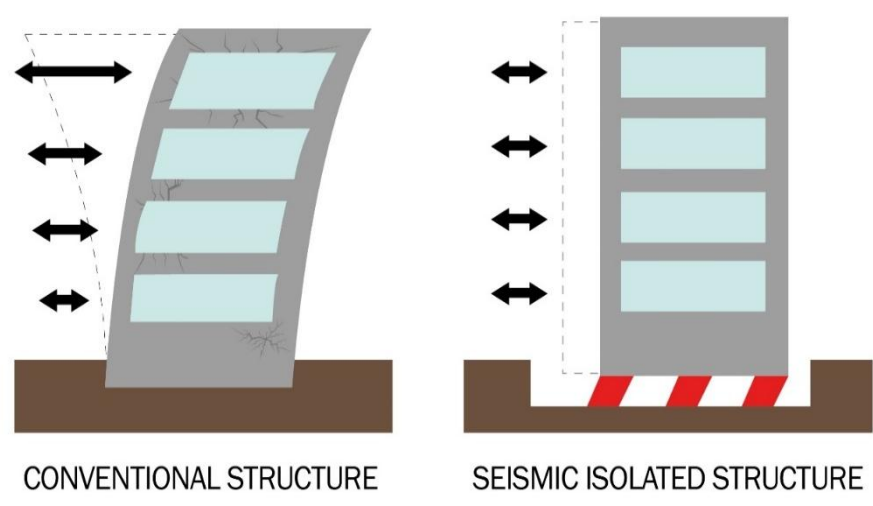


Figure 1.1 Seismic Isolation Systems on Building

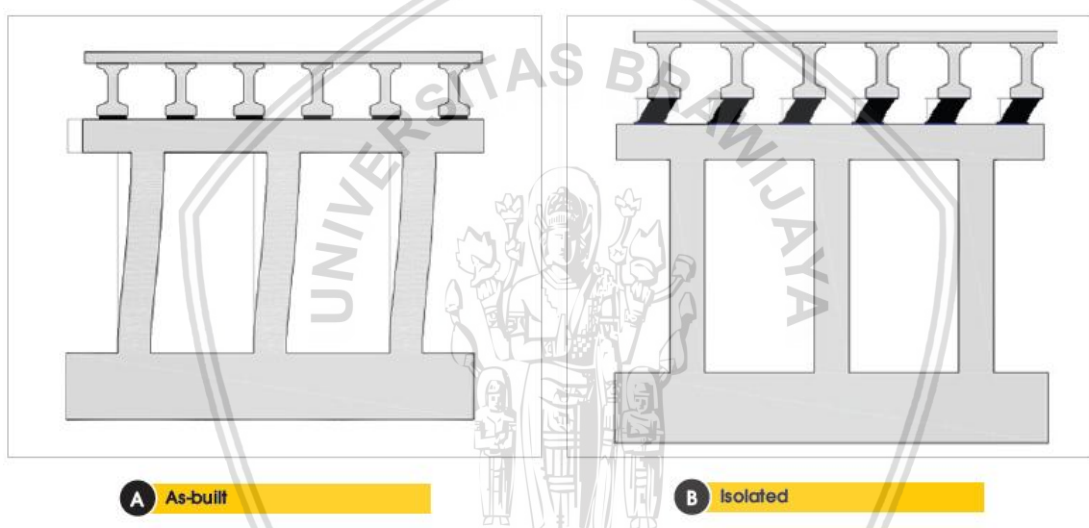


Figure 1.2 Seismic Isolation Systems on Bridge

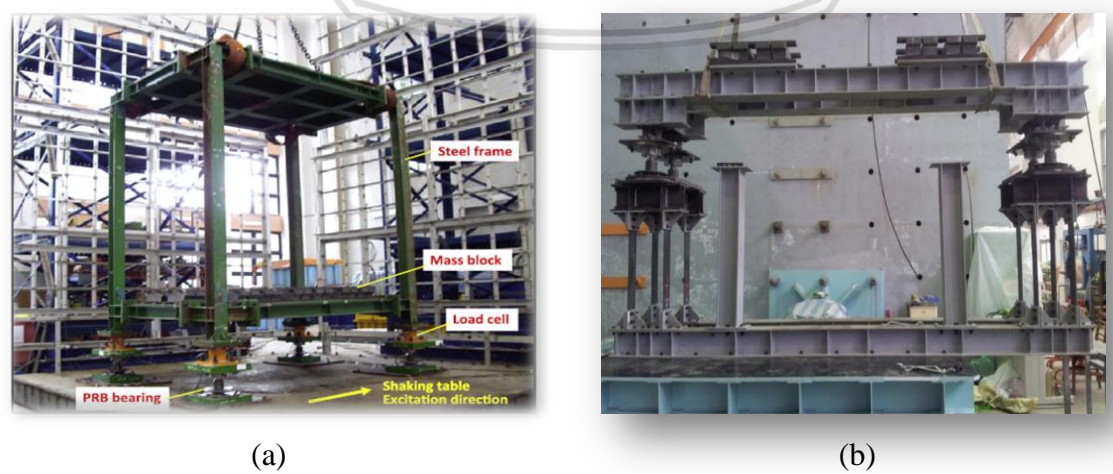


Figure 1.3 Experimental Test (a) PRBs Installed on Building; (b) PRBs Installed on Regular Bridge

CHAPTER II: POLYNOMIAL ROCKING BEARINGS

2.1 Configuration of a General Polynomial Rocking Bearing

Polynomial rocking bearing (PRB) is an axially symmetric rocking surface with a variable curvature. It has an articular (ball and socket) joint on the upper part and a concave rocking surface with a base plate on the lower part (Lu *et al*, 2013:117). The articular joint is mounted on the footing of the superstructure, while the base plate is mounted on the foundation (Lu *et al*, 2013:117). When the earthquake occurred, the rocking surface of the bearing will rock back and forth on the base plate, thus provide an isolation layer to reduce the ground motion transmitted into the super-structure. The geometry of the rocking surface must be concave. In order to provide variable isolation frequency, the rocking surface may have a variable curvature that can be determined depend on the designer.

Based on the experiment, PRB is able to suppress excessive isolator displacement induced by a near-fault earthquake (Lu *et al*, 2013:118). PRB is one of the seismic isolation systems. It has 2 main functions, first is to protect the structural systems and their facilities inside from earthquakes, another is to mitigate the seismic load transmitted onto the structure. Based on the Figure 2.1, PRB has 3 design parameters: height of bearing (h), the radius of the spherical head (r), and the geometrical function of rocking surface $Y = G(X)$. In this study, the sixth-order polynomial function is chosen to make the bearing with variable stiffness. Therefore, it will be an even function which is symmetrical about Y -axis.

$$G(X) = c_1X^6 + c_2X^4 + c_3X^2 \quad (2.1)$$

Note: c_1 , c_2 , c_3 are determined by using numerical optimization

2.2 Horizontal Restoring Force of a Polynomial Rocking Bearing

The mechanical properties of an isolator are also important besides the configuration. However, before discussing mechanical properties, for simplicity, some assumptions will be made. First, rocking surface and base plate of bearing should have a point contact anytime. Second, the friction coefficient between them should be large enough to prevent slippage (both of them are always in rolling contact). Third, the inertial moment due to the rocking motion is negligible as compared to the forces

applied to the bearing. At last, the radius of curvature should be larger than height to retain stability.

There are 2 coordinate systems on this isolator, x - y and X - Y . The x - y is a fixed coordinate system which x -axis attached to the ground. The X - Y is moving coordinate system of PRB attached to bearing and will rock along the bearing. Therefore, when the bearing is on its origin position, both of the coordinate systems coincides each other. However, when the systems are on rocking state, there will be a rotation angle between x - y and X - Y that denoted by θ_a . In Figure 2.3, since it assumed that the rocking surface of PRB has a point contact with ground, so the x -axis is tangent to the contact point A.

$$\tan \theta_a = \frac{\sin \theta_a}{\cos \theta_a} = G'(X_a), \quad -\frac{\pi}{2} \leq \theta_a \leq \frac{\pi}{2} \quad (2.2)$$

Note:

θ_a = rotation angle

X_a = moving coordinate for contact point

Other parameters are four forces that work on the isolator. W is the structural weight, U is the horizontal resultant forces, N is the normal forces at contact point A, and F is the friction forces at contact point A. W and U are actually the forces that occur between superstructure and the bearing. Moreover, the force U as horizontal resultant forces transmitted onto isolated structure is an important parameter. The force U is defined by taking the moment equilibrium at contact point A and written as follows:

$$\sum F_x = 0 \rightarrow U = F \quad (2.3)$$

$$\sum F_y = 0 \rightarrow W = N \quad (2.4)$$

$$\sum M_A = 0 \rightarrow U = u_r = \frac{W(x_a - x_b)}{y_b} \quad (2.5)$$

Note:

W = structural weight

U = horizontal resultant forces

N = normal forces at contact point A

F = friction forces at contact point A

u_r = bearing restoring force

x_a = x coordinate of the contact point A in the x - y coordinates

x_b = x coordinates of the point B

y_b = y coordinates of the point B

Since it assumed that friction coefficient between the rocking surface and base plate should be large enough to prevent slippage, so x_a should be equal to the arc length (S_a) between A and center axis of moving coordinate system.

$$x_a = S_a = \int_0^{X_a} \sqrt{1 + G'(X_a)^2} dX \quad (2.6)$$

Using the coordinate transformation relation between x - y and X - Y systems, the value of x_b and y_b can be determined as:

$$x_b = (h - G(X_a)) \sin \theta_a - X_a \cos \theta_a + x_a \quad (2.7)$$

$$y_b = (h - G(X_a)) \cos \theta_a + X_a \sin \theta_a \quad (2.8)$$

Refer to equation 2.2, with eliminating variable θ_a , the value of x_b and y_b can be determined in another form.

$$x_b = S_a + \frac{-X_a + (h - G(X_a))G'(X_a)}{\sqrt{1 + G'(X_a)^2}} \quad (2.9)$$

$$y_b = \frac{X_a G'(X_a) + (h - G(X_a))}{\sqrt{1 + G'(X_a)^2}} \quad (2.10)$$

From the equations above, variables x_a , x_b , and y_b are depend on variable X_a which represents the X coordinate of the contact point A. Refer to equation 2.5, equation 2.6, equation 2.9, and equation 2.10, the existence of restoring force u_r can be shown as:

$$u_r = u_r(X_a) = \frac{W[-(h - G(X_a))G'(X_a) + X_a]}{(h - G(X_a)) + X_a G'(X_a)} \quad (2.11)$$

Thus, to express the restoring force u_r of Polynomial Rocking Bearing, it should be defined first about the geometric function of Polynomial Rocking Bearing.

2.3 Isolation Stiffness and Frequency of a Polynomial Rocking Bearing

The stiffness (k_r) of an isolator can be defined as the rate of change or first derivative of the restoring force (u_r) respect to the isolator displacement (x_b). However, since the u_r is not an explicit function of x_b , so the stiffness should derive one by one like equation below:

$$k_r = k_r(X_a) = \frac{du_r(X_a)}{dx_b(X_a)} = \frac{\frac{du_r(X_a)}{dX_a}}{\frac{dx_b(X_a)}{dX_a}} \quad (2.12)$$

Once the geometric function $G(X)$ is known, the stiffness (k_r) can be calculated by the equation above. It should be noted that the equation above is just for a single isolator. For the multi-stiffness isolation system, the total stiffness is equal to the sum of all the

stiffness (K_r). This provision also applies to the mass of the super-structure. Finally, the total mass is also equal to the sum of all the mass (M).

$$K_r = \sum_{i=1}^n k_{r,i} \quad (2.13)$$

$$\sum_{i=1}^n W_i = Mg \quad (2.14)$$

Note:

$k_{r,i}$ = stiffness of the i^{th} bearing

W_i = vertical load of the i^{th} bearing

n = total number of bearings used in the system

g = gravitational acceleration

With assuming that the superstructure is a rigid body and all of the bearings are designed identically and have the same displacement, so we can calculate the period T of the overall Polynomial Rocking Bearing as:

$$T = 2\pi \sqrt{\frac{M}{K_r}} \quad (2.15)$$

$$T = 2\pi \sqrt{\frac{1}{g} \frac{\sum_{i=1}^n W_i}{\sum_{i=1}^n k_i}} \quad (2.16)$$

$$T = 2\pi \frac{x'_b(X_a)}{g \bar{u}'_r(X_a)} \quad (2.17)$$

From some equations above, the restoring force (u_r), stiffness (k_r), and period (T) of the Polynomial Rocking Bearing are depend on the geometric function of isolator $G(X)$ and its derivatives. In another hand, the isolation stiffness and period are also a function of X_a . It is different from the conventional system that the isolation stiffness and period are constant. Therefore, it becomes important to choose the proper geometric function to achieve the desired properties. Moreover, from equation 2.17, period T is independent of the isolated structure mass. Hence, this property can be advantageous for the structure with a variable mass that needs to be isolated.

2.4 Horizontal Friction Force of a Polynomial Rocking Bearing

Since the spherical head of Polynomial Rocking Bearing has the friction effect, it will provide the energy dissipation of the bearing. So, when the friction is considered, the behavior of spherical head will change like the Figure 2.4. This figure represents the resultant friction force and resultant normal force with the symbol F

and N , respectively. For the resultant normal force, because it measured from the vertical axis, so there will be an angle ϕ . Note that the force N and F are perpendiculars each other.

For the convenience, the force system in the Figure 2.4(a) is slightly replaced by the equivalent calculation of force system in the Figure 2.4(b), in which W and U are the equivalents vertical and horizontal force components. The Force W and U are interactive forces between the structure and bearing, so it should be affected by the structural weight and dynamic response. Furthermore, in the Figure 2.4(b), the equivalent couple moment produce by friction force F to point B can be expressed as:

$$M_f = rF \tag{2.18}$$

Note:

M_f = moment produce by F

Looking back to the Figure 2.4, it is assumed that the bearing has a positive displacement and its rocking outward (the articular joint moving away from the neutral position). If the bearing has the opposite direction, so the directions of F and M_f should be reversed. Generally, the directions of F and M_f should be determined by the rocking direction of the bearing, once it moving outward or inward.

Horizontal force U is consists of restoring force and friction force.

$$U = u_r + u_f \tag{2.19}$$

Note:

$$u_r = \frac{We}{y_b} = \frac{W(x_a - x_b)}{y_b} \tag{2.20}$$

$$u_f = \frac{M_f}{y_b} = \frac{rF}{y_b} \tag{2.21}$$

Unlike the restoring force, the friction force cannot be easily expressed as an explicit function of the system response, because it has two possible states, slip state and stick state. When F in the slip state, it means its absolute value should be equal to its slip force. When F is in stick state, its value will be determined by the current excitation and motion of superstructure. Using the Coulomb's friction law to express the friction force, and it should satisfy the condition below:

$$|F| = F_{max} = \mu N \quad \rightarrow \text{slip state} \tag{2.22}$$

$$|F| < F_{max} \quad \rightarrow \text{stick state} \tag{2.23}$$

Note:

μ = friction coefficient in articular joint

F_{max} = maximum friction force

Since Figures 2.4(a) and 2.4 (b) are equivalent, so the normal force can be expressed as:

$$N = W \cos \phi + U \sin \phi \quad (2.24)$$

W is known value, however, U is the unknown value. So, it will be more complicated to find the N when the U is still unknown. To simplify this condition, it assumes that the horizontal force is smaller than vertical force ($U < W$) and also the angle ϕ is small enough ($\phi \approx 0$), thus $N \approx W$. By using the previous condition, finally the friction force can be shown as:

$$|u_f| = u_{f,max} = \beta(X_a)\mu W \quad \rightarrow \text{slip state} \quad (2.25)$$

$$|u_f| < u_{f,max} \quad \rightarrow \text{stick state} \quad (2.26)$$

Note:

$u_{f,max}$ = maximum value of u_f

$$\beta(X_a) = \frac{r\sqrt{1+G'(X_a)^2}}{h-G(X_a)+X_aG'(X_a)} \quad = \text{modification factor of } \mu \quad (2.27)$$

Since u_r and u_f are proportional to the vertical load W based on previous equations, so when the superstructure experience rocking behavior, it causes the vertical load W varies, so the total horizontal force U will be varied also. If W decreases to zero, so U will also approach to zero. Hence, as long as the assumption $\phi \approx 0$ is true, the derived formula of PRB is applicable even though the vertical load W is a variable.

2.5 Equivalent Horizontal Friction Coefficient

The friction coefficient of a sliding isolator can be defined as the ratio between the maximum friction force and vertical load.

$$\bar{\mu} = \frac{u_{f,max}}{W} = \beta(X_a)\mu \quad (2.28)$$

Therefore, if the chosen geometric function is symmetric about Y -axis and passes through the origin of X - Y coordinate, then we have $G(0) = G'(0) = 0$ at $X_a = 0$.

$$\bar{\mu}_0 = \bar{\mu}(0) = \beta(0)\mu = \frac{r}{h}\mu \quad (2.29)$$

$\bar{\mu}_0$ = the initial equivalent friction coefficient.

Initial equivalent friction coefficient is the friction coefficient when the bearing is at its neutral position. Its value is important since it determines the threshold seismic force that will activate the PRB. For the given material friction coefficient, the value of initial equivalent friction coefficient can be easily adjusted by change the design value of $\left(\frac{r}{h}\right)$.



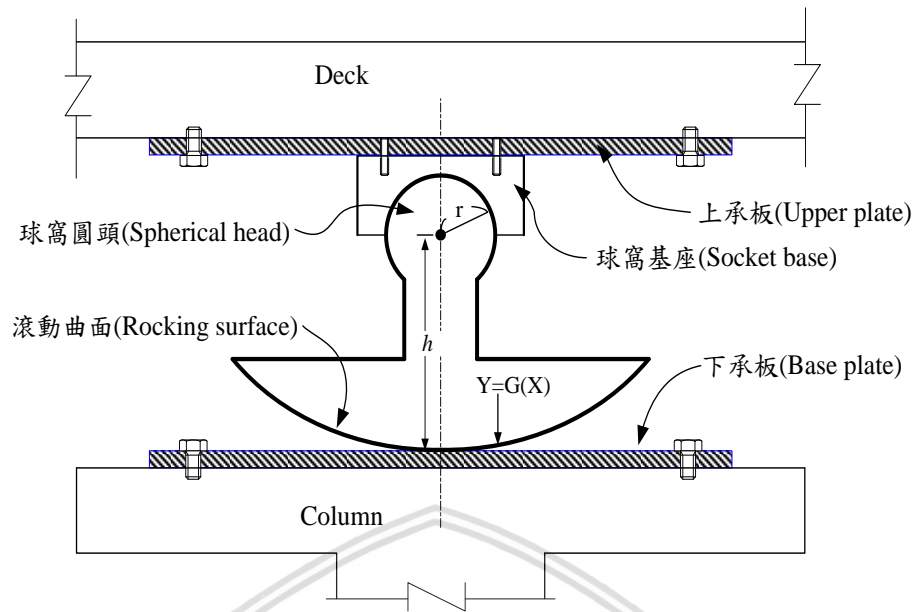


Figure 2.1 Polynomial Rocking Bearings Installed under Bridge's Deck



Figure 2.2 Polynomial Rocking Bearings

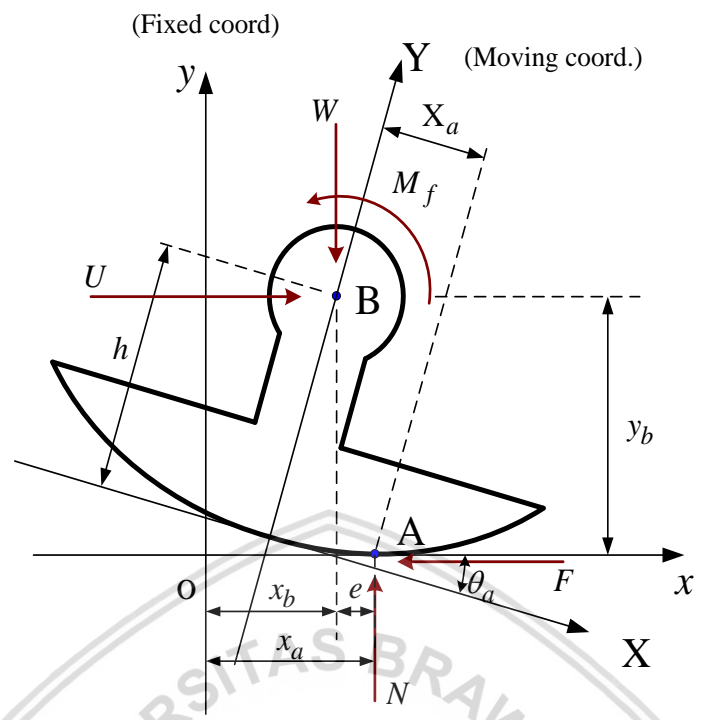


Figure 2.3 Free Body Diagram of Polynomial Rocking Bearings

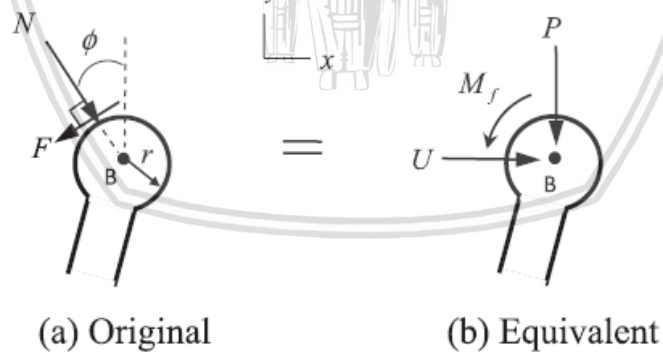


Figure 2.4 Equivalent Force Systems at Spherical Head of PRBs

CHAPTER III: NUMERICAL ANALYSIS MODEL AND ANALYSIS METHOD

This chapter describes the numerical analysis model of PRB isolation system that applied on the irregular bridge and uses the numerical analysis method called discrete-time state-space method to analyze the behavior of PRB under the seismic loading.

3.1 Design of Target of Bridge

The bridge which consists the superstructures, bearing isolation systems, columns are designed based on the Japan Highway Bridge Design Codes. As shown in the Figure 3.1, the bridges consist of the three-span deck with 2 abutments and 2 different heights of piers. The detail parameters of irregular bridges are shown in the Table 3.1. This study is based on single span bridge deck with a different high of the pier. The following assumption is considered to simplify the analysis. First, the soil condition along the bridge is uniform. Second, the vertical ground motion characteristics of the structure are not considered. Third, the friction coefficient of the bearing is constant. Lastly, the maximum static friction coefficient is equal to its dynamic friction coefficient.

3.2 Equation of Motion Derivation

Figure 3.2 shows the mathematical model of the irregular bridge. In order to simplify the calculation, free body diagram is presented on Figure 3.3 and it will divide the system into two parts, the upper part and a lower part. The upper part is a bridge's deck, and the lower part is bridge's pier. m_d denotes the mass of deck, m_c denotes the mass of pier, c_c denotes the damping of the pier, and k_c denotes the stiffness of pier. The horizontal force of bearing is denoted by U , it is the combination from restoring force (u_r) and friction force (u_f). x_d , x_c are the relative displacement of the bearing and the pier, respectively. \ddot{x}_g is the ground motion acceleration. The equation of motion can be obtained from the Figure 3.3.

$$m_d \ddot{x}_d = -(U_1 + U_2) - m_d \ddot{x}_g \quad (3.1)$$

$$m_{c1} \ddot{x}_{c1} + c_{c1} \dot{x}_{c1} + k_{c1} x_{c1} = U_1 - m_{c1} \ddot{x}_g \quad (3.2)$$

$$m_{c2} \ddot{x}_{c2} + c_{c2} \dot{x}_{c2} + k_{c2} x_{c2} = U_2 - m_{c2} \ddot{x}_g \quad (3.3)$$

Equations 3.1 to 3.3 are transformed into the matrix form.

$$\begin{bmatrix} m_d & 0 & 0 \\ 0 & m_{c1} & 0 \\ 0 & 0 & m_{c2} \end{bmatrix} \begin{bmatrix} \ddot{x}_d \\ \ddot{x}_{c1} \\ \ddot{x}_{c2} \end{bmatrix} + \begin{bmatrix} 0 & 0 & 0 \\ 0 & c_{c1} & 0 \\ 0 & 0 & c_{c2} \end{bmatrix} \begin{bmatrix} \dot{x}_d \\ \dot{x}_{c1} \\ \dot{x}_{c2} \end{bmatrix} + \begin{bmatrix} 0 & 0 & 0 \\ 0 & k_{c1} & 0 \\ 0 & 0 & k_{c2} \end{bmatrix} \begin{bmatrix} x_d \\ x_{c1} \\ x_{c2} \end{bmatrix} = \begin{bmatrix} -1 & -1 \\ 1 & 0 \\ 0 & 1 \end{bmatrix} \begin{bmatrix} U_1 \\ U_2 \end{bmatrix} + \begin{bmatrix} m_d & 0 & 0 \\ 0 & m_{c1} & 0 \\ 0 & 0 & m_{c2} \end{bmatrix} \begin{bmatrix} -1 \\ -1 \\ -1 \end{bmatrix} \ddot{x}_g \quad (3.4)$$

Generally, from the matrix form above, the equation of motion can be obtained as:

$$\mathbf{M}\ddot{\mathbf{x}}(t) + \mathbf{C}\dot{\mathbf{x}}(t) + \mathbf{K}\mathbf{x}(t) = \mathbf{M}\mathbf{L}_1\ddot{x}_g(t) + \mathbf{L}_2\mathbf{U}(t) \quad (3.5)$$

For the mass (\mathbf{M}), damping (\mathbf{C}), and stiffness (\mathbf{K}) matrix can be defined as:

$$\mathbf{M} = \begin{bmatrix} m_d & 0 & 0 \\ 0 & m_{c1} & 0 \\ 0 & 0 & m_{c2} \end{bmatrix}; \mathbf{C} = \begin{bmatrix} 0 & 0 & 0 \\ 0 & c_{c1} & 0 \\ 0 & 0 & c_{c2} \end{bmatrix}; \mathbf{K} = \begin{bmatrix} 0 & 0 & 0 \\ 0 & k_{c1} & 0 \\ 0 & 0 & k_{c2} \end{bmatrix} \quad (3.6)$$

\mathbf{L}_1 and \mathbf{L}_2 are the seismic force distribution vector and the total horizontal force distribution matrix, respectively.

$$\mathbf{L}_1 = \begin{bmatrix} -1 \\ -1 \\ -1 \end{bmatrix}; \mathbf{L}_2 = \begin{bmatrix} -1 & -1 \\ 1 & 0 \\ 0 & 1 \end{bmatrix} \quad (3.7)$$

$x(t)$ and $\mathbf{U}(t)$ are the structure displacement vector and total horizontal force vector, respectively.

$$x(t) = \begin{bmatrix} x_d(t) \\ x_{c1}(t) \\ x_{c2}(t) \end{bmatrix}; \mathbf{U}(t) = \begin{bmatrix} U_1(t) \\ U_2(t) \end{bmatrix} \quad (3.8)$$

The equation 3.5 is rewritten as the state space equation of motion as follows:

$$\dot{\mathbf{Z}}(t) = \mathbf{A}\mathbf{Z}(t) + \mathbf{E}\ddot{x}_g(t) + \mathbf{B}\mathbf{U}(t) \quad (3.9)$$

Note:

$$\mathbf{Z}(t) = \begin{bmatrix} \dot{\mathbf{x}}(t) \\ \mathbf{x}(t) \end{bmatrix}; \mathbf{A} = \begin{bmatrix} -\mathbf{M}^{-1}\mathbf{C} & -\mathbf{M}^{-1}\mathbf{K} \\ \mathbf{I} & \mathbf{0} \end{bmatrix}; \mathbf{E} = \begin{bmatrix} -\mathbf{M}^{-1}\mathbf{M}\mathbf{L}_1 \\ \mathbf{0} \end{bmatrix}; \mathbf{B} = \begin{bmatrix} \mathbf{M}^{-1}\mathbf{L}_2 \\ \mathbf{0} \end{bmatrix} \quad (3.10)$$

Equation 3.9 is a continuous-time system. It will be converted into a discrete-time system using external linear interpolation as follows:

$$\mathbf{Z}[k+1] = \mathbf{A}_d\mathbf{Z}[k] + \mathbf{E}_0\ddot{x}_g[k] + \mathbf{E}_1\ddot{x}_g[k+1] + \mathbf{B}_0\mathbf{U}[k] + \mathbf{B}_1\mathbf{U}[k+1] \quad (3.11)$$

Note:

$$\mathbf{Z}[k + 1] = \begin{bmatrix} \dot{\mathbf{x}}[k + 1] \\ \mathbf{x}[k + 1] \end{bmatrix} \quad (3.12)$$

$$\mathbf{U}[k + 1] = u_f[k + 1] + u_r[k + 1] \quad (3.13)$$

$$\mathbf{A}_d = e^{\mathbf{A}\Delta t} = \sum_{i=0}^{\infty} \frac{\Delta t^i}{i!} \mathbf{A}^i \quad (3.14)$$

$$\mathbf{B}_0 = \left(\sum_{i=0}^{\infty} \frac{(\Delta t)^{i+1}}{i!(i+2)} \mathbf{A}^i \right) \mathbf{B} \quad (3.15)$$

$$\mathbf{B}_1 = \left(\sum_{i=0}^{\infty} \frac{(\Delta t)^{i+1}}{i!(i+1)} \mathbf{A}^i - \sum_{i=0}^{\infty} \frac{(\Delta t)^{i+1}}{i!(i+2)} \mathbf{A}^i \right) \mathbf{B} \quad (3.16)$$

$$\mathbf{E}_0 = \left(\sum_{i=0}^{\infty} \frac{(\Delta t)^{i+1}}{i!(i+2)} \mathbf{A}^i \right) \mathbf{E} \quad (3.17)$$

$$\mathbf{E}_1 = \left(\sum_{i=0}^{\infty} \frac{(\Delta t)^{i+1}}{i!(i+1)} \mathbf{A}^i - \sum_{i=0}^{\infty} \frac{(\Delta t)^{i+1}}{i!(i+2)} \mathbf{A}^i \right) \mathbf{E} \quad (3.18)$$

From above equations 3.11-3.18, k is the k^{th} step and $(k+1)$ is the $(k^{\text{th}}+1)$ step, Δ_t is the time step.

3.3 Horizontal Friction Force of PRB

In equation 3.13, the component u_r that represents the restoring force can be determined by the bearing geometric parameters as shown in the previous chapter. Because the physical properties of the PRBs are complex, then the behavior of PRBs must be obtained by two coordinate systems, namely fixed coordinate system (x - y) and moving coordinate system (X - Y). As describe in second chapter, the value of X_a , $x_b(X_a)$, $y_b(X_a)$, $x_a(X_a)$ are obtained by coordinate transformation systems. In this study, the bisection method is selected as the numerical solver to find X_a and others parameters.

Unlike the restoring force (u_r), the friction force (u_f) cannot be easily expressed as an explicit function of the system response, because the friction forces have two possible states, namely sticking state and rocking state. Furthermore, because the bridge model has different height for each column, it may cause the friction force has one another possible state, namely partial rocking state. Thus, in this case, the friction force totally has three possible states: sticking state (all bearing is sticking), rocking state (all bearing is rocking), and partial rocking state (partial bearing is sticking while the partial bearing is rocking). When the moment of the bearing (M_f) is less than the maximum moment ($M_{f,max}$), it is called the sticking state. On the other hand, when the moment (M_f) is equal or more than the maximum moment ($M_{f,max}$), it will be in rocking state. For the third state, it may happen because the bridge has different height for the both columns, so this state needs to be considered. For the detail, analysis process will be shown in the Figure 3.4.

Before doing the calculation about the three possible states, some assumption needs to be considered. When the sticking state occurred in $[k+1]$ step, so the velocity of the bearing is equal to zero.

$$\dot{x}_b[k + 1] = \mathbf{DZ}[k + 1] = 0 \quad (3.19)$$

$$\mathbf{D} = [-\mathbf{L}_2^T \quad \mathbf{0}] \quad (3.20)$$

Matrix \mathbf{D} is the configuration matrix.

Based on the discrete-time system in equation 3.11, by the assumption above, the internal force in the sticking state will be like equation below.

$$\mathbf{B}_1\mathbf{U}[k + 1] = \mathbf{Z}[k + 1] - \mathbf{A}_d\mathbf{Z}[k] - \mathbf{E}_0\ddot{x}_g[k] - \mathbf{E}_1\ddot{x}_g[k + 1] - \mathbf{B}_0\mathbf{U}[k] \quad (3.21)$$

$$\mathbf{DB}_1\mathbf{U}[k + 1] = -\mathbf{D}(\mathbf{A}_d\mathbf{Z}[k] + \mathbf{E}_0\ddot{x}_g[k] + \mathbf{E}_1\ddot{x}_g[k + 1] + \mathbf{B}_0\mathbf{U}[k]) \quad (3.22)$$

$$(\mathbf{DB}_1)^{-1}\mathbf{DB}_1\mathbf{U}[k + 1] = -(\mathbf{DB}_1)^{-1}\mathbf{D}(\mathbf{A}_d\mathbf{Z}[k] + \mathbf{E}_0\ddot{x}_g[k] + \mathbf{E}_1\ddot{x}_g[k + 1] + \mathbf{B}_0\mathbf{U}[k]) \quad (3.23)$$

$$\bar{\mathbf{U}}[k + 1] = -(\mathbf{DB}_1)^{-1}\mathbf{D}(\mathbf{A}_d\mathbf{Z}[k] + \mathbf{E}_0\ddot{x}_g[k] + \mathbf{E}_1\ddot{x}_g[k + 1] + \mathbf{B}_0\mathbf{U}[k]) \quad (3.24)$$

The internal force is also equal to:

$$\bar{\mathbf{U}}[k + 1] = \bar{u}_f[k + 1] + u_r[k + 1] \quad (3.25)$$

$$\bar{u}_f[k + 1] = \bar{\mathbf{U}}[k + 1] - u_r[k + 1] \quad (3.26)$$

Moment of the bearing and the maximum moment can be shown as:

$$\bar{M}_f[k + 1] = \bar{u}_f[k + 1]y_b[k + 1] \quad (3.27)$$

$$M_{f,max} = W\mu r\beta(X_a) \quad (3.28)$$

Note:

W = vertical force/structural weight.

μ = friction's coefficient.

r = radius of spherical head.

3.3.1 Sticking State

$$|\bar{M}_f[k + 1]| < M_{f,max} \quad (3.29)$$

It means all of the bearings are in the sticking state.

$$u_f[k + 1] = \bar{u}_f[k + 1] \quad (3.30)$$

$$\mathbf{U}[k + 1] = \bar{u}_f[k + 1] + u_r[k + 1] \quad (3.31)$$

3.3.2 Rocking State

$$|\bar{M}_f[k + 1]| \geq M_{f,max} \quad (3.32)$$

It means all of the bearings are in the rocking state. The friction force should be updated into $u_{f,max}$.

$$u_{f,max}[k + 1] = \frac{M_{f,max}[k+1]}{y_b[k+1]} \quad (3.33)$$

$$\mathbf{U}[k + 1] = u_{f,max}[k + 1] + u_r[k + 1] \quad (3.34)$$

3.3.3 Partial Rocking State

It means at the same time, both of bearings may have different state, one is sticking state and the other is rocking state. Because the restoring force (u_r) can be defined easily by the bearing geometric parameters, so for this condition just need to concern for the friction force (u_f). When one of the bearings is in the sticking state, so equation 3.29-3.31 can be considered. And for another bearing is in the rocking state, so equation 3.32-3.34 can be used to calculate the friction force.

Table 3.1 Parameter of Irregular Bridges

Mass of Bridge's deck		2038.8 ton
Short Column	Mass of column	37.1 ton
	Stiffness of column	124400 kN/m
Long Column	Mass of column	74.2 ton
	Stiffness of column	15740 kN/m



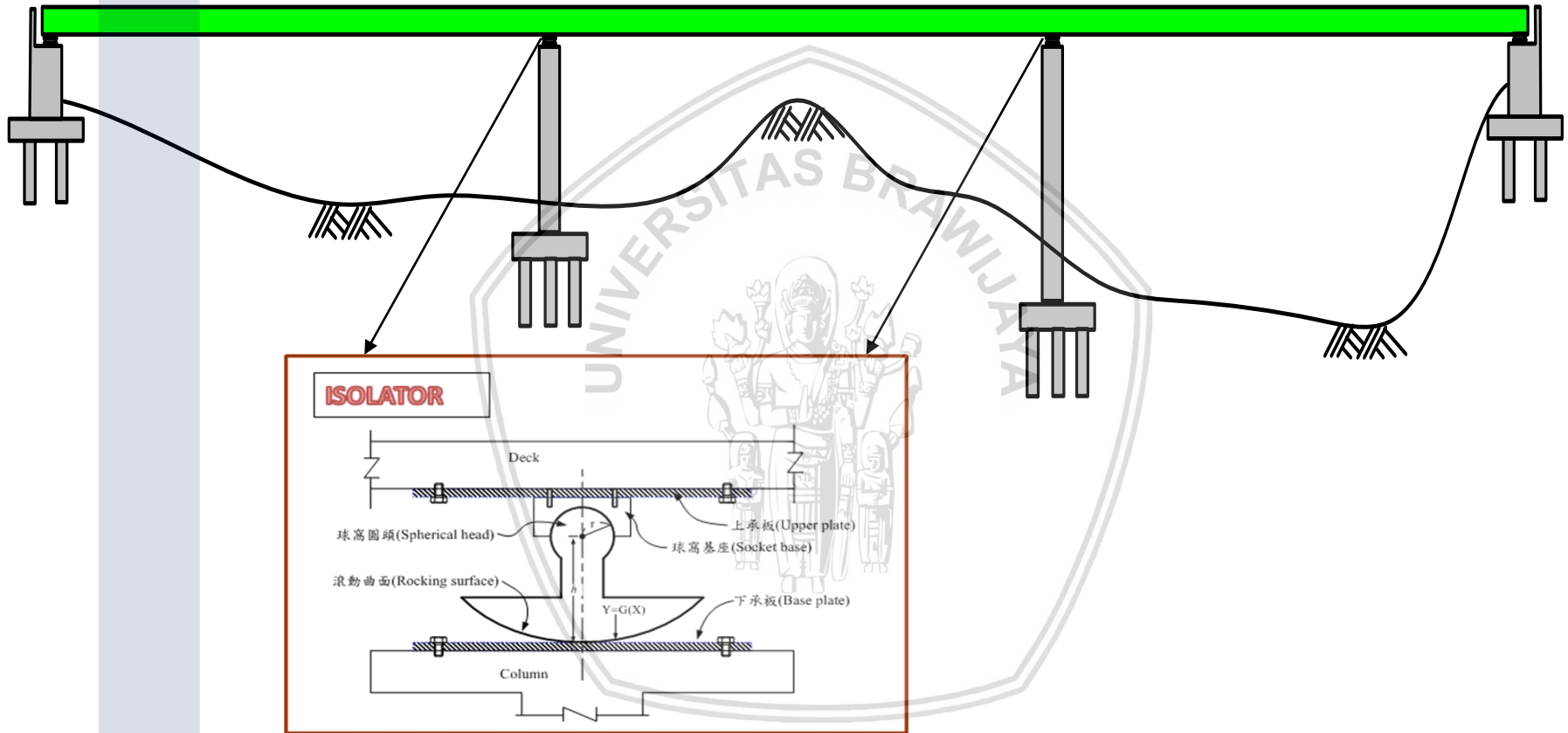


Figure 3.1 Model of Irregular Bridges

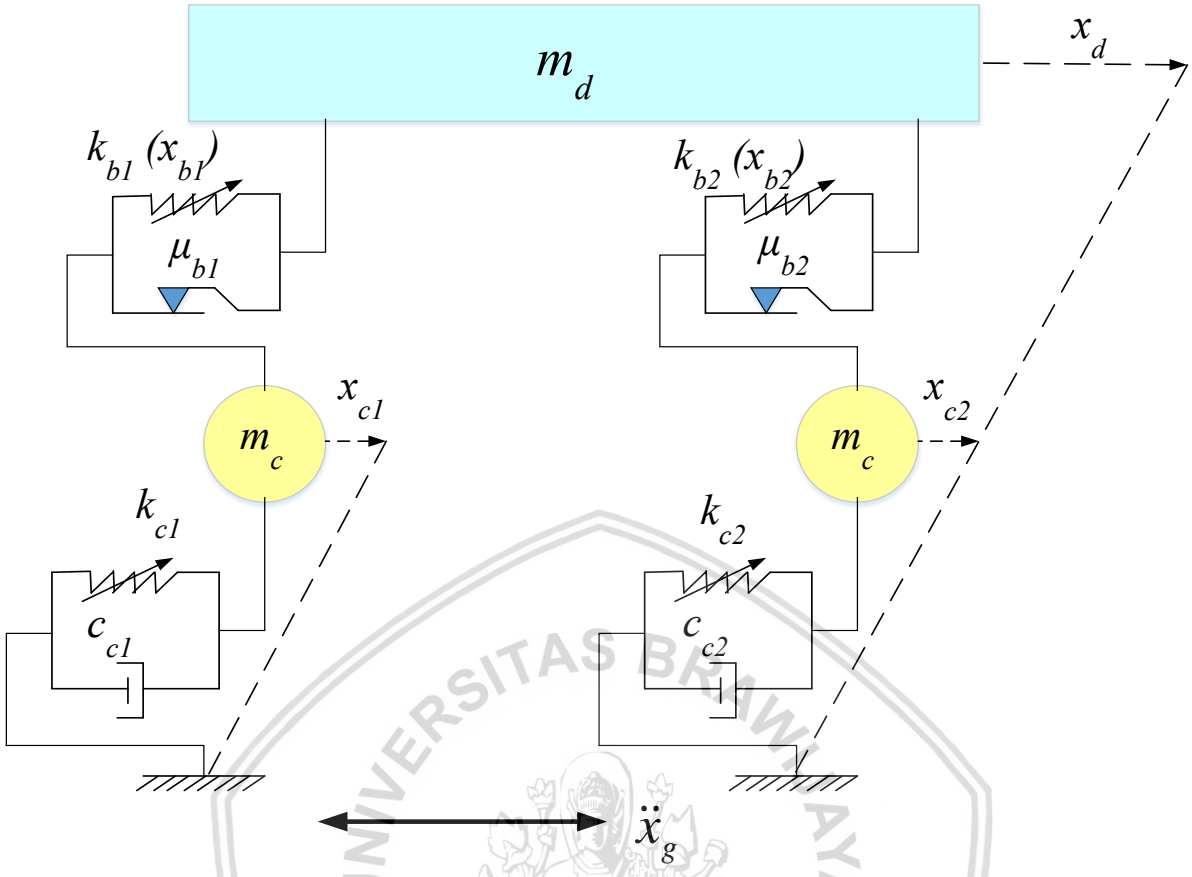


Figure 3.2 Mathematical Model of Irregular Bridges

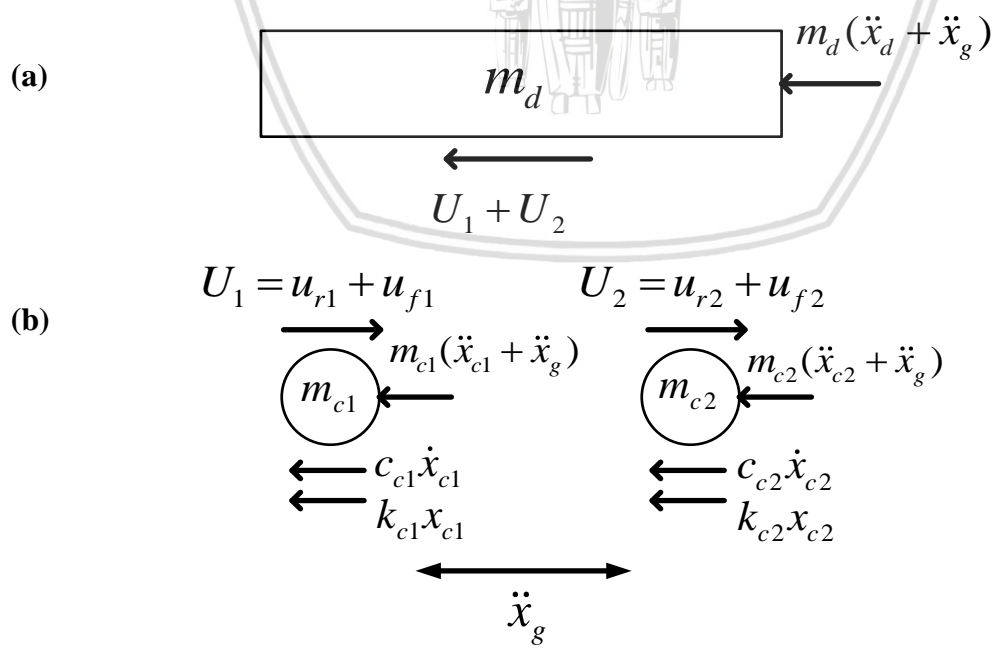


Figure 3.3 Free Body Diagram of Irregular Bridges: (a) Upper Part (b) Lower Part

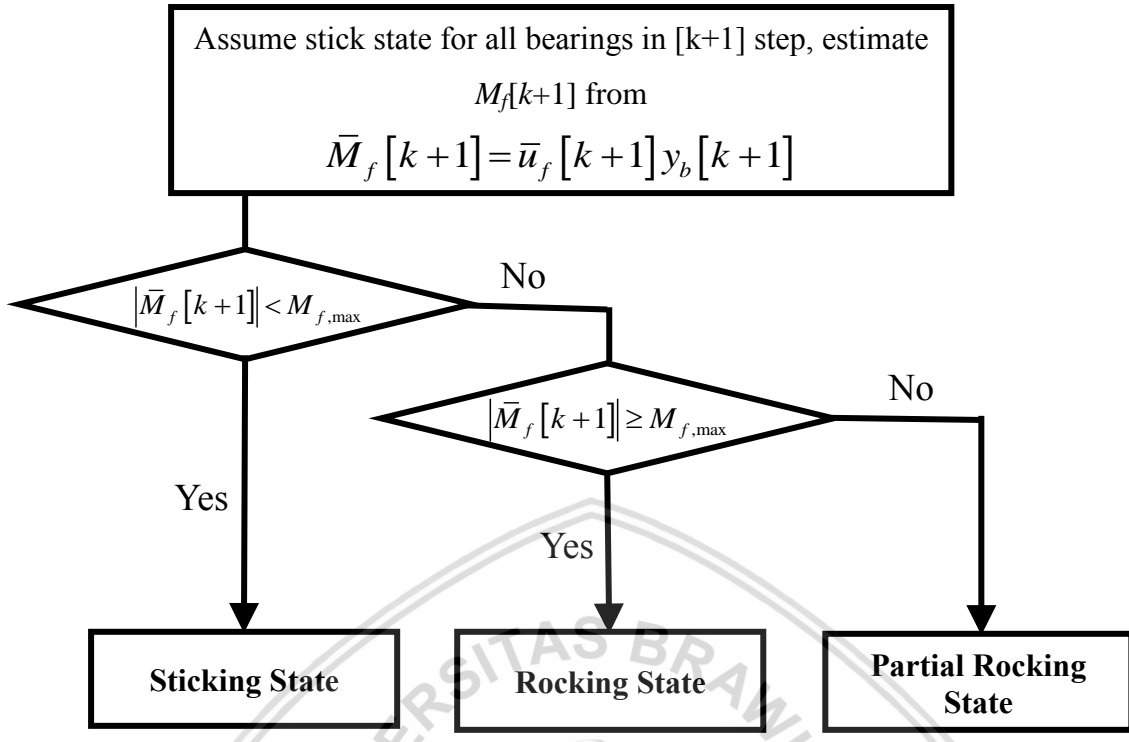
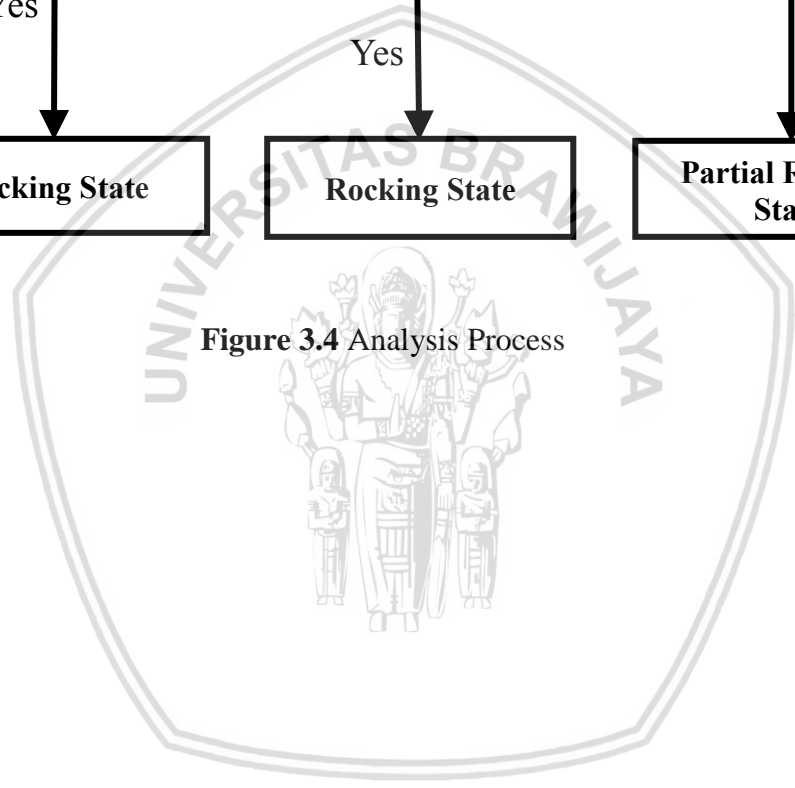


Figure 3.4 Analysis Process



CHAPTER IV: OPTIMAL DESIGN OF POLYNOMIAL ROCKING BEARINGS USING PSO-SA METHOD

PRBs use the sixth-order polynomial function at the rocking surface in order to provide variable isolation frequency. PRBs have three key design parameters: the geometric function $Y=G(X)$ which equal to the sixth-order polynomial function, the bearing height (h), and the radius of the spherical head (r). Thus, by properly choosing the value of these parameters, the mechanical properties of the PRBs may get the desired specifications. Lu et al. have studied about the sliding isolators with variable curvatures (SIVCs) which stiffness is a function of the isolator displacement. They proposed a fifth-order polynomial function with the proper coefficient values to define the restoring force as a function of displacement. Nevertheless, the restoring force of the PRBs actually cannot be expressed as a fifth-order polynomial, so their study cannot be used for the PRBs case. Therefore, in this study, PSO-SA hybrid searching algorithm based on Particle Swarm Optimization (PSO) and Simulated Annealing (SA) is adopted to explore the optimal parameters of the PRB isolation system.

4.1 PSO-SA Hybrid Searching Method

This section introduces the mathematical model of the optimization problem, as well as the Particle Swarm Optimization (PSO) and Simulated Annealing (SA) method, and also the combining of PSO method and SA method becoming PSO-SA hybrid searching method.

4.1.1 Mathematical Model of Optimization Problem

The optimization problem should be based on the description of the problem. Then, the mathematical model can build from this optimization problem and after that using a mathematical model to optimize the design. Considering the structural optimization problem of the inequality beam condition, then the mathematical model can be expressed as:

$$\text{Minimize } f(\mathbf{X}) \quad (4.1)$$

$$\text{Subject to } g_j(\mathbf{X}) = \left| \frac{b_j}{(b_a)_j} \right| - 1 \leq 0, \quad j = 1 \sim n \quad (4.2)$$

$$\mathbf{X}_{lb} \leq \mathbf{X} \leq \mathbf{X}_{ub} \quad (4.3)$$

The above formulas mean the way to determine the design variable \mathbf{X} in order to minimize the objective function $f(\mathbf{X})$ and correspond to the constraint function $g_j(\mathbf{X})$. b_j is the structural response and $(b_a)_j$ is the structure response allowable value, n is the total of constraint function. The design variables \mathbf{X} must be between the lower bound (\mathbf{X}_{lb}) and the upper bound (\mathbf{X}_{ub}). The combination of the objective function $f(\mathbf{X})$ and the constraint functions $g_j(\mathbf{X})$ multiplied by the penalty parameters lead to the fitness function like the equation 4.4.

$$\tilde{f} = f(\mathbf{X}) + \lambda \sum_{j=1}^n \max(0, g_j(\mathbf{X})) \quad (4.4)$$

λ is the penalty parameters ($\lambda=10^6$).

4.1.2 Particle Swarm Optimization (PSO)

Optimization techniques have been widely applied in numerous fields of engineering. Recently, evolutionary computation techniques have become more popular, such as Genetic Algorithms (GAs) and Particle Swarm Optimization (PSO) (Kennedy and Blackwell, 2007). Particle Swarm Optimization, a population-based stochastic optimization, was motivated from the optimization of the social behavior of animals, such as the flocking of birds and schooling of fish (Kennedy and Eberhart, 1995). In the implementation of the PSO, a candidate solution of the concern problem is called a particle. In the beginning of searching, the population of particles, i.e. a swarm of particles, are initialized with random “positions” (i.e. solutions) and “velocities” in an l -dimensional search space where l denotes the number of design variables. All particles in the swarm exchange information about their best solutions with one another and then each particle adjusts its searching “velocity” for the next “position” according to its own “experience” as well as the group “experiences”. The position and velocity of the i^{th} particle updated from the current generation t to the next generation $t+1$ and it can be related by the following equations:

$$\mathbf{v}_{t+1}^i = \mathbf{v}_t^i + c_1 r_1 (p_t^i - \mathbf{X}_t^i) + c_2 r_2 (p_t^g - \mathbf{X}_t^i) \quad (4.5)$$

$$\mathbf{X}_{t+1}^i = \mathbf{X}_t^i + \mathbf{v}_{t+1}^i \quad (4.6)$$

The superscript i indicates the i^{th} particle while the subscript t indicates the generation number; \mathbf{v} and \mathbf{X} are the velocity and position vectors of the particle, respectively; p_t^i is the best position vector of the i^{th} particle, corresponding to the individual best fitness value obtained so far, and p_t^g is the global best position vector, corresponding to the overall previous best fitness value in the whole swarm; r_1 and r_2

are two independent uniform random numbers between 0 and 1; c_1 and c_2 are positive acceleration constants denoting the weights of the stochastic acceleration terms that drag each particle toward the positions of the global and local best solutions, usually uses the value is 2.

In the original process of the PSO, the velocities of the particles on each dimension should be limited between $-\mathbf{v}^{\max}$ and \mathbf{v}^{\max} . A larger value of \mathbf{v}^{\max} promotes global exploration, while a smaller \mathbf{v}^{\max} inspires local exploitation. Thus, the parameter \mathbf{v}^{\max} is an important one for the PSO. Shi and Eberhart (1998b) introduced the inertia weight (w) with constant \mathbf{v}^{\max} to balance the global exploration and local exploitation, aimed at improving the performance of the PSO within a reasonable number of generations.

$$\mathbf{v}_{t+1}^i = w\mathbf{v}_t^i + c_1r_1(p_t^i - \mathbf{X}_t^i) + c_2r_2(p_t^g - \mathbf{X}_t^i) \quad (4.7)$$

$$\mathbf{v}^{\max} = \gamma(\mathbf{X}_{ub} - \mathbf{X}_{lb}) \quad (4.8)$$

In which \mathbf{X}_{ub} is the upper bound of particles and \mathbf{X}_{lb} is the lower bound of particles, and γ is a fraction for decreasing the initial search space, usually uses the value is 1.

Fourie and Groenwold (2002) proposed a rule to dynamically decrease the inertia weight and maximum velocity if no more improved solutions are obtained after running h consecutive generations. Such a rule is utilized in this study, which can be written as:

$$\text{If } \tilde{f}(p_t^g) \geq \tilde{f}(p_{t-h}^g) \text{ then,} \quad (4.9)$$

$$w_{t+1} = \alpha w_t \text{ and } \mathbf{v}_{t+1}^{\max} = \beta \mathbf{v}_t^{\max} \quad (4.10)$$

In which α and β are the decrease factors between 0 and 1.

When the global best solution is entrapped in a poor local optimal solution, then the searching efficiency decreases significantly. In this connection, the global best solution plays a more important role in guiding the search direction than the local one. In order to prevent the solution of the PSO from converging early to a poor local minimum, Juang and Chuang (2007) proposed inserting a simulated annealing algorithm into the PSO procedure to provide the possibility of jumping away from a local minimum.

4.1.3 Simulated Annealing (SA)

Simulated Annealing (SA) is an optimization algorithm motivated by an analogy to the annealing in solids in statistical mechanics (Kirkpatrick et al., 1983). SA

is also a generic probabilistic meta-heuristic for the global optimization problem, can be seen as analogous to the behavior of physical systems in a heat bath (Kirkpatrick *et al.*, 1983). When no further improvements to the global best solution can be found after h consecutive generations, a new solution in the neighborhood of the global best solution p_t^g is generated by using two uniform random numbers, R_1 and R_2 in the range from 0 to 1.

$$\text{If } R_1 > 0.5, \hat{p}_t^g = p_t^g + R_2(\mathbf{X}_{ub} - p_t^g) \quad (4.11)$$

$$\text{If } R_1 \leq 0.5, \hat{p}_t^g = p_t^g - R_2(p_t^g - \mathbf{X}_{lb}) \quad (4.12)$$

SA is not only accepted a near local optimal but also a worse solution, so it offers the possibility of escaping from poor local optimal, where the solutions are entrapped during the process of the PSO. Whether the new solution can be accepted or not is decided according to the Boltzmann probability factor P :

$$P = \exp\left(-\frac{\Delta\tilde{f}}{kT_j}\right) \quad (4.13)$$

In which, $\Delta\tilde{f}$ is the difference of the fitness value between the new solution and the current global solution, k is Boltzmann's constant, usually the value is 1, and T_j is the current temperature.

If $\Delta\tilde{f}$ is smaller than or equal to zero, the new solution is accepted as the new global best solution. If $\Delta\tilde{f}$ is larger than zero, a uniform random number is generated in the value between 0 and 1 and then compared with the Boltzmann probability factor P . If the generated random number is smaller than P , the new solution is accepted as the new global best one. Otherwise, the current global best solution is maintained.

In processing the SA, the initial temperature (T_{start}) and the final temperature (T_{end}) are chosen in advance. At each iterative search, the temperature T_i is updated by multiplying the previous temperature T_{i-1} by a reduction factor (T_{red}). The searching process is continued until the temperature reaches the final temperature T_{end} . Then, the final solution is saved as the new global best solution.

4.1.4 Particle Swarm Optimization-Simulated Annealing (PSO-SA)

As mentioned above, a hybrid searching algorithm combining the PSO with the SA is employed in this study to find the optimal parameters of the PRB isolation system for an irregular isolated bridge. An inner loop of the SA is inserted in the

process of the PSO, giving an interference to create a new solution and then determine the acceptance based on the Boltzmann probability factor if the new solution moves up. After completing a cooling cycle, the operation returns to the PSO algorithm. The procedure of the hybrid searching algorithm is summarized as follows:

- (i) Create an initial population array of particles with random positions and velocities on l dimensions in the searching space.
- (ii) Select \mathbf{v}^{\max} according to equation 4.8.
- (iii) Loop of PSO.
- (iv) Evaluate the fitness function of the t^{th} generation according to equation 4.4 for each particle i .
- (v) Compare each particle's fitness function value with its previous best value. If the fitness function value $<$ previous best value, so the best position vector of the i^{th} particle is equal to position vectors of the particle, also the best value is equal to the fitness function value.
- (vi) Compare each particle's fitness function value with the previous global best value. If the fitness function value $<$ previous global best value, so the global best position vector is equal to position vectors of the particle, also the global best value is equal to the fitness function value.
- (vii) If no more improved solutions obtained after running h consecutive generations like equation 4.9, do the following:
 - (a) Decrease inertia weight (w) and maximum velocity (\mathbf{v}^{\max}) according to equation 4.10.
 - (b) Choose the initial temperature (T_{start}), final temperature (T_{end}), and reduction factor (T_{red}) for the SA algorithm.
 - (c) Loop of SA.
 - (d) Generate two uniform random numbers (R_1 and R_2) in the range from 0 to 1.
 - (e) Create a new solution according to equations 4.11 and 4.12, then calculate the difference of the fitness value ($\Delta\tilde{f}$) between the new solution and the current global best solution.
 - (f) If $\Delta\tilde{f}$ is smaller than or equal to zero, the new solution is accepted as the new global best solution.

- (g) If $\Delta\tilde{f}$ is larger than zero, generate a random number in the value between 0 and 1 and then compared with the Boltzmann probability factor (P) according to equation 4.13.
- (h) If the final temperature T_{end} is reached, exit loop of SA.
- (i) End the loop of SA.
- (viii) Change the velocity according to equation 4.7 and the position of a particle according to equation 4.8 for each particle.
- (ix) If the specific number of generations is reached, exit loop of PSO.
- (x) End the loop of PSO.

In order to select a suitable set of parameters in the process of optimization to control the structure response of irregular isolated bridge, a number of running cases were carried out with various sets of parameters. The population size was 30, the number of generation was 100, and the set of other parameters used is listed in Table 4.1.

4.2 Bearing's Objective Function

PSO-SA is adopted to explore the optimal parameters and solution of the PRB isolation system. Based on the mathematical model of optimization problem, equations 4.1 to 4.3 are used to determine the design variable \mathbf{X} in order to minimize the objective function $f(\mathbf{X})$ correspond to the constraint function $g_j(\mathbf{X})$. In this paper, the objective function depends on the deck displacement and the horizontal force of each column.

$$f(\mathbf{X}) = w_c x \frac{\max(|V_{c1}|) + \max(|V_{c2}|)}{D_c} + w_d x \frac{\max(|x_d|)}{D_d} \quad (4.14)$$

V_{c1} is the horizontal force of short column, V_{c2} is the horizontal force of long column, x_d is deck displacement. D_c and D_d are the normalized denominators. D_c is a maximum horizontal force (using hinged support) for each column, and D_d is maximum deck displacement (using roller support). Because in this study has two different height of columns, so D_c has two numbers, for the first column $D_{c1}=7168.304$ kN, and for the second column $D_{c2}=912.9679$ kN. The maximum deck displacement $D_d=0.058$ m. w_c and w_d are scalar weights related to the peak of column horizontal forces and the peak of deck displacement, respectively. Because the bridge is not expected to have a large displacement when an earthquake occurs, hence set $w_d > w_c$, $w_c=0.35$ and $w_d=0.65$. However, it is also not expected the horizontal force of columns will be too large and make the columns going into non-linear stage, therefore it needs to use the fitness

function as the combination of the objective function $f(\mathbf{X})$ and the constraint functions $g_j(\mathbf{X})$ multiplied by the penalty parameters to avoid this situation.

$$g_j(\mathbf{X}) = \frac{\max|x_{b,j}|}{x_{b,j_limit}} - 1 \quad (4.15)$$

$$\tilde{f} = f(\mathbf{X}) + \lambda_1 \max(0, g_1(\mathbf{X})) + \lambda_2 \max(0, g_2(\mathbf{X})) \quad (4.16)$$

$$\lambda_1 = \lambda_2 = 10^6 \quad (4.17)$$

4.3 PRB Parameter Setting

PRB has three key design parameters: the geometric function $Y=G(X)$ which equal to the sixth-order polynomial function, the bearing height (h), and the radius of the spherical head (r). For the spherical head radius, the value of this parameter is fixed in 0.044 m, because the size of the spherical head cannot too big. Thus, it has 4 parameters need to find the optimal value in order to get the desired specifications. Before doing the PSO-SA, it needs to make the limitation value for each parameter. For the sixth-order polynomial function with 3 coefficients, the value of c_1 is set between -20 and 700, the value of c_2 is set between -40 and 20, and the value of c_3 is set between 0 and 3. The value of bearing height (h) is set between 0.15 m and 0.65 m. For the friction coefficient, because it assumes using the steel material for the spherical head and brass material for the ball socket, so the friction coefficient is 0.3. The summary of PRB parameter setting is listed in Table 4.2 and the result of design parameters is listed in Tables 4.4 and 4.5.

4.4 FPS Parameter Setting

FPS has two design parameters, the coefficient of friction and the radius of curvature, respectively. The friction coefficient depends on the types of material that used. Because it assumes using the steel material for the spherical surface and polytetrafluoroethylene (PTFE) material for the bearing material at articulated slider, so the friction coefficient is 0.1. Another important parameter of FPS is the radius of curvature. The radius of curvature determines the bearing stiffness and isolation period.

$$K = \frac{W}{R \cos \theta} \quad (4.18)$$

$$T = 2\pi \sqrt{\frac{W/g}{K}} = 2\pi \sqrt{\frac{R}{g}} \quad (4.19)$$

Note:

W = weight of super-structure

K = bearing stiffness

T = isolation period

Since the commonly used isolation period is range between 1.5 seconds and 3 seconds, so the range of curvature's radius is converted from 0.56 m to 2.236 m based on the equation 4.19. The summary of FPS parameter setting is listed in Table 4.3 and the result of design parameters is listed in Tables 4.6.

4.5 Ground Motion Input

Ground motions generated from earthquakes differ from one another in characteristics, magnitude, source, distance and direction from the rupture location, and also local soil conditions. These ground motions generally divide into two groups, near-fault earthquakes and far-fault earthquakes, respectively. Near-fault earthquakes are the earthquakes which occur in fields close to the fault. Generally, the distance is less than 15 kilometers from earthquake epicenter. Otherwise, the distance for far-fault earthquakes is more than 15 kilometers. Besides, the characteristics of near-fault earthquakes are linked to the fault geometry and the orientation of the traveling seismic waves. The primary characteristics of near-fault earthquakes are the forward directivity and fling step effects which have caused severe structural damage in recent major earthquake. The velocity pulse duration in the near-fault earthquakes is larger than 1.0 s. In addition, the ratio of the peak ground velocity (PGV) to the peak ground acceleration (PGA) of the near-fault ground motions is larger than 0.1 s. On the contrary, another set of ground motion records, recorded at the same site condition from the same earthquake events with epicenter far away from the site, is employed to represent the characteristics of far-fault earthquakes. In this simulation, 7 ground motions are used to simulate the behavior of irregular bridge. For the near-fault earthquake, it has 5 ground motions, Imperial Valley, TCU068, Sylmar, JMA Kobe, and Northridge. The rest is for the far-fault earthquake, Hachinohe and El Centro.

The 1979 Imperial Valley Earthquake affected Imperial Valley in Southern California and Mexicali Valley in Northern Baja California. This earthquake had a relatively shallow hypocenter. It caused by rupture along parts of the Imperial Fault, the Brawley fault zone, and the Rico Fault. Imperial Valley measured the surface acceleration from east to west. TCU068 is the 1999 Chi-Chi Earthquake, also known

as the 921 Earthquakes, was an earthquake in the central part of Taiwan. The depth of the epicenter was 7.0 km. This earthquake happened along the Chelungpu fault line in western part of the island of Taiwan. The fault is located along the foot hills of the Central Mountains in Nantou and Taichung counties. TCU068 measured the surface acceleration from east to west. The 1994 Sylmar Earthquake is also known as The 1994 Northridge Earthquake. The difference is the direction measurement for surface acceleration. For the Sylmar, it is measured from east to west, while for the Northridge is from north to south. Its epicenter is located in Reseda, a neighborhood in the north-central San Fernando Valley region of Los Angeles, California. The earthquake struck in the San Fernando Valley about 20 miles (31 km) northwest of downtown Los Angeles. The depth of hypocenter was 11.4 miles (18.3 km). The 1995 Great Hanshin Earthquake or JMA Kobe Earthquake struck Kobe, Japan, and its surrounding area. The focus of the earthquake was located 17 km beneath its epicenter, on the northern end of Awaji Island, 20 km away from the city of Kobe. The Great Hanshin Earthquake called an "inland shallow earthquake". Earthquakes of this type occur along active faults. Even at lower magnitudes, they can be very destructive because they often occur near populated areas and their hypocenters are located less than 20 km below the surface. It measured the surface acceleration from north to south.

The 1968 Tokachi Earthquake is also known as Hachinohe Earthquake. It was located near the junction of the Kuril Trench and the Japan Trench. It is an inter-plate earthquake. The focal mechanism of this earthquake shows movement on a thrust fault with a considerable slip-strike component. This earthquake measured the surface acceleration from north to south. The 1940 El Centro Earthquake occurred in the Imperial Valley in south eastern Southern California near the international border of the United States and Mexico. It was characterized as a typical moderate-sized destructive event with a complex energy release signature. It was the result of a rupture along the Imperial Fault, with its epicenter 5 miles (8.0 km) north of Calexico, California. It measured the surface acceleration from north to south. The time history of ground motion is divided into two groups, the near-fault ground motions are shown in Figures 4.1(a) to 4.1(e), and the far fault ground motions are shown in Figures 4.2(a) and 4.2 (b).

4.6 Numerical Analysis Results and Discussions

In this section, the optimal parameters of PRB and FPS obtained by PSO-SA and their seismic isolation performance will be presented and compared each other. Tables 4.4-4.6 show the best parameter of PRB and FPS based on PSO-SA method. Figures 4.3(a) to 4.3(g) show the PRB convergence characteristics. With the 100 iterations, overall PRB obtained by PSO-SA present the constant solutions after the 60th iteration. Figures 4.4 to 4.10 show the PRB curvature for each of column. PRB curvatures obtained by PSO-SA present the reasonable curvature. It means that PSO-SA method is appropriate to find the best parameter of PRB. Figures 4.11(a) to 4.11(g) show the FPS convergence characteristics. With the 100 iterations, overall FPS obtained by PSO-SA present the constant solutions after some first iteration. It means that PSO-SA method is suitable to find the best parameter of FPS.

Figures 4.12 to 4.25 are the dynamic response of the irregular bridge subjected to 7 ground motions. Each of ground motion has 9 figures which are divided into two parts, the time history of structure's displacement and the hysteretic loop of structures. For time history of displacement, there are 5 figures, (a) time history of deck displacement, (b) time history of bearing displacement in short column, (c) time history of bearing displacement in long column, (d) time history of short column displacement, (e) time history of long column displacement. For the hysteretic loop, there are 4 figures, (a) hysteretic loop of bearing in short column, (b) hysteretic loop of bearing in long column, (c) hysteretic loop of short column, (d) hysteretic loop of long column. For all the figures will have 2 lines, the blue solid line is for the PRB response and the red dash line is for the FPS response. Table 4.7 compares the maximum displacement of bearing in short and long column for PRB and FPS. Table 4.8 compares the maximum displacement of deck, short column, and long column for PRB and FPS. Table 4.9 compares the maximum horizontal force of bearing in each column for PRB and FPS.

Overall for the deck displacement, PRB has better isolation effect than FPS. For 7 kinds of ground motions, PRB just has the larger displacement at Sylmar ground motion. Nevertheless, even though PRB has larger displacement, FPS still has the residual deck displacement about 0.025 m at the end of ground motion. It means that PRB still have the better isolation effect than the FPS. For the bearing displacement and column displacement have opposite results for PRB in Northridge, TCU068, Imperial, and Sylmar. For example, when the bearing displacement in short column is

smaller, then it is getting larger in short column displacement and vice versa. However, for Hachinohe, JMA Kobe, and El Centro, the bearing displacement and column displacement have equal results. In FPS case, the bearing displacement and column displacement have opposite results in Northridge, Hachinohe, Sylmar, JMA Kobe, and El Centro. In another hand, for TCU068 and Imperial, the bearing displacement and column displacement have equal results.

Based on the numerical results above, some figures about the structure's responses are not satisfactory, such as the hysteretic loop of the bearing. For example is the hysteretic loop of PRB in Northridge Earthquake. Theoretically, in the short column case, the displacement of PRB in short column should be larger than longer column, because short column's stiffness is larger than longer column, so the stiffness of the bearing should be smaller than in longer bearing. However, the results show that displacement of PRB in short column is smaller than PRB in long column. It means that the stiffness of PRB in short column is larger than PRB in long column. This phenomenon is also occurred in the long column case. It may happened because in this research using two different analysis for the seismic isolation system and the bridge structure. Non-linear analysis is performed in the seismic isolation system while linear analysis in the bridge structure. Nevertheless, generally, the performance of PRB isolation system is better than FPS because it can effectively suppress the displacement of the bridge deck in both near and far-fault earthquakes.

Table 4.1 Parameter of PSO-SA Hybrid Searching Algorithm

Parameter	Value	Parameter	Value
c_1	0.5	w_{max}	1.4
c_2	1.6	w_{min}	0.8
γ	1	T_{start}	450
α	0.99	T_{red}	0.97
β	0.95	T_{end}	300
h	3		

Table 4.2 PRB Parameter Setting in PSO-SA Hybrid Searching Method

Parameter		Lower Bound	Upper Bound
Coefficient of Sixth-Order Polynomial Function	c_1	-20	700
	c_2	-40	20
	c_3	0	3
Height of Bearing (h)		0.15	0.65

*Friction coefficient is 0.3 (steel-brass)

Table 4.3 FPS Parameter Setting in PSO-SA Hybrid Searching Method

Parameter	Lower Bound	Upper Bound
Radius of Curvature in Short Column (r_1)	0.56	2.236
Radius of Curvature in Short Column (r_2)	0.56	2.236

*Friction coefficient is 0.1 (steel-PTFE)



Table 4.4 The Optimal Parameter of PRB in Short Column Based on PSO-SA

Earthquake's name	Bearing in short column			
	c_1	c_2	c_3	$h (m)$
Imperial Valley	141.2325	20	0	0.1643
TCU068	700	20	0	0.15
Sylmar	700	20	0	0.15
JMA Kobe	-20	20	3	0.15
Northridge	525.9088	-2.467	0.8332	0.15
Hachinohe	700	-7.244	3	0.15
El Centro	700	20	3	0.15

Table 4.5 The Optimal Parameter of PRB in Long Column Based on PSO-SA

Earthquake's name	Bearing in long column			
	c_1	c_2	c_3	$h (m)$
Imperial Valley	-20	5.8497	0.7563	0.65
TCU068	-20	20	0.7266	0.65
Sylmar	173.0106	20	0.9873	0.4807
JMA Kobe	-20	20	0.7333	0.65
Northridge	216.1577	32.5545	1.0704	0.4938
Hachinohe	700	-10.5177	0.7924	0.65
El Centro	700	2.9801	0.7737	0.65

Table 4.6 The Optimal Parameter of FPS Based on PSO-SA

Earthquake's name	Radius of FPS in short column $r_1 (m)$	Radius of FPS in long column $r_2 (m)$
Imperial Valley	0.56	2.236
TCU068	0.56	2.236
Sylmar	2.236	2.236
JMA Kobe	2.236	0.6796
Northridge	2.236	2.236
Hachinohe	0.56	2.236
El Centro	1.5924	1.762

Table 4.7 Maximum Displacement of Bearing

Earthquake's name	Maximum displacement of bearing in short column (m)		Maximum displacement of bearing in long column (m)	
	PRB	FPS	PRB	FPS
Imperial Valley	0.0109	0.1583	0.0457	0.1001
TCU068	0.0198	0.1983	0.0634	0.1477
Sylmar	0.0392	0.0729	0.0935	0.0206
JMA Kobe	0.0339	0.0433	0.0402	0.0008
Northridge	0.0158	0.0688	0.0489	0.0097
Hachinohe	0.0533	0.0725	0.0586	0.0181
El Centro	0.0335	0.0423	0.0384	0.0008

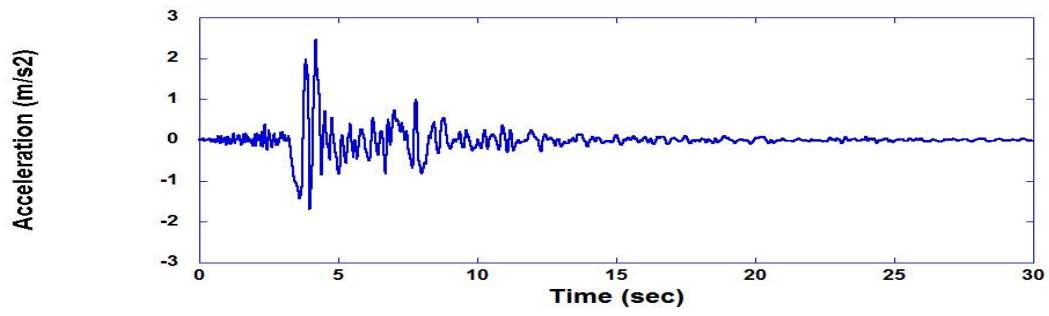
Table 4.8 Maximum Displacement of Bridge Structure

Earthquake's name	Maximum displacement of deck (m)		Maximum displacement of short column (m)		Maximum displacement of long column (m)	
	PRB	FPS	PRB	FPS	PRB	FPS
Imperial Valley	0.0566	0.1662	0.0459	0.0103	0.0408	0.0841
TCU068	0.0692	0.2062	0.0496	0.0115	0.0426	0.0928
Sylmar	0.0854	0.0808	0.0503	0.0114	0.0589	0.0747
JMA Kobe	0.0426	0.0511	0.0118	0.0121	0.0347	0.0503
Northridge	0.0488	0.0761	0.0331	0.0108	0.0484	0.0734
Hachinohe	0.0662	0.08	0.0134	0.0114	0.035	0.0747
El Centro	0.0428	0.0507	0.0107	0.0121	0.0294	0.0499

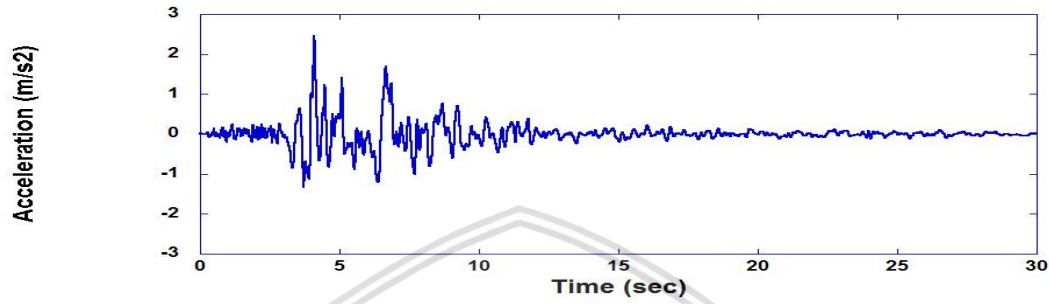
Table 4.9 Maximum Horizontal Force of Bearing

Earthquake's name	Maximum horizontal force of bearing in short column (kN)		Maximum horizontal force of bearing in long column (kN)		Total horizontal force (kN)	
	PRB	FPS	PRB	FPS	PRB	FPS
Imperial Valley	5653.117	3827.083	244.822	1447.797	5897.939	5274.881
TCU068	6121.616	4540.909	332.166	1659.706	6453.782	6200.614
Sylmar	6125.589	1324.731	623.433	1092.248	6749.022	2416.979
JMA Kobe	1280.018	1193.808	254.005	742.515	1534.023	1936.324
Northridge	4079.545	1306.923	452.223	1043.515	4531.769	2350.438
Hachinohe	1683.780	2289.156	272.186	1081.157	1955.967	3370.313
El Centro	1278.113	1268.676	248.695	729.827	1526.808	1998.503

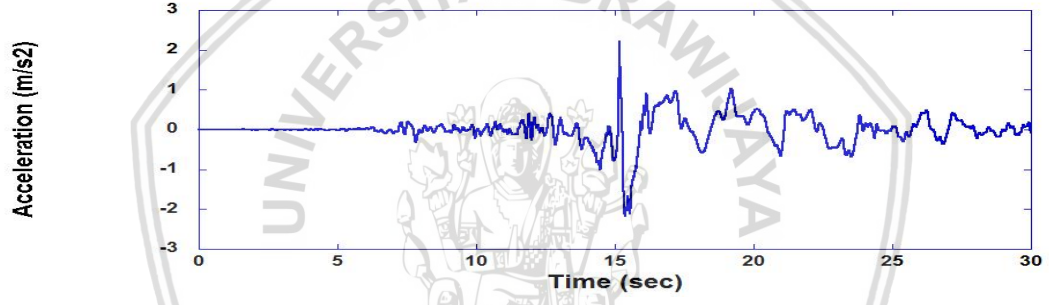




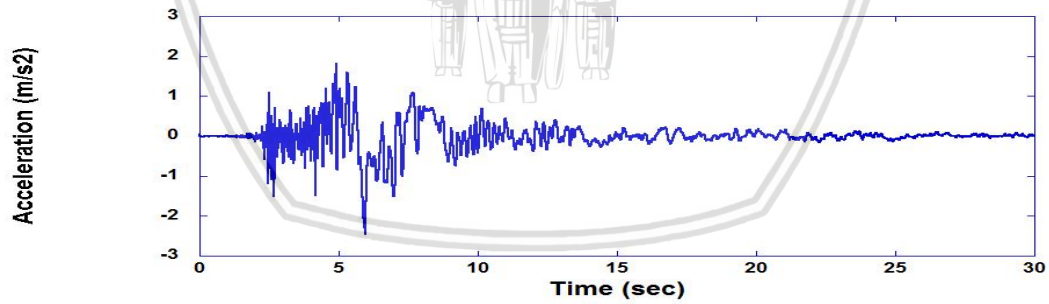
(a) Northridge Ground Motion



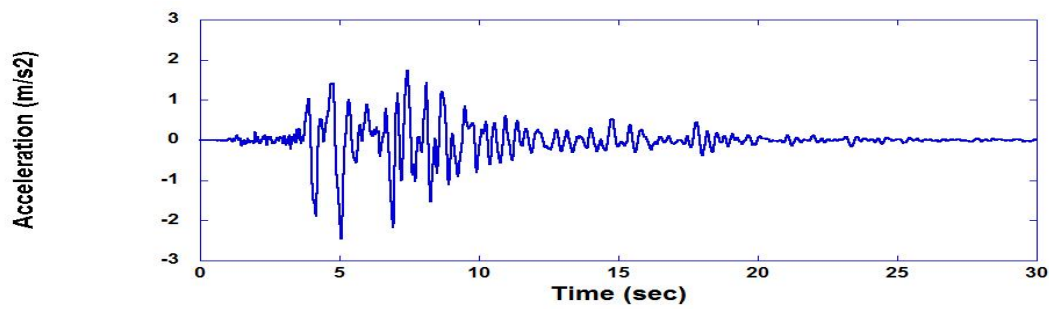
(b) Sylmar Ground Motion



(c) TCU068 Ground Motion



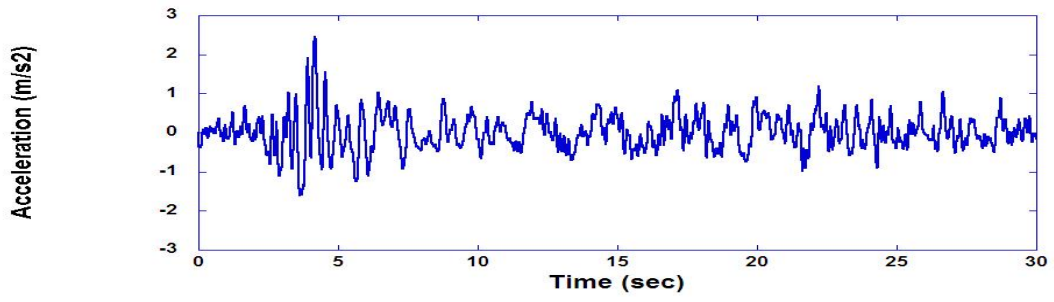
(d) Imperial Ground Motion



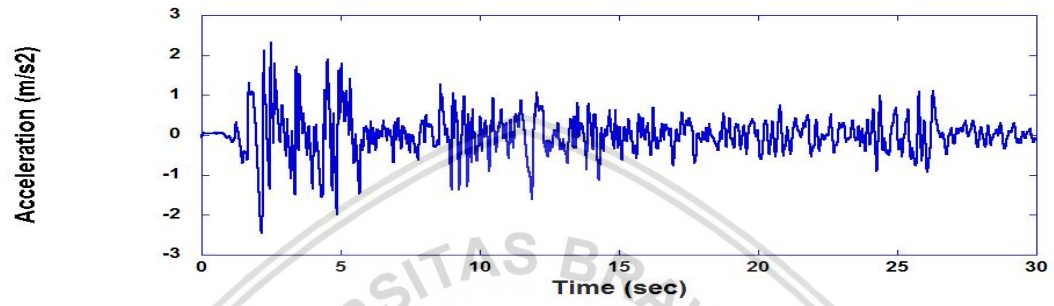
(e) JMA Kobe Ground Motion

Figure 4.1 Time History of Near-Fault Ground Motions, PGA = 250 gal



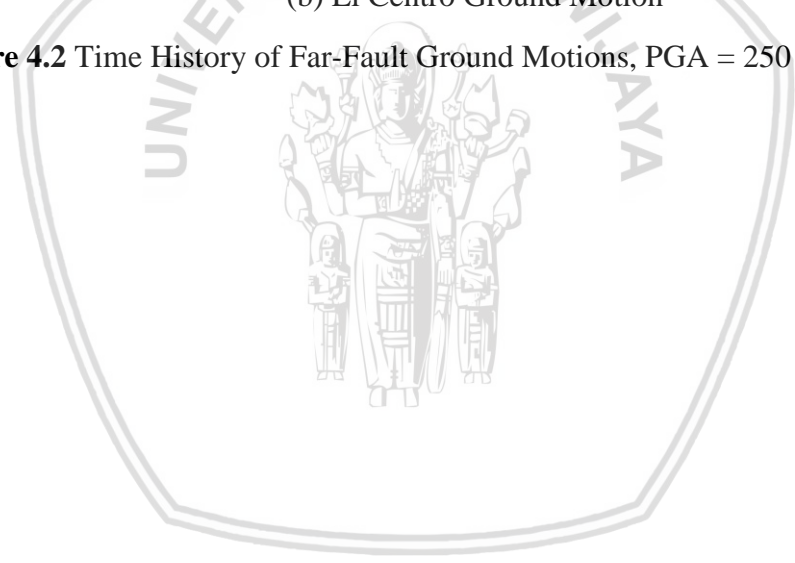


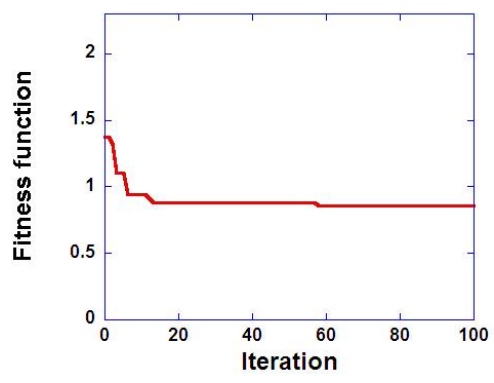
(a) Hachinohe Ground Motion



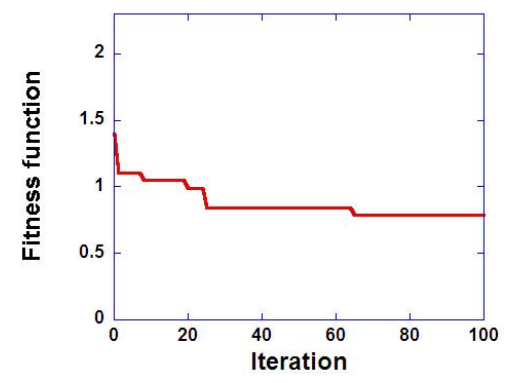
(b) El Centro Ground Motion

Figure 4.2 Time History of Far-Fault Ground Motions, PGA = 250 gal

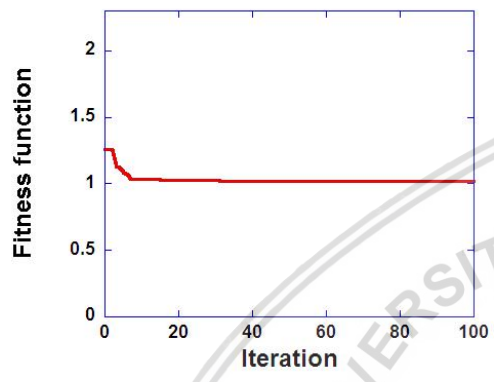




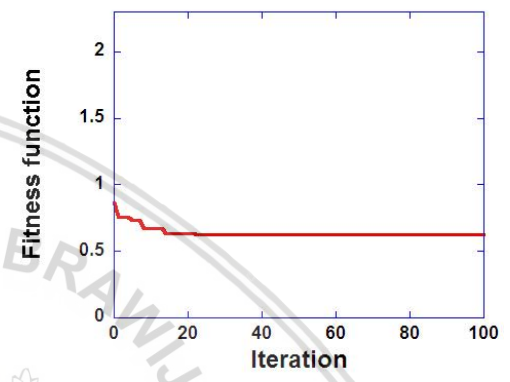
(a) Northridge Ground Motion



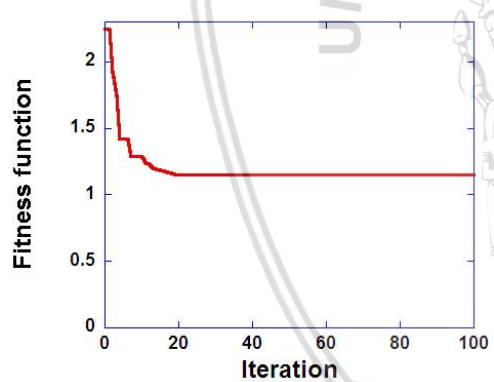
(e) Sylmar Ground Motion



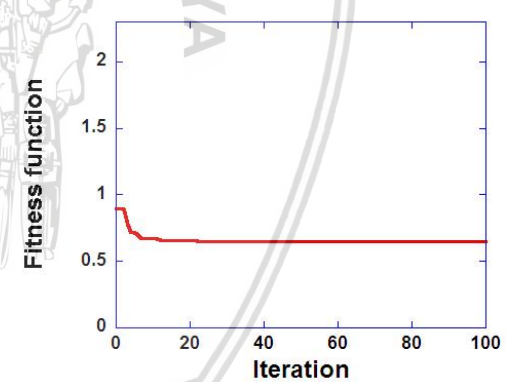
(b) Hachinohe Ground Motion



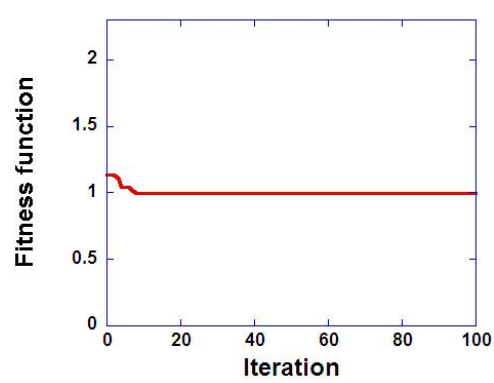
(f) JMA Kobe Ground Motion



(c) TCU086 Ground Motion



(g) El Centro Ground Motion



(d) Imperial Ground Motion

Figure 4.3 PRB Convergence Characteristics by PSO-SA

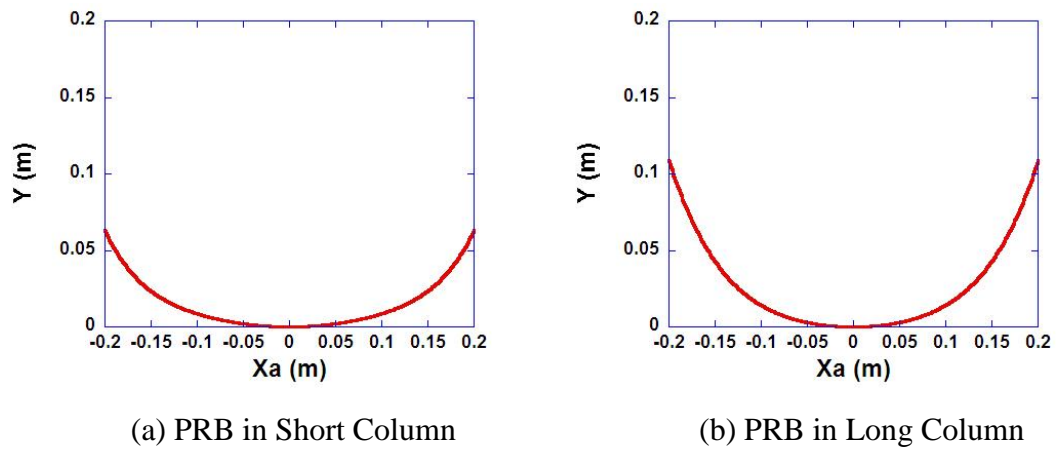


Figure 4.4 PRB Curvature by PSO-SA Subjected to Northridge Ground Motion

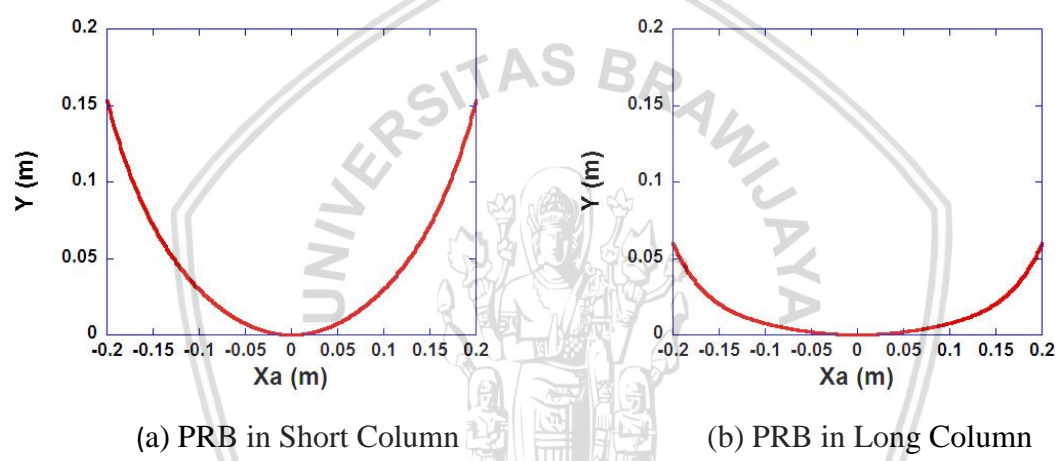


Figure 4.5 PRB Curvature by PSO-SA Subjected to Hachinohe Ground Motion

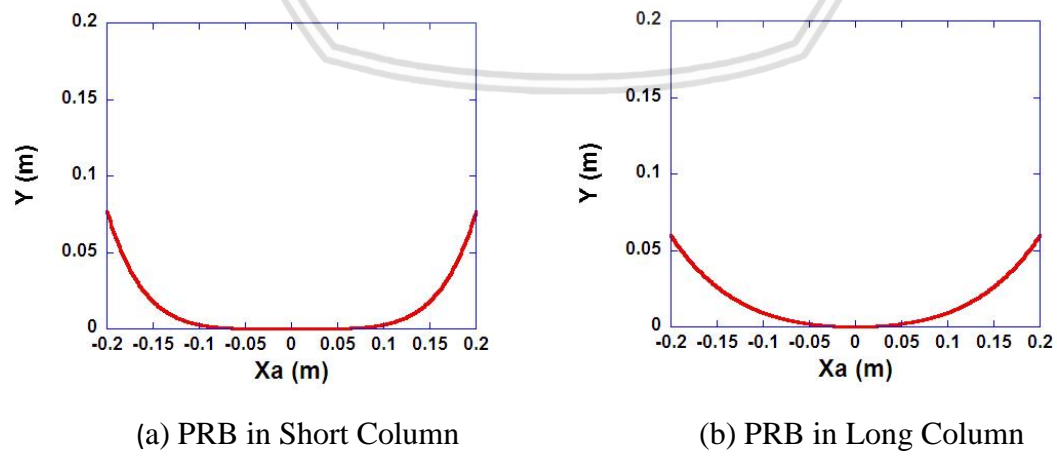
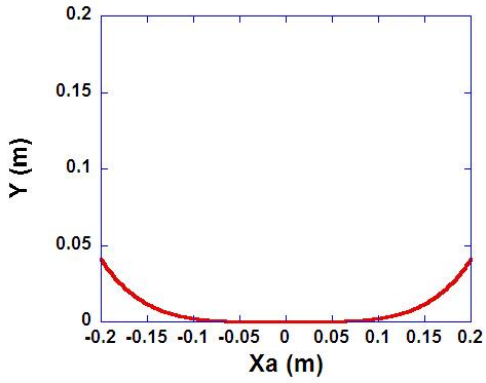
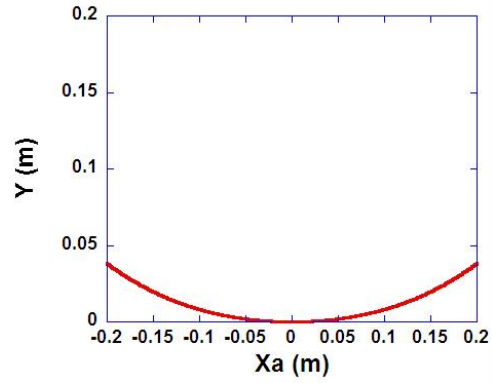


Figure 4.6 PRB Curvature by PSO-SA Subjected to TCU068 Ground Motion

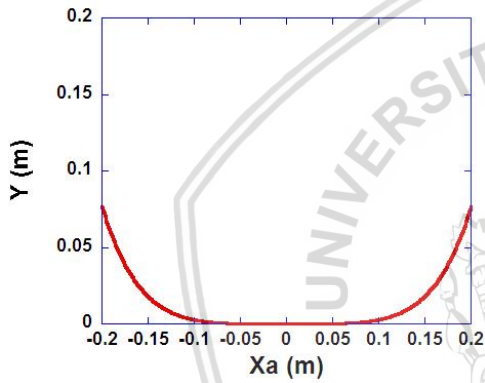


(a) PRB in Short Column

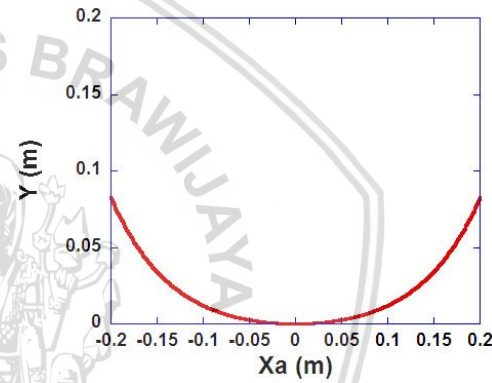


(b) PRB in Long Column

Figure 4.7 PRB Curvature by PSO-SA Subjected to Imperial Ground Motion

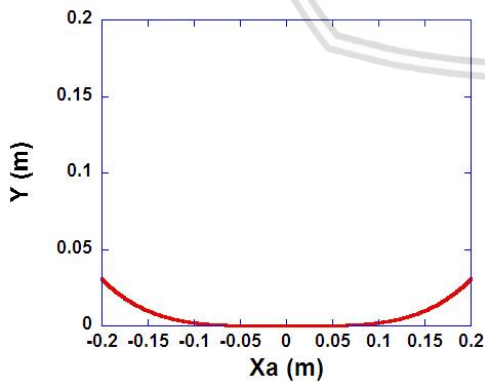


(a) PRB in Short Column

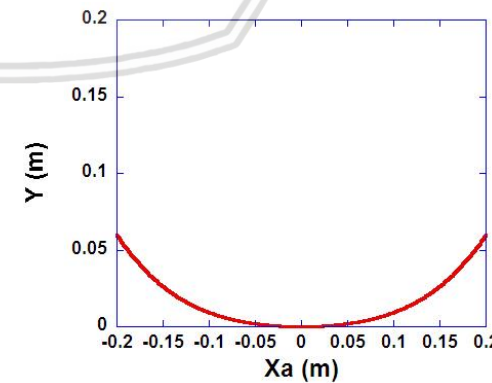


(b) PRB in Long Column

Figure 4.8 PRB Curvature by PSO-SA Subjected to Sylmar Ground Motion

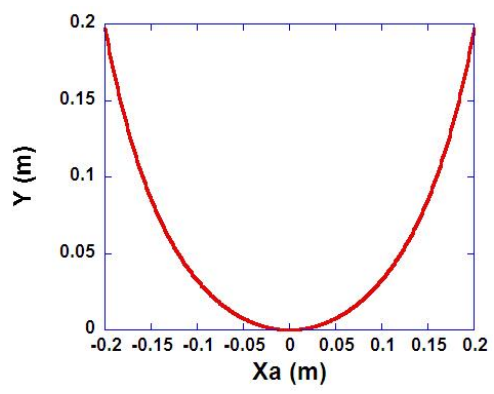


(a) PRB in Short Column

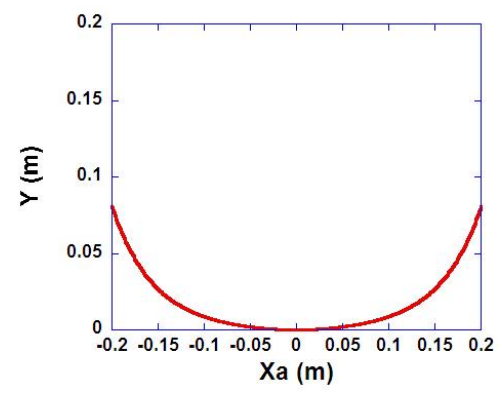


(b) PRB in Long Column

Figure 4.9 PRB Curvature by PSO-SA Subjected to JMA Kobe Ground Motion



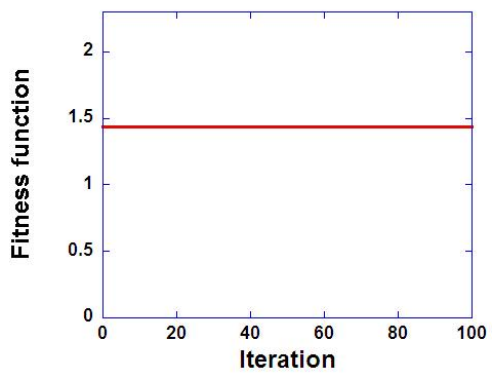
(a) PRB in Short Column



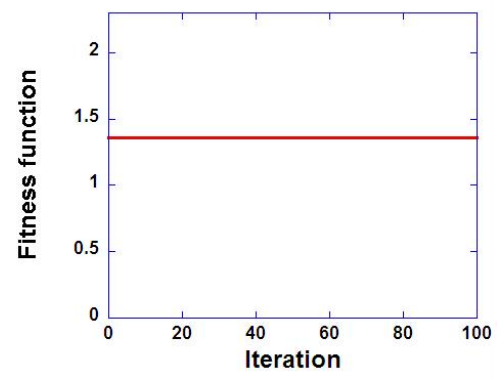
(b) PRB in Long Column

Figure 4.10 PRB Curvature by PSO-SA Subjected to El Centro Ground Motion

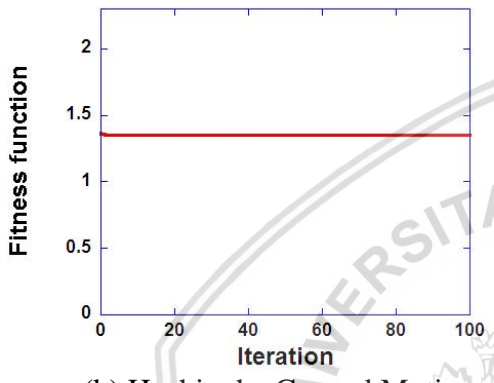




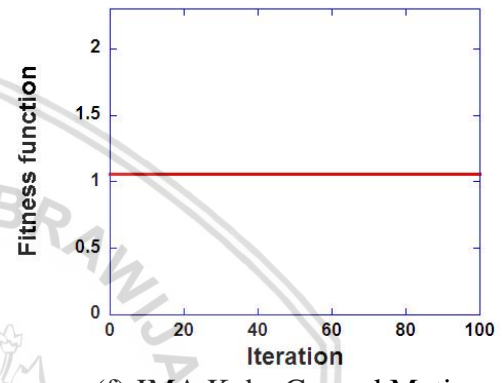
(a) Northridge Ground Motion



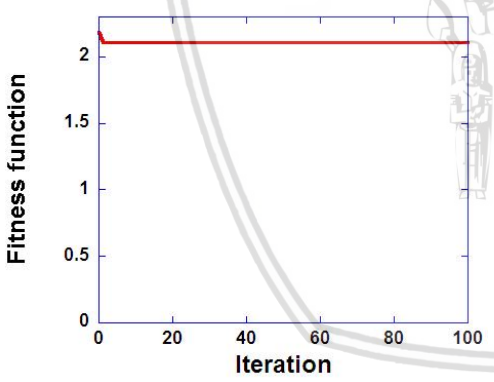
(e) Sylmar Ground Motion



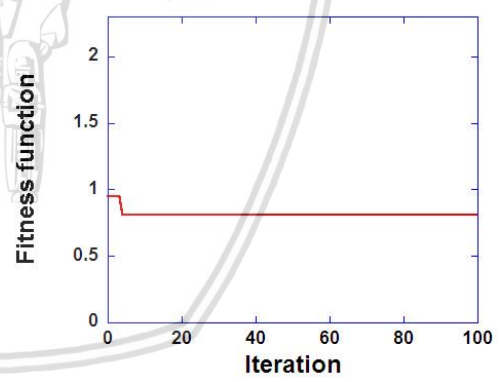
(b) Hachinohe Ground Motion



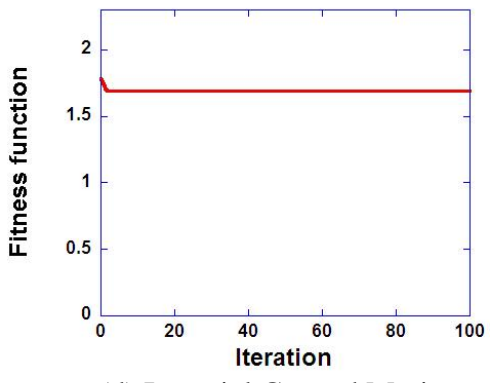
(f) JMA Kobe Ground Motion



(c) TCU068 Ground Motion



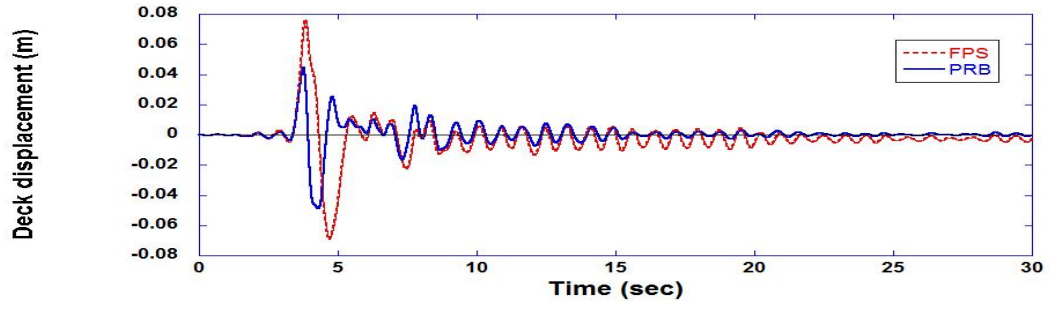
(g) El Centro Ground Motion



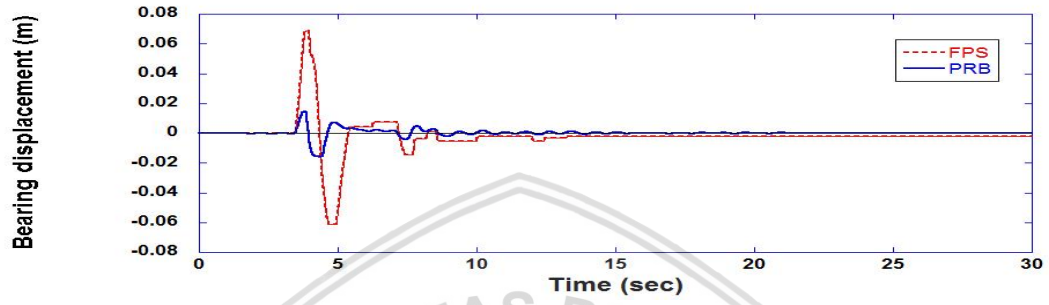
(d) Imperial Ground Motion

Figure 4.11 FPS Convergence Characteristics by PSO-SA

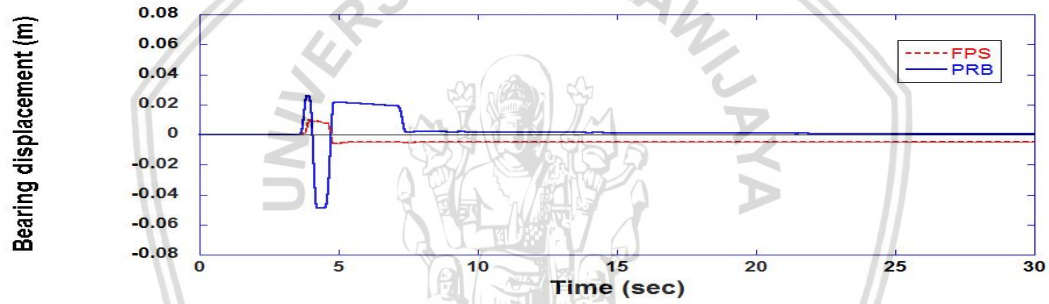




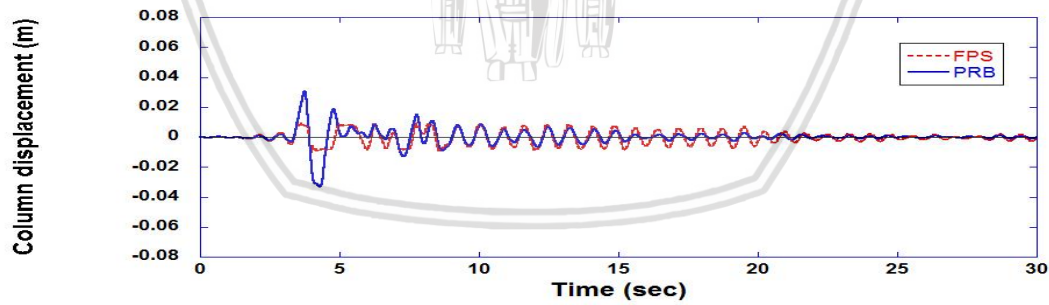
(a) Time History of Deck Displacement



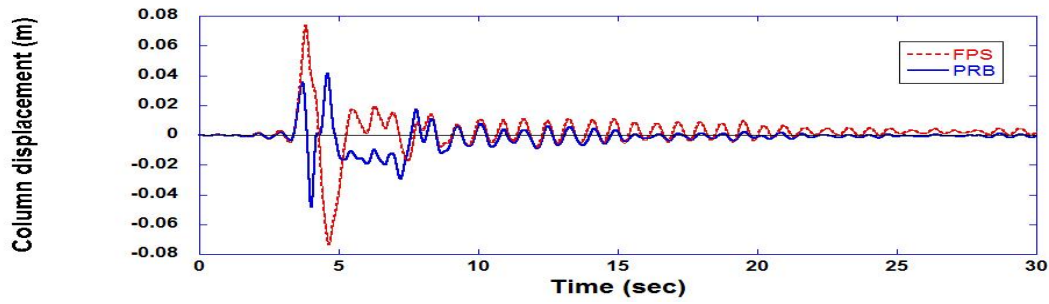
(b) Time History of Bearing Displacement in Short Column



(c) Time History of Bearing Displacement in Long Column



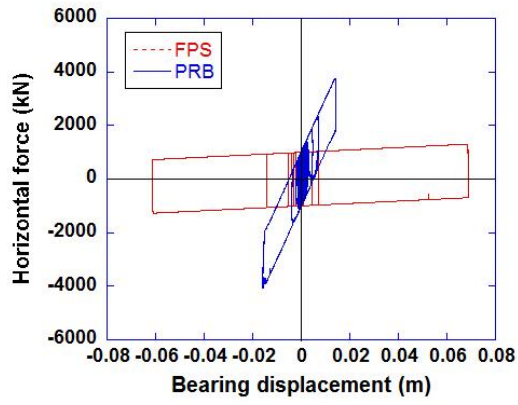
(d) Time History of Short Column Displacement



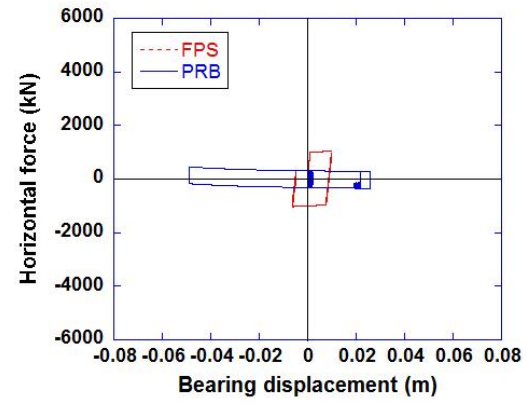
(e) Time History of Long Column Displacement

Figure 4.12 Bridge's Time History Displacement Subjected to Northridge Earthquake

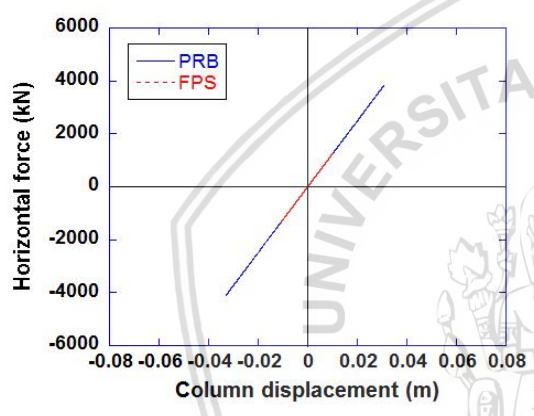




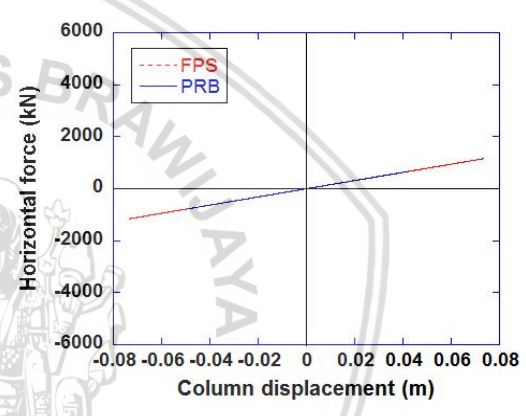
(a) Hysteretic Loop of Bearing in Short Column



(b) Hysteretic Loop of Bearing in Long Column

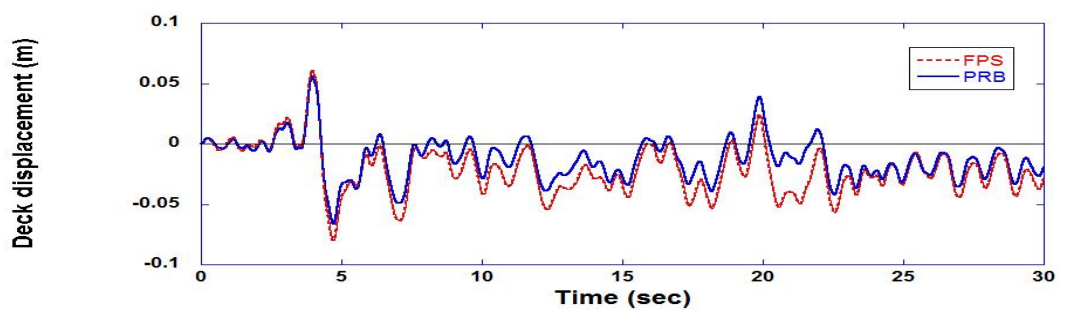


(c) Hysteretic Loop of Short Column

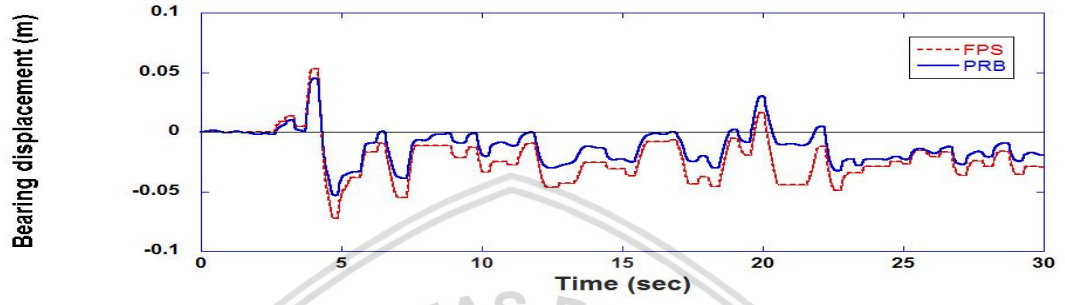


(d) Hysteretic Loop of Long Column

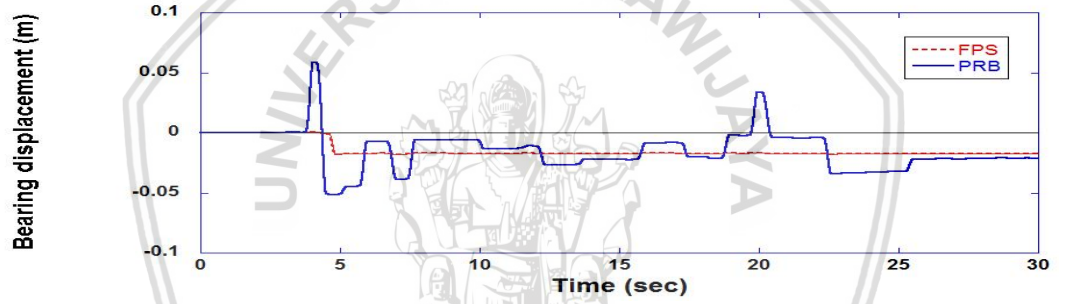
Figure 4.13 Bridge's Hysteretic Loop Subjected to Northridge Earthquake



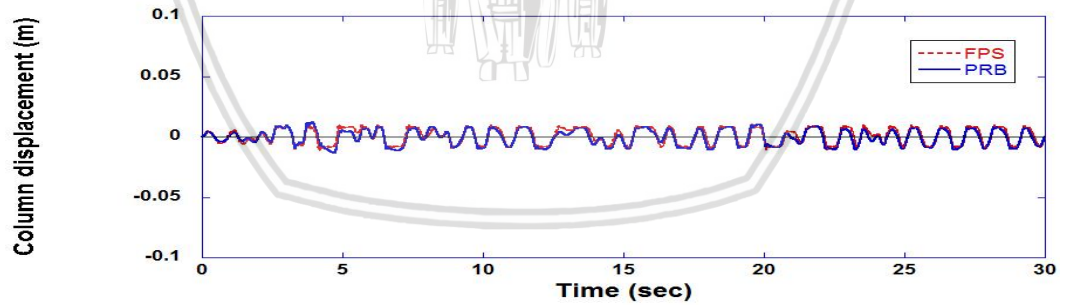
(a) Time History of Deck Displacement



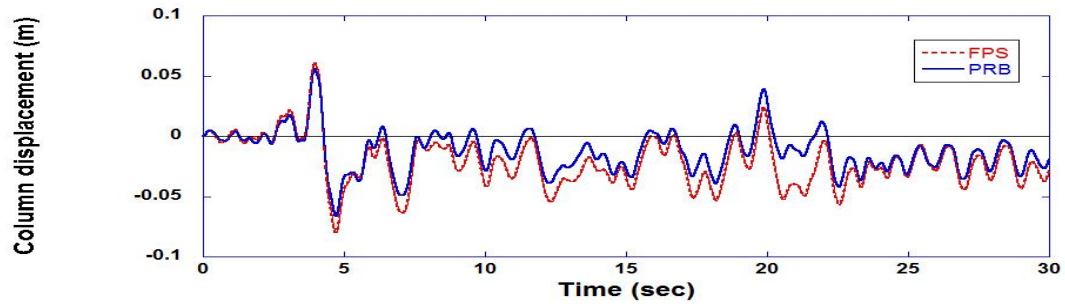
(b) Time History of Bearing Displacement in Short Column



(c) Time History of Bearing Displacement in Long Column

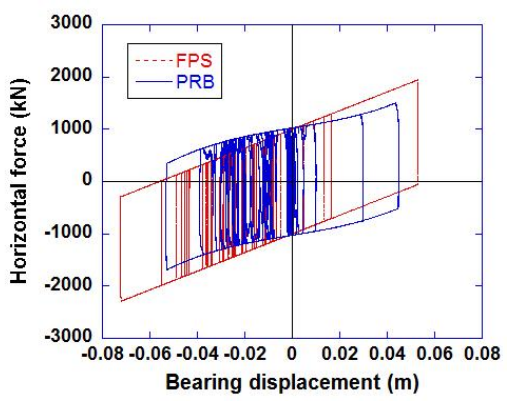


(d) Time History of Short Column Displacement

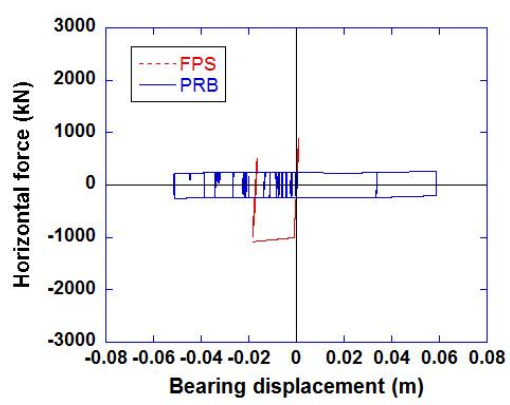


(e) Time History of Long Column Displacement

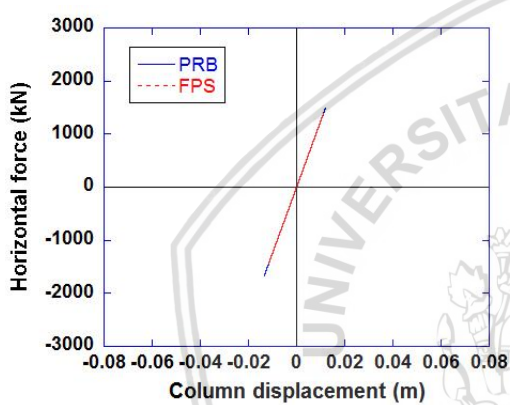
Figure 4.14 Bridge's Time History Displacement Subjected to Hachinohe Earthquake



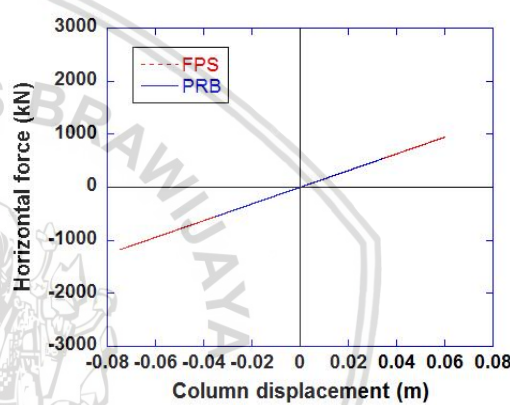
(a) Hysteretic Loop of Bearing in Short Column



(b) Hysteretic Loop of Bearing in Long Column

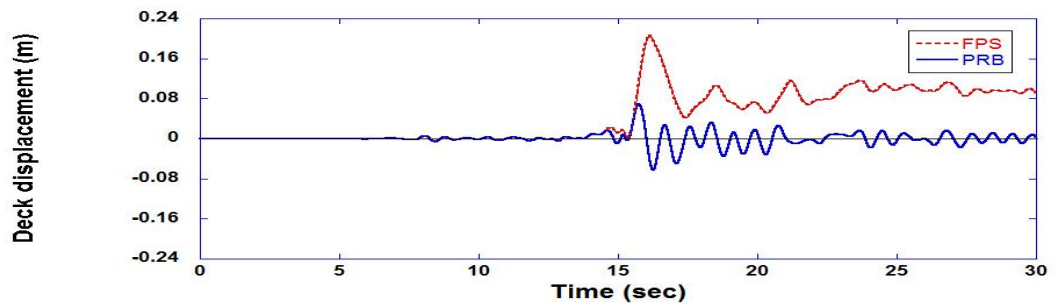


(c) Hysteretic Loop of Short Column

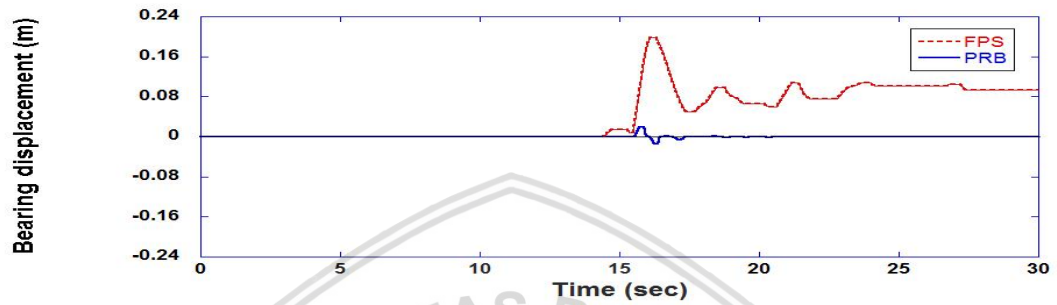


(d) Hysteretic Loop of Long Column

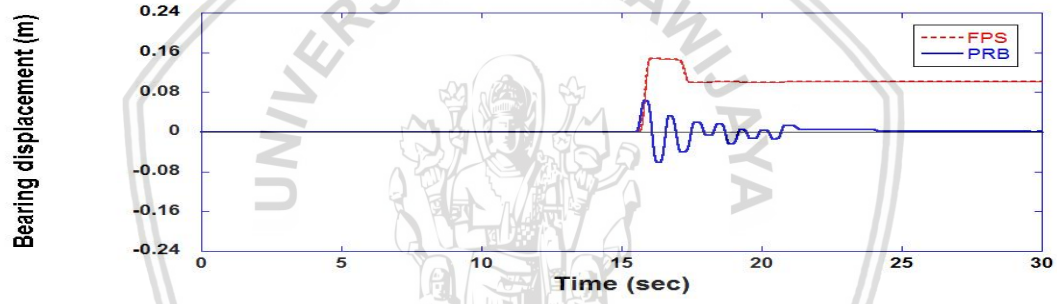
Figure 4.15 Bridge's Hysteretic Loop Subjected to Hachinohe Earthquake



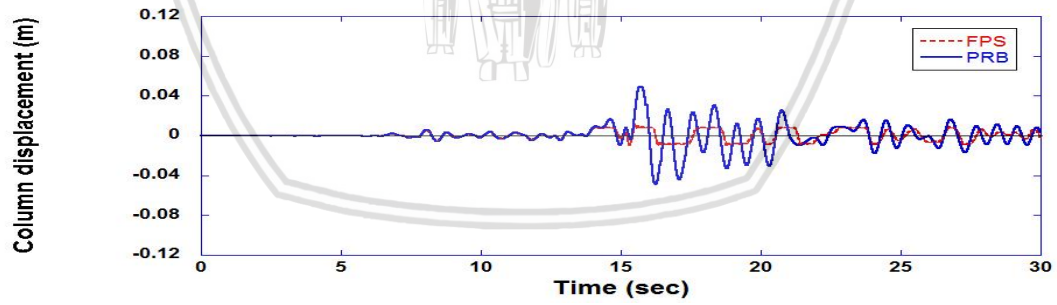
(a) Time History of Deck Displacement



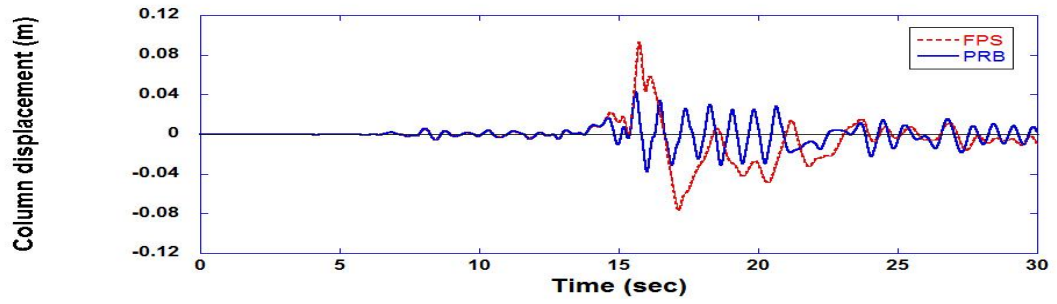
(b) Time History of Bearing Displacement in Short Column



(c) Time History of Bearing Displacement in Long Column

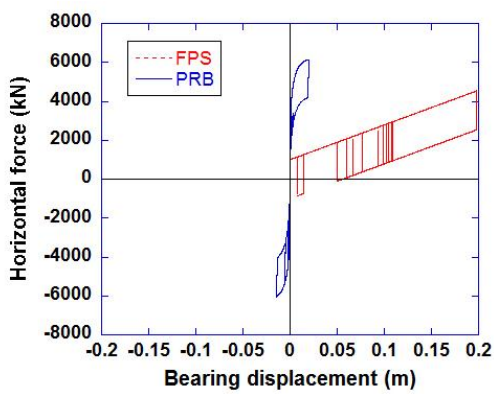


(d) Time History of Short Column Displacement

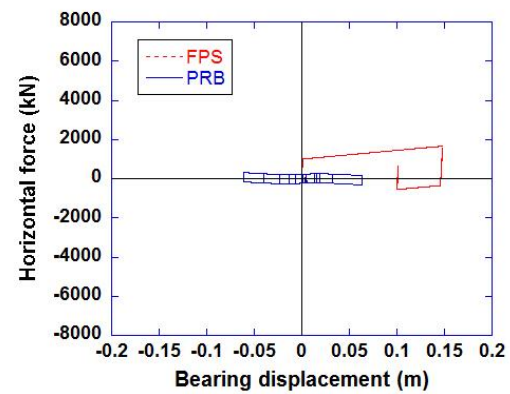


(e) Time History of Long Column Displacement

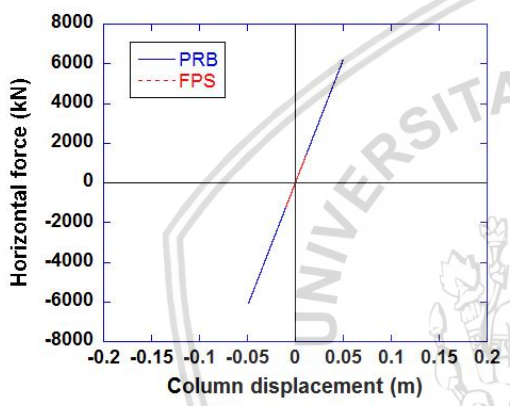
Figure 4.16 Bridge's Time History Displacement Subjected to TCU068 Earthquake



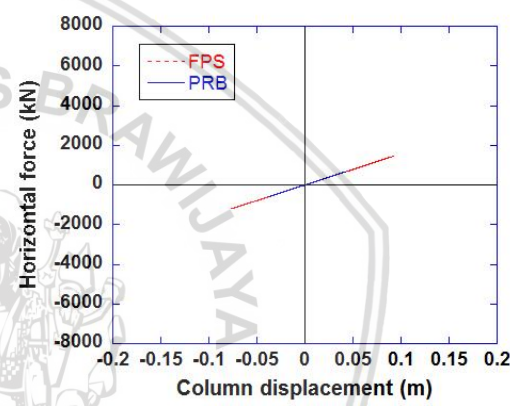
(a) Hysteretic Loop of Bearing in Short Column



(b) Hysteretic Loop of Bearing in Long Column

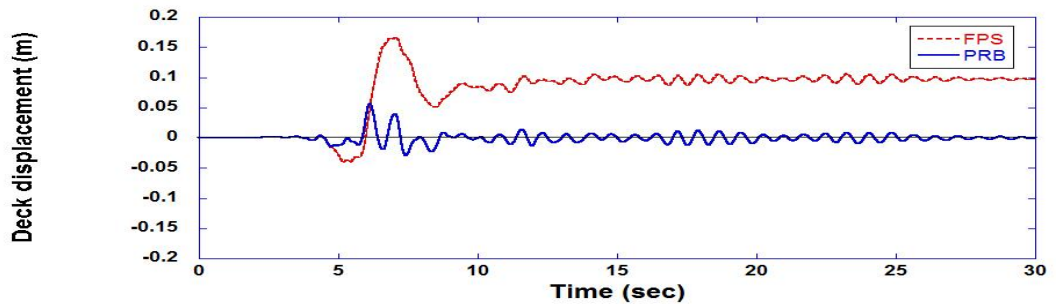


(c) Hysteretic Loop of Short Column

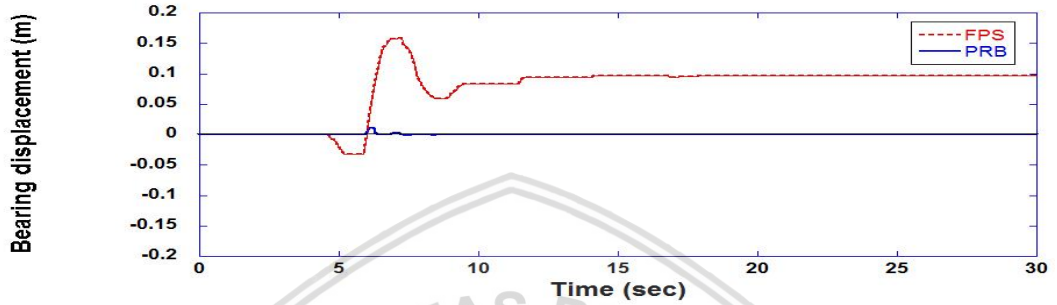


(d) Hysteretic Loop of Long Column

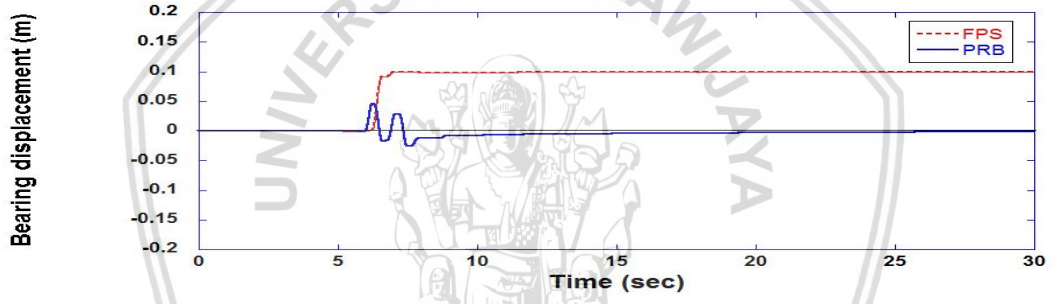
Figure 4.17 Bridge's Hysteretic Loop Subjected to TCU068 Earthquake



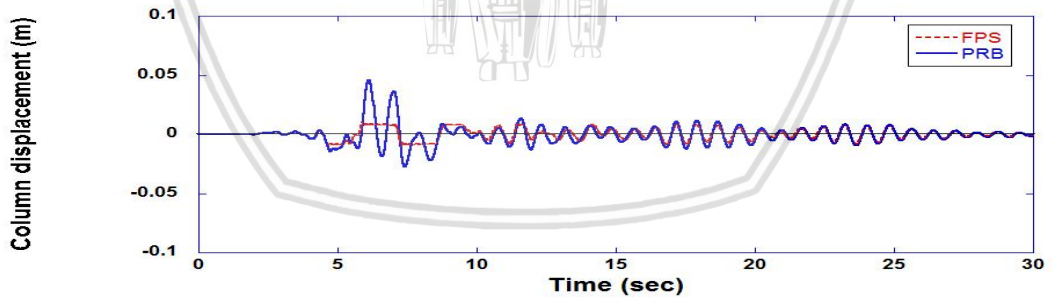
(a) Time History of Deck Displacement



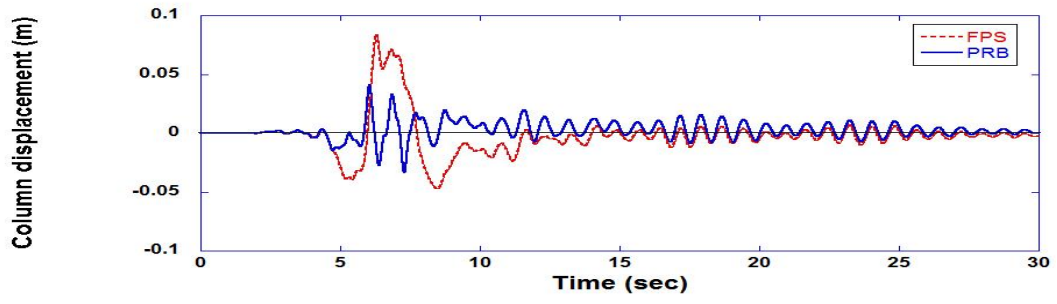
(b) Time History of Bearing Displacement in Short Column



(c) Time History of Bearing Displacement in Long Column

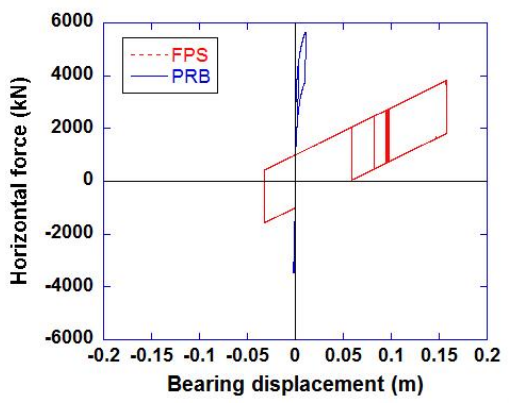


(d) Time History of Short Column Displacement

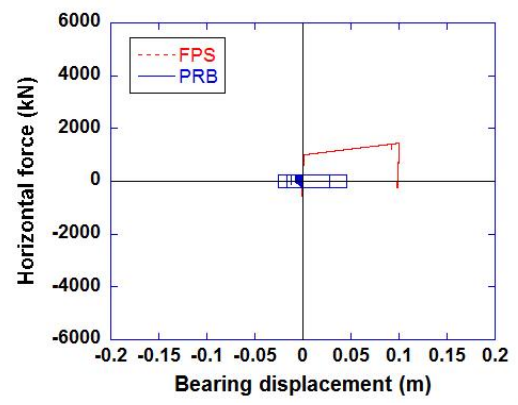


(e) Time History of Long Column Displacement

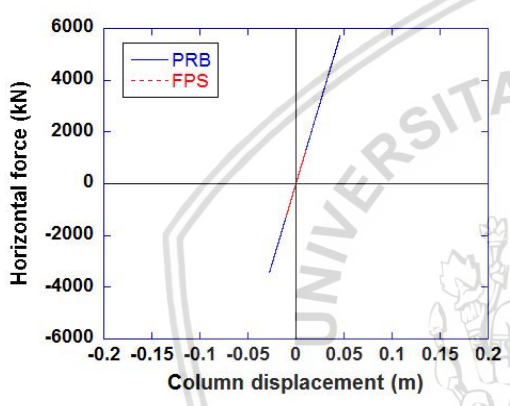
Figure 4.18 Bridge's Time History Displacement Subjected to Imperial Earthquake



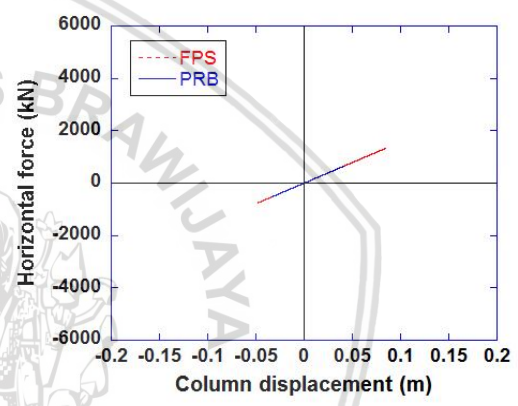
(a) Hysteretic Loop of Bearing in Short Column



(b) Hysteretic Loop of Bearing in Long Column

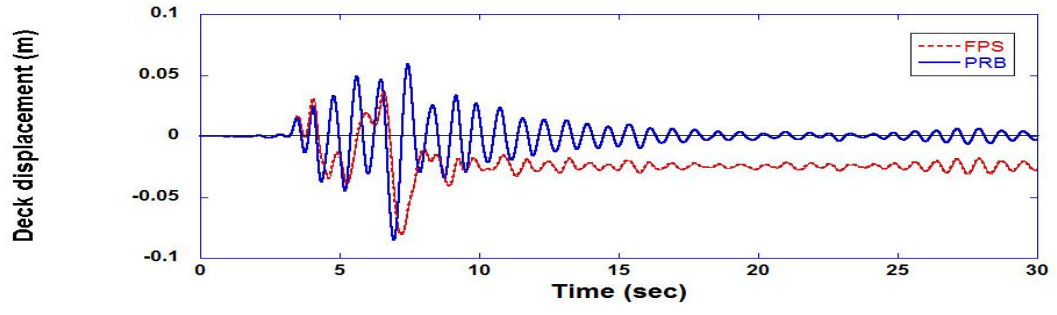


(c) Hysteretic Loop of Short Column

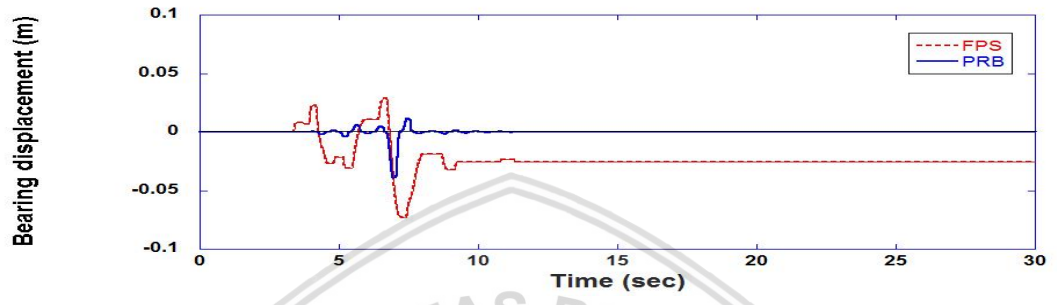


(d) Hysteretic Loop of Long Column

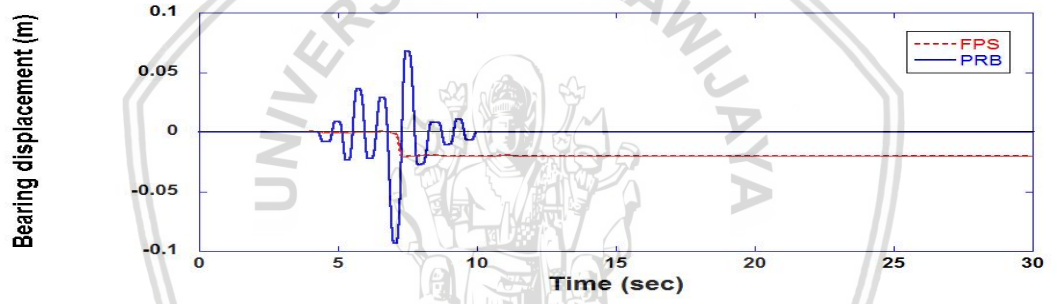
Figure 4.19 Bridge's Hysteretic Loop Subjected to Imperial Earthquake



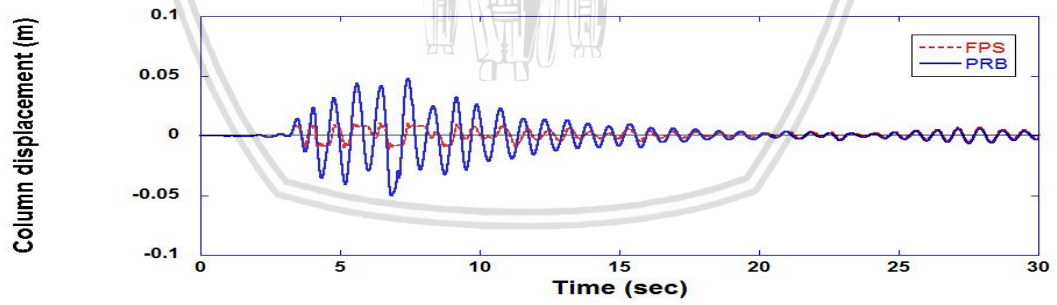
(a) Time History of Deck Displacement



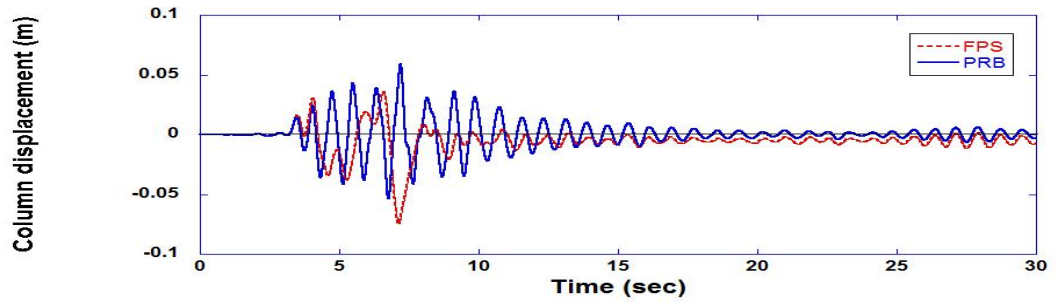
(b) Time History of Bearing Displacement in Short Column



(c) Time History of Bearing Displacement in Long Column

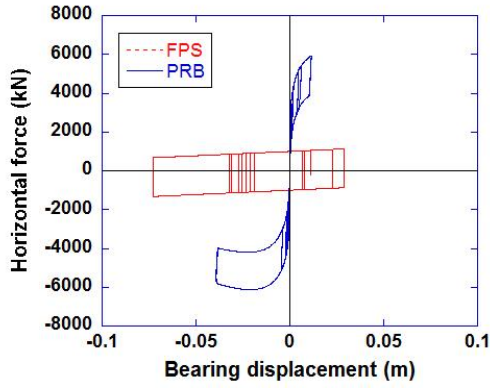


(d) Time History of Short Column Displacement

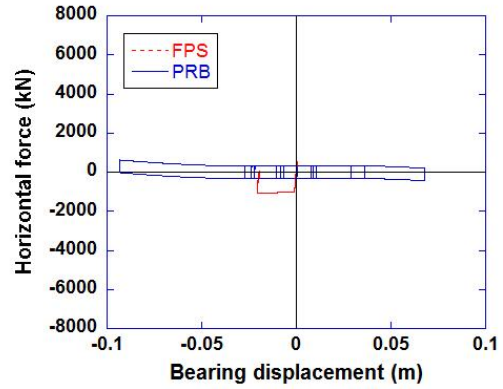


(e) Time History of Long Column Displacement

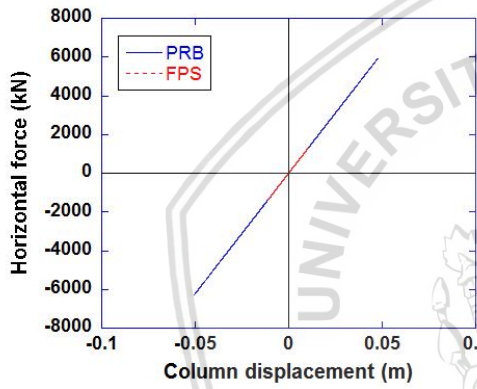
Figure 4.20 Bridge's Time History Displacement Subjected to Sylmar Earthquake



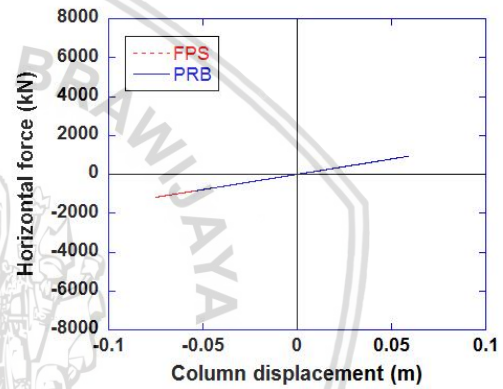
(a) Hysteretic Loop of Bearing in Short Column



(b) Hysteretic Loop of Bearing in Long Column



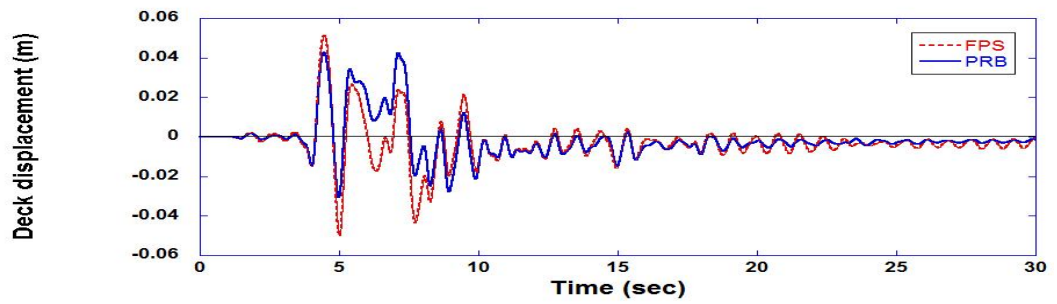
(c) Hysteretic Loop of Short Column



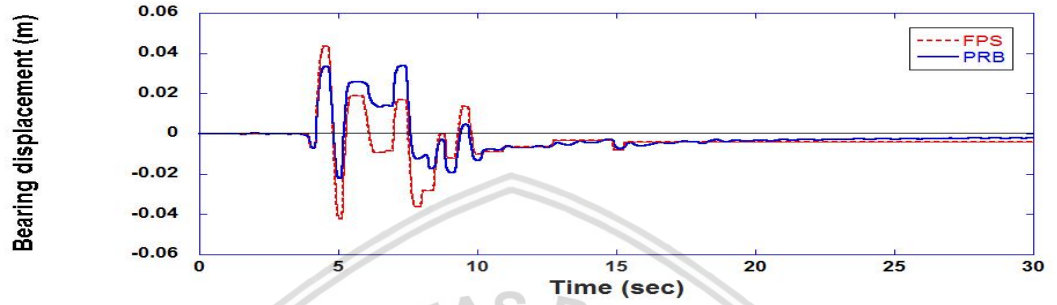
(d) Hysteretic Loop of Long Column

Figure 4.21 Bridge's Hysteretic Loop Subjected to Sylmar Earthquake

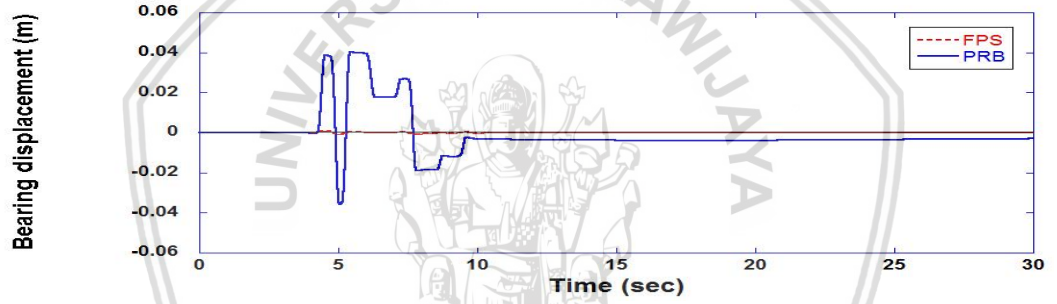




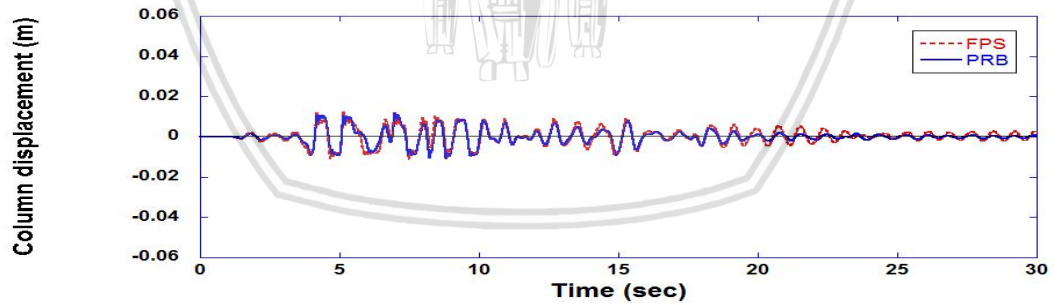
(a) Time History of Deck Displacement



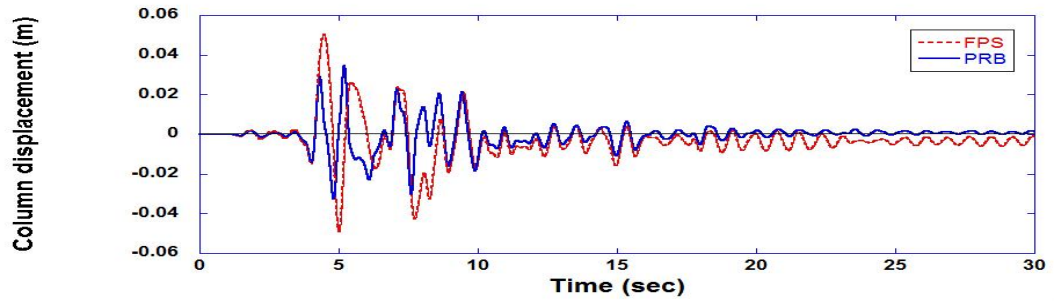
(b) Time History of Bearing Displacement in Short Column



(c) Time History of Bearing Displacement in Long Column

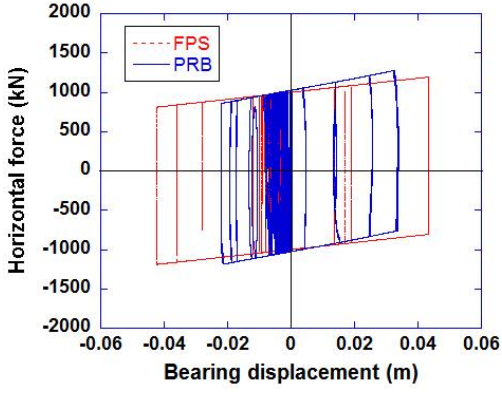


(d) Time History of Short Column Displacement

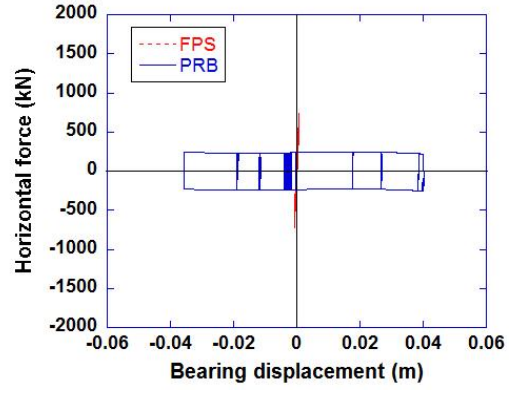


(e) Time History of Long Column Displacement

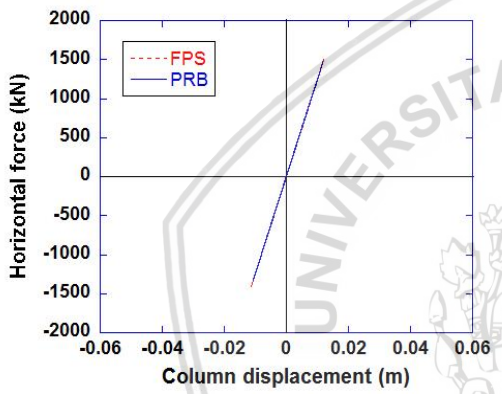
Figure 4.22 Bridge's Time History Displacement Subjected to JMA Kobe Earthquake



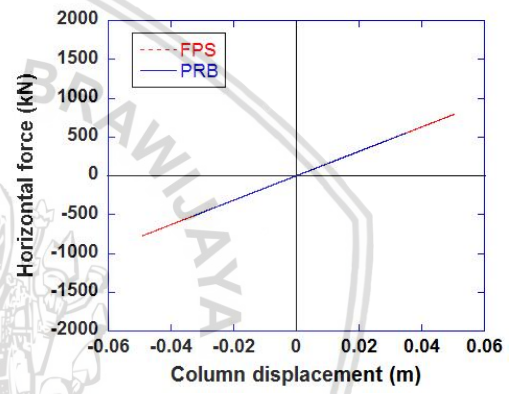
(a) Hysteretic Loop of Bearing in Short Column



(b) Hysteretic Loop of Bearing in Long Column

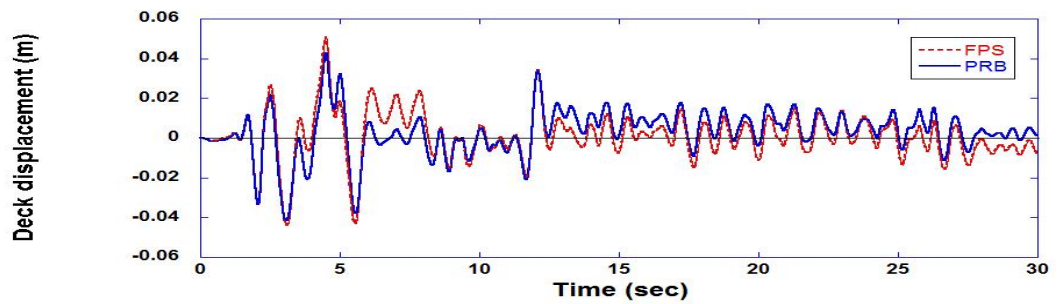


(c) Hysteretic Loop of Short Column

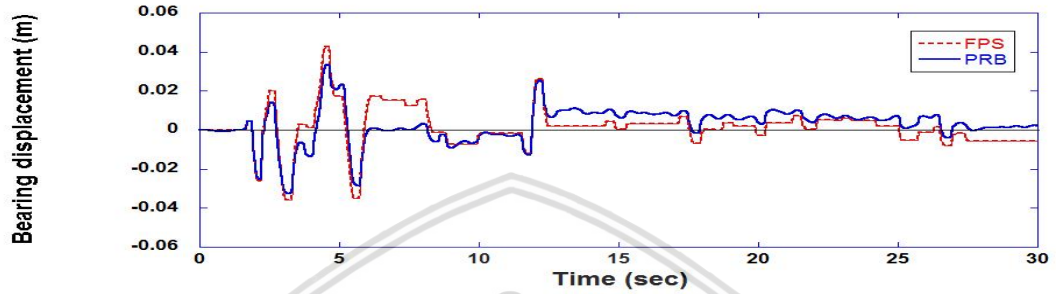


(d) Hysteretic Loop of Long Column

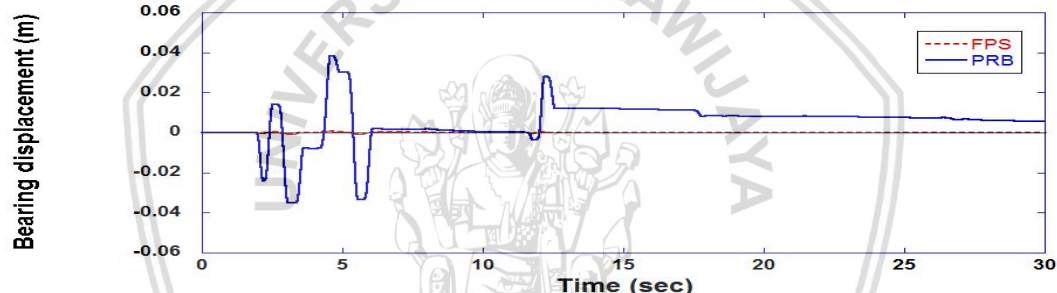
Figure 4.23 Bridge's Hysteretic Loop Subjected to JMA Kobe Earthquake



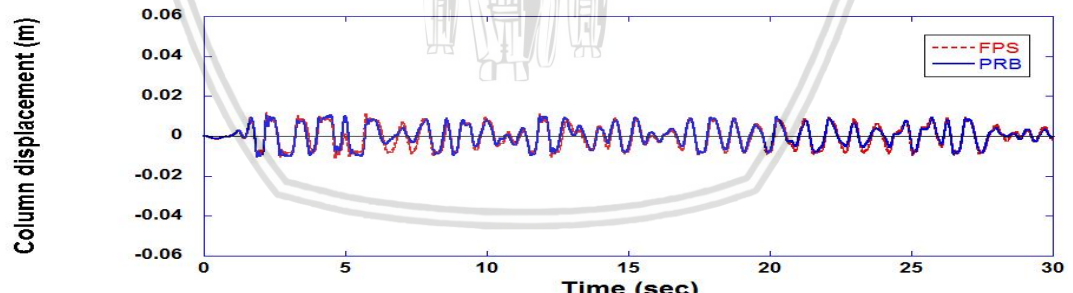
(a) Time History of Deck Displacement



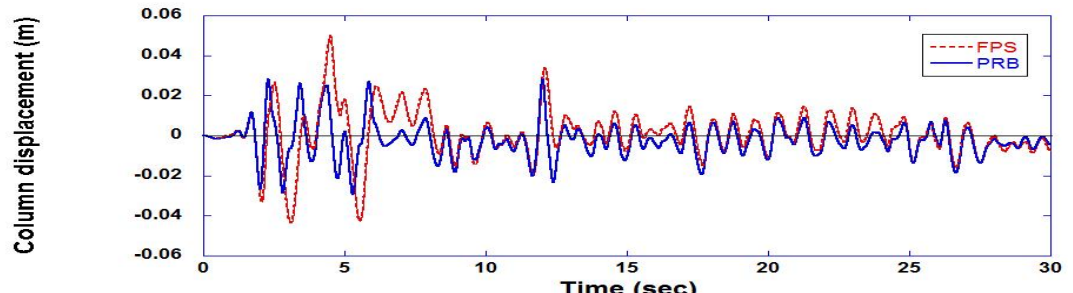
(b) Time History of Bearing Displacement in Short Column



(c) Time History of Bearing Displacement in Long Column

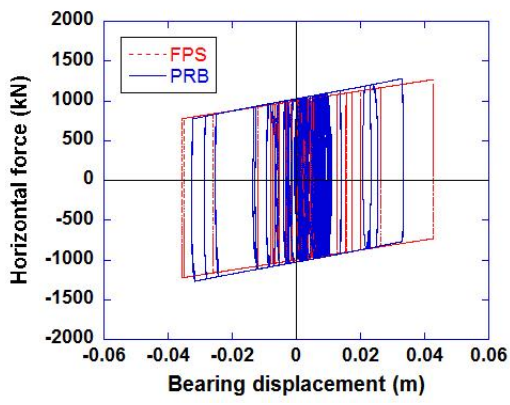


(d) Time History of Short Column Displacement

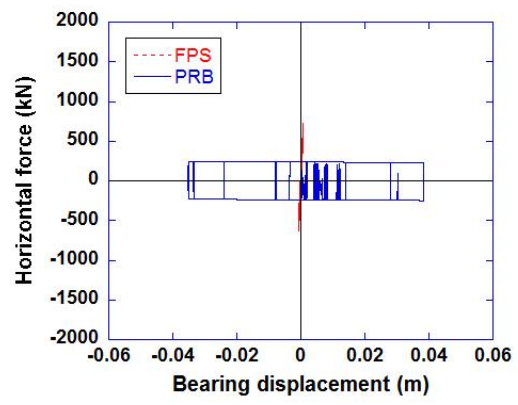


(e) Time History of Long Column Displacement

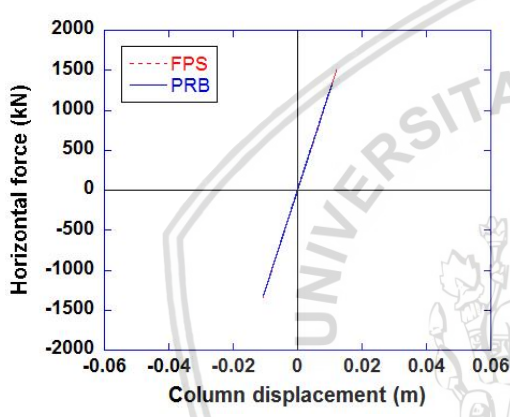
Figure 4.24 Bridge's Time History Displacement Subjected to El Centro Earthquake



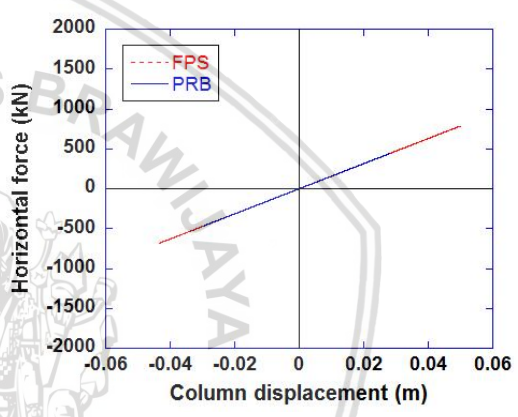
(a) Hysteretic Loop of Bearing in Short Column



(b) Hysteretic Loop of Bearing in Long Column



(c) Hysteretic Loop of Short Column



(d) Hysteretic Loop of Long Column

Figure 4.25 Bridge's Hysteretic Loop Subjected to El Centro Earthquake

CHAPTER V: CONCLUSIONS AND RECOMMENDATIONS

5.1 Conclusions

According to the previous studies, the conventional sliding bearing such as FPS has good isolation effect under far-fault earthquakes. However, under near fault earthquakes, the isolation period is highly probable to resonate so as to result excessive displacements. To overcome such a problem, the PRB which has variable isolation stiffness is used to improve the performance of irregular bridges. By properly selecting the geometry function of the rocking surface, the isolation stiffness of the PRB changes with the bearing displacement. Hence, the isolation stiffness becomes variable. This study employs a sixth-order polynomial function to define the rocking surface of the PRB.

Totally 7 ground motions are selected to simulate the dynamic behavior of irregular bridges with the PRBs. Five near-fault ground motions recorded at the 1979 Imperial Valley Earthquake in California, the 1999 Chi-Chi Earthquake in Taiwan (TCU068), the 1994 Sylmar Earthquake in California, the 1994 Northridge Earthquake in California, and the 1995 JMA Kobe Earthquake in Japan. The other two are far-fault ground motions recorded at the 1968 Tokachi Earthquake in Japan (Hachinohe) and the 1940 El Centro Earthquake in California.

The PSO-SA hybrid searching method is used to find out the optimal design parameters of the PRB and FPS. Observed from the analytical results, the PSO-SA can obtain effective isolation effect of the PRB and FPS bearing parameters. However, some structural responses are not satisfactory because in this research two different analysis for the seismic isolation system and for the bridge structure are used. Non-linear analysis is performed in the seismic isolation system while linear analysis in the bridge structure. Nevertheless, compared with the FPS, generally PRB can effectively suppress the displacement of the bridge deck under both near and far-fault earthquakes.

5.2 Recommendations

For the future research, it is suggested to consider the non-linear behavior of bridges, namely, non-linear analysis to achieve more realistic results for the structure

response. In the PSO-SA results, the limit of the PRB bearing height is up to 0.65 m. This value may have stability problem on the real structure. Actually this numerical study just wants to know the optimal parameters of the PRBs to achieve the isolation effect. So, in the real application, the PRB's height should be carefully selected.



REFERENCES

Asher, J. W., Hoskere, S. N., Ewing, R. D., Van Volkinburg, D. R., Mayes, R. L., and Button, M. (1995). Seismic performance of the base isolated USC University Hospital in the 1994 Northridge earthquake. *ASME-PUBLICATIONS-PVP*, 319, 147-154.

ATC. (1993). *Proceedings of seminar on seismic isolation, passive energy dissipation, and active control* (Report No.ATC-17-1). San Francisco, CA: Applied Technology Council.

ATC. (1994). *Guidelines and commentary for the seismic rehabilitation of buildings* (Report No. 33-02). Redwood City, CA: Applied Technology Council.

Basoz, N., and Kiremidjian, A. S. (1998). *Evaluation of bridge damage data from the Loma Prieta and Northridge, California earthquakes* (No. MCEER-98-0004).

Basoz, N. I., Kiremidjian, A. S., King, S. A., and Law, K. H. (1999). Statistical analysis of bridge damage data from the 1994 Northridge, CA, earthquake. *Earthquake Spectra*, 15(1), 25-54.

Bozorgnia, Y., Mahin, S. A., and Brady, A. G. (1998). Vertical response of twelve structures recorded during the Northridge earthquake. *Earthquake Spectra*, 14(3), 411-432.

Bruneau, M., Wilson, J. C., and Tremblay, R. (1996). Performance of steel bridges during the 1995 Hyogo-ken Nanbu (Kobe, Japan) earthquake. *Canadian Journal of Civil Engineering*, 23(3), 678-713.

Buckle, I. G., and Mayes, R. L. (1990). Seismic isolation: history, application, and performance-a world view. *Earthquake spectra*, 6(2), 161-201.

Calvi, G. M., and Pavese, A. (1997). Conceptual design of isolation systems for bridge structures. *Journal of Earthquake Engineering*, 1(01), 193-218.

Çelebi, M. (1996). Successful performance of a base-isolated hospital building during the 17 January 1994 Northridge earthquake. *The Structural Design of Tall and Special Buildings*, 5(2), 95-109.

Chen, W. F., and Duan, L. (Eds.). (2014). *Bridge engineering handbook: construction and maintenance*. CRC press.

Chen, L., Sun, L., and Nagarajaiah, S. (2015). Cable with discrete negative stiffness device and viscous damper: passive realization and general characteristics. *Smart Struct. Syst*, 15(3), 627-643.

Cheng, C. T., and Chao, C. H. (2017). Seismic behavior of rocking base-isolated structures. *Engineering Structures*, 139, 46-58.

Coburn, A., and Spence, R. (2003). *Earthquake protection*. John Wiley & Sons.

Constantinou, M. C., Soong, T. T., and Dargush, G. F. (1998). Passive energy dissipation systems for structural design and retrofit.

Corana, A., Marchesi, M., Martini, C., and Ridella, S. (1987). Minimizing multimodal functions of continuous variables with the simulated annealing algorithm. *ACM Transactions on Mathematical Software (TOMS)*, 13(3), 262-280.

Eberhart, R., and Kennedy, J. (1995). A new optimizer using particle swarm theory. *Proceedings of the Sixth International Symposium on* (pp. 39-43). IEEE.

Eberhart, R. C., and Shi, Y. (1998). Comparison between genetic algorithms and particle swarm optimization. *International conference on evolutionary programming* (pp. 611-616). Springer, Berlin, Heidelberg.

Fenz, D. M., and Constantinou, M. C. (2008). Spherical sliding isolation bearings with adaptive behavior: Theory. *Earthquake engineering & structural dynamics*, 37(2), 163-183.

Fourie, P. C., and Groenwold, A. A. (2002). The particle swarm optimization algorithm in size and shape optimization. *Structural and Multidisciplinary Optimization*, 23(4), 259-267.

Fujita, T. (1998). Seismic isolation of civil buildings in Japan. *Progress in Structural Engineering and Materials*, 1(3), 295-300.

Ghobarah, A., and Ali, H. M. (1988). Seismic performance of highway bridges. *Engineering Structures*, 10(3), 157-166.

Heydari, M., and Mousavi, M. (2015). The comparison of seismic effects of near-field and far-field earthquakes on relative displacement of seven-storey concrete building with shear wall. *Current World Environment*, 10(1), 0-46.

Jangid, R. S., and Kelly, J. M. (2001). Base isolation for near-fault motions. *Earthquake engineering & structural dynamics*, 30(5), 691-707.

Japan Road Association. (1996). Design Specifications of Highway Bridges, Part V Seismic Design, Maruze, Tokyo.

Juang, D. S. and Chuang, W.S. (2007). "A PSO-SA hybrid searching algorithm for least weight design of structures (in Chinese)." 31th National Conference on Theoretical and Applied Mechanics, ISU, Kaohsiung, Taiwan.

Kawashima, K., and Unjoh, S. (1989). Development of hybrid control technology. *Civil Engineering Journal*, 32(6), 2-5.

Kawashima, K., Hasegawa, K., Unjoh, S., and Nagashima, H. (1991). Current research efforts in Japan for passive and active control of highway bridges against earthquake. In *PROCEEDINGS OF THE 23RD JOINT MEETING OF THE US-JAPAN COOPERATIVE PROGRAM IN NATURAL RESOURCES PANEL ON WIND AND SEISMIC EFFECTS*.

Kawashima, K., Unjoh, S. and Shimizu, H. (1992a). "Experiments on Dynamic Characteristics of Variable Damper." *Proc. Japan National Symposium on Structural Response Control*, Japan, 121-128.

Kawashima, K., Unjoh, S. and Shimizu, H. (1992b). "Experiments on Dynamic Characteristics of Variable Damper." *Proc. Japan National Symposium on Structural Response Control*, Japan, 311-317.

Kawashima, K. (2002). Damage of bridges resulting from fault rupture in the 1999 Kocaeli and Duzce, Turkey earthquakes and the 1999 Chi-Chi, Taiwan earthquake. *Structural Engineering/Earthquake Engineering*, 19(2), 179s-197s.

Kelly, J. M. (1986). Aseismic base isolation: review and bibliography. *Soil Dynamics and Earthquake Engineering*, 5(4), 202-216.

Kelly, J. M. (1998). Seismic isolation of civil buildings in the USA. *Progress in Structural Engineering and Materials*, 1(3), 279-285.

Kennedy, J. and Eberhart, R.C. (1995). "Particle swarm optimization". *Proceedings of IEEE International Conference on Neural Networks*, Perth, Australia, vol. 4, 1942-1948.

Kennedy, J., and Eberhart, R. C. (2001). *Swarm Intelligence*, Morgan Kaufmann.

Kirkpatrick, S., Gelatt, C. D., and Vecchi, M. P. (1983). Optimization by simulated annealing. *Science*, 220(4598), 671-680.

Koh, C. G., and Kelly, J. M. (1988). A simple mechanical model for elastomeric bearings used in base isolation. *International journal of mechanical sciences*, 30(12), 933-943.

Kosa, K., Tazaki, K., and Yamaguchi, E. (2002). Mechanism of damage to Shiwei Bridge caused by 1999 Chi-Chi earthquake. *Structural Engineering/Earthquake Engineering*, 19(2), 221s-226s.

Lee, G. C., and Loh, C. H. (1999). Preliminary report from MCEER-NCREE workshop on the 921 Taiwan earthquake. *Multidisciplinary Center for Earthquake Engineering Research*.

Liao, W. I., Loh, C. H., and Wan, S. (2000). Responses of isolated bridges subjected to near-fault ground motions recorded in Chi-Chi earthquake. *International Workshop on Annual Commemoration of Chi-Chi Earthquake, Sep* (pp. 18-20).

Lu, L. Y., Shih, M. H., Tzeng, S. W., and Chang Chien, C. S. (2003). Experiment of a sliding isolated structure subjected to near-fault ground motion. In *Proceedings of the 7th pacific conference on earthquake engineering* (pp. 13-15).

Lu, L. Y., Shih, M. H., and Wu, C. Y. (2004). Near-fault seismic isolation using sliding bearings with variable curvatures. *Proceedings of the 13th World Conference on Earthquake Engineering* (No. 3264).

Lu, L. Y., Chung, L. L., Wu, L. Y., and Lin, G. L. (2006). Dynamic analysis of structures with friction devices using discrete-time state-space formulation. *Computers & structures*, 84(15), 1049-1071.

Lu, L. Y., Wang, J., and Yeh, S. W. (2007). Experimental verification of polynomial friction pendulum isolator for near-fault seismic isolation. *Proceedings of the 4th International Structural Engineering and Construction Conference (ISEC-4)*.

Lu, L. Y., Lin, G. L., and Kuo, T. C. (2008). Stiffness controllable isolation system for near-fault seismic isolation. *Engineering Structures*, 30(3), 747-765.

Lu, L. Y., Lee, T. Y., Yeh, I. L., and Chang, H. (2010). Rocking bearings with variable frequency for near-fault seismic isolation. *Journal of the Chinese Institute of Civil and Hydraulic Engineering*, 22(3), 283-298.

Lu, L. Y., Lee, T. Y., and Yeh, S. W. (2011). Theory and experimental study for sliding isolators with variable curvature. *Earthquake Engineering & Structural Dynamics*, 40(14), 1609-1627.

Lu, L. Y., and Hsu, C. C. (2013). Experimental study of variable-frequency rocking bearings for near-fault seismic isolation. *Engineering structures*, 46, 116-129.

Lu, L. Y., Lee, T. Y., Juang, S. Y., and Yeh, S. W. (2013). Polynomial friction pendulum isolators (PFPIs) for building floor isolation: An experimental and theoretical study. *Engineering Structures*, 56, 970-982.

Martelli, A., and Forni, M. (1998). Seismic isolation of civil buildings in Europe. *Progress in structural engineering and materials*, 1(3), 286-294.

Matsagar, V. A., and Jangid, R. S. (2006). Seismic response of simply supported base-isolated bridge with different isolators. *International Journal of Applied Science and Engineering*, 4(1), 53-69.

MATLAB (2000). The Math Works, Inc., Massachusetts, USA.

Otsuka, H. (1997). Report on the Disaster Caused by the 1995 Hyogoken Nanbu Earthquake, Chapter 5, Damage to Highway Bridges. *Journal of Research*.

Naeim, F., and Kelly, J. M. (1999). *Design of seismic isolated structures: from theory to practice*. John Wiley & Sons.

Poli, Riccardo, James Kennedy, and Tim Blackwell. "Particle swarm optimization." *Swarm intelligence* 1.1 (2007): 33-57.

Pranesh, M., and Sinha, R. (2000). VFPI: an isolation device for aseismic design. *Earthquake engineering & structural dynamics*, 29(5), 603-627.

Priestley, M. N., Seible, F., and Calvi, G. M. (1996). *Seismic design and retrofit of bridges*. John Wiley & Sons.

Rådeström, S., Ü lker-Kaustell, M., Andersson, A., Tell, V., and Karoumi, R. (2017). Application of fluid viscous dampers to mitigate vibrations of high-speed railway bridges. *International Journal of Rail Transportation*, 5(1), 47-62.

Roberts, J. E. (2005). Caltrans structural control for bridges in high-seismic zones. *Earthquake engineering & structural dynamics*, 34(4- 5), 449-470.

Robinson, W., and Greenbank, L. (1976). An extrusion energy absorber suitable for the protection of structures during an earthquake. *Earthquake Engineering & Structural Dynamics*, 4(3), 251-259.

Shi, Y., and Eberhart, R. C. (1998a). Parameter selection in particle swarm optimization. In *International conference on evolutionary programming* (pp. 591-600). Springer, Berlin, Heidelberg.

Shi, Y., and Eberhart, R. (1998b). A modified particle swarm optimizer. In *Evolutionary Computation Proceedings, 1998. IEEE World Congress on Computational Intelligence. The 1998 IEEE International Conference on* (pp. 69-73). IEEE.

Shi, X., Zhu, S., Li, J. Y., and Spencer Jr, B. F. (2016). Dynamic behavior of stay cables with passive negative stiffness dampers. *Smart Materials and Structures*, 25(7), 075044.

Soong, T. T. and Constantinou, M. C. (1994). *Passive and Active Structural Control in Civil Engineering*, Springer: Vienna, New York

Symans, M. D., and Constantinou, M. C. (1999). Semi-active control systems for seismic protection of structures: a state-of-the-art review. *Engineering structures*, 21(6), 469-487.

Taflanidis, A. A. (2011). Optimal probabilistic design of seismic dampers for the protection of isolated bridges against near-fault seismic excitations. *Engineering structures*, 33(12), 3496-3508.

Vaurigaud, B., Manevitch, L. I., and Lamarque, C. H. (2011). Passive control of aeroelastic instability in a long span bridge model prone to coupled flutter using targeted energy transfer. *Journal of Sound and Vibration*, 330(11), 2580-2595.

Wang, Y. P., Chung, L. L., and Liao, W. H. (1998). Seismic response analysis of bridges isolated with friction pendulum bearings. *Earthquake Engineering & Structural Dynamics*, 27(10), 1069-1093.

Zhang, S., and Wang, G. (2013). Effects of near-fault and far-fault ground motions on nonlinear dynamic response and seismic damage of concrete gravity dams. *Soil Dynamics and Earthquake Engineering*, 53, 217-229.



APPENDIX A

This appendix derives the relationship between two coordinates (fixed coordinate and moving coordinate) of the PRB in second chapter. As shown in figure 2.3, it has two different coordinates, fixed coordinate and moving coordinate. $x-y$ is the fixed coordinate with the x -axis attached to the ground, while $X-Y$ is the moving coordinate that is attached to the bearing, with the Y -axis being the symmetric axis of the bearing. The $X-Y$ coordinate will rock along with the bearing. When the bearing is in its neutral position, the origins of the two coordinate systems will coincide with each other. Because it has two different coordinates, so it needs the transformation equation to make this two coordinates connect each other. Thus, as shown in Figure A.1, (\vec{i}, \vec{j}) is the unit vector of the fixed coordinate $x-y$; (\vec{i}', \vec{j}') is the unit vector for the moving coordinate $X-Y$. The relationship between this two unit vectors are:

$$\begin{cases} \vec{i} = \cos\theta_a \vec{i}' + \sin\theta_a \vec{j}' \\ \vec{j} = -\sin\theta_a \vec{i}' + \cos\theta_a \vec{j}' \end{cases} \quad (\text{A.1})$$

$$\begin{cases} \vec{i}' = \cos\theta_a \vec{i} - \sin\theta_a \vec{j} \\ \vec{j}' = \sin\theta_a \vec{i} + \cos\theta_a \vec{j} \end{cases} \quad (\text{A.2})$$

As shown in Figure A.1, o and C are the origin points of the fixed coordinate and moving coordinate, respectively. P is any point on the hypothetical plane. The relative vector between o and C is as follows:

$$\vec{r}_{oC} = x_C \vec{i} + y_C \vec{j} \quad (\text{A.3})$$

Equation (A.3) also can be expressed as:

$$\vec{r}_{Co} = X_o \vec{i}' + Y_o \vec{j}' = -\vec{r}_{oC} \quad (\text{A.4})$$

Assuming P is any point on the plane, P is described by moving coordinate system $X-Y$ can be written as:

$$\vec{r}_{CP} = X_P \vec{i}' + Y_P \vec{j}' \quad (\text{A.5})$$

If the equation (A.5) is described by fixed coordinate $x-y$, so it can be written as:

$$\vec{r}_{oP} = x_P \vec{i} + y_P \vec{j} \quad (\text{A.6})$$

So, it can be directly as:

$$\vec{r}_{oP} = \vec{r}_{oC} + \vec{r}_{CP} \quad (\text{A.7})$$

Or in another form:

$$\vec{r}_{CP} = \vec{r}_{oP} - \vec{r}_{oC} = \vec{r}_{oP} + \vec{r}_{Co} \quad (\text{A.8})$$

Substituting equations (A.4), (A.5) and (A.6) into equation (A.8):

$$X_P \vec{i}' + Y_P \vec{j}' = (x_P \vec{i} + y_P \vec{j}) + (X_o \vec{i}' + Y_o \vec{j}') \quad (\text{A.9})$$

Substituting equation (A.2) into equation (A.9):

$$X_P \vec{i}' + Y_P \vec{j}' = (x_P (\cos\theta_a \vec{i}' + \sin\theta_a \vec{j}') + y_P (-\sin\theta_a \vec{i}' + \cos\theta_a \vec{j}')) + (X_o \vec{i}' + Y_o \vec{j}') \quad (\text{A.10})$$

Separate the vectors:

$$\begin{cases} X_P = x_P \cos\theta_a - y_P \sin\theta_a + X_o \\ Y_P = x_P \sin\theta_a + y_P \cos\theta_a + Y_o \end{cases} \quad (\text{A.11})$$

As shown in Figure 2.3, PRB has two kinds of coordinates, the fixed coordinate and moving coordinate for the contact surface A, respectively.

$$\begin{cases} \text{Fixed coordinate} = (x_a, y_a) \\ \text{Moving coordinate} = (X_a, Y_a) \\ \text{Fixed coordinate} = (x_b, y_b) \\ \text{Moving coordinate} = (X_b, Y_b) \end{cases} \quad (\text{A.12})$$

Using the equation (A.11) to describe the coordinate in (A.12):

$$\begin{cases} X_a = x_a \cos\theta_a - y_a \sin\theta_a + X_o \\ Y_a = x_a \sin\theta_a + y_a \cos\theta_a + Y_o \\ X_b = x_b \cos\theta_a - y_b \sin\theta_a + X_o \\ Y_b = x_b \sin\theta_a + y_b \cos\theta_a + Y_o \end{cases} \quad (\text{A.13})$$

These following known conditions are given according to the geometric conditions in Figure 2.3:

$$y_a = 0 \quad (\text{A.14})$$

$$Y_a = G(X_a) \quad (\text{A.15})$$

$$X_b = 0 \quad (\text{A.16})$$

$$Y_b = h \quad (\text{A.17})$$

$G(X_a)$ is the geometric function of rocking surface, h is the bearing height. Substituting the above equations (A.14), (A.15), (A.16) and (A.17) into equation (A.13):

$$X_a = x_a \cos \theta_a + X_o \quad (\text{A.18})$$

$$G(X_a) = x_a \sin \theta_a + Y_o \quad (\text{A.19})$$

$$x_b \cos \theta_a - y_b \sin \theta_a + X_o = 0 \quad (\text{A.20})$$

$$x_b \sin \theta_a + y_b \cos \theta_a + Y_o = h \quad (\text{A.21})$$

Substituting equation (A.18) to (A.20), and equation (A.19) to (A.21), so it will be as follows:

$$-X_a = x_b \cos \theta_a - y_b \sin \theta_a - x_a \cos \theta_a \quad (\text{A.22})$$

$$h - G(X_a) = x_b \sin \theta_a + y_b \cos \theta_a - x_a \sin \theta_a \quad (\text{A.23})$$

Moving x_b and y_b into the left side:

$$x_b = [h - G(X_a)] \sin \theta_a - X_a \cos \theta_a + x_a \quad (\text{A.24})$$

$$y_b = [h - G(X_a)] \cos \theta_a + X_a \sin \theta_a \quad (\text{A.25})$$

From Figure 2.3, since it assumed that the rocking surface and the ground have point contact, the x -axis is actually tangent to the rocking surface at the contact point A.

$$G'(X_a) = \tan \theta_a \quad (\text{A.26})$$

Equation (A.26) can be change based on the trigonometric relationship, and further rewritten as a function as follows:

$$\begin{cases} \sin \theta_a = \frac{\tan \theta_a}{\sqrt{1 + \tan^2 \theta_a}} = \frac{G'(X_a)}{[1 + (G'(X_a))^2]^{\frac{1}{2}}} \\ \cos \theta_a = \frac{1}{\sqrt{1 + \tan^2 \theta_a}} = \frac{1}{[1 + (G'(X_a))^2]^{\frac{1}{2}}} \end{cases} \quad (\text{A.27})$$

Since it assumed that slippage will not occur at the contact point, x_a should be equal to the arc length between points A and C, which can be computed by:

$$x_a(X_a) = \int_0^{X_a} [1 + (G'(X_a))^2]^{\frac{1}{2}} dX \quad (\text{A.28})$$

Furthermore by using coordinate transformation relation between fixed and moving coordinates systems, x_b and y_b can be written as:

$$x_b = \frac{G'(X_a)(h-G(X_a))-X_a}{[1+(G(X_a))^2]^{\frac{1}{2}}} + \int_0^{X_a} [1 + (G(X_a))^2]^{\frac{1}{2}} dX \quad (\text{A.29})$$

$$y_b = \frac{h-G(X_a)+X_a G'(X_a)}{[1+(G(X_a))^2]^{\frac{1}{2}}} \quad (\text{A.30})$$



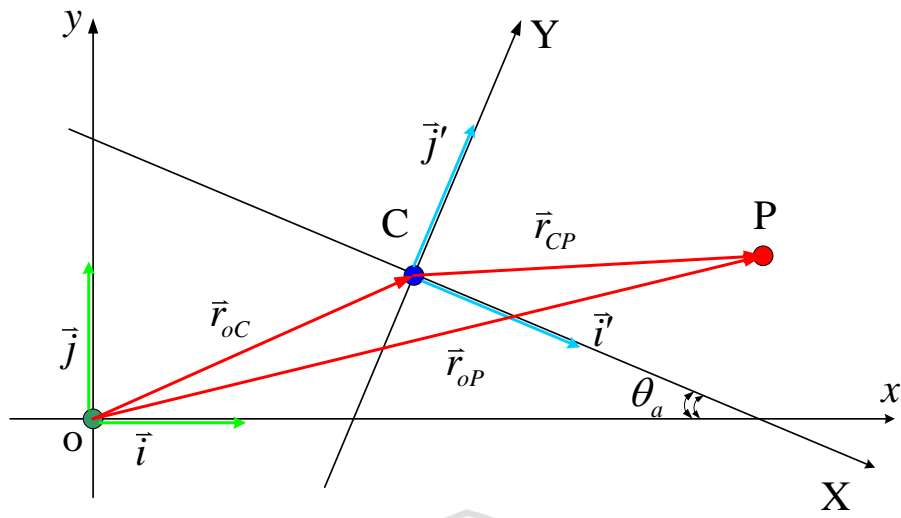
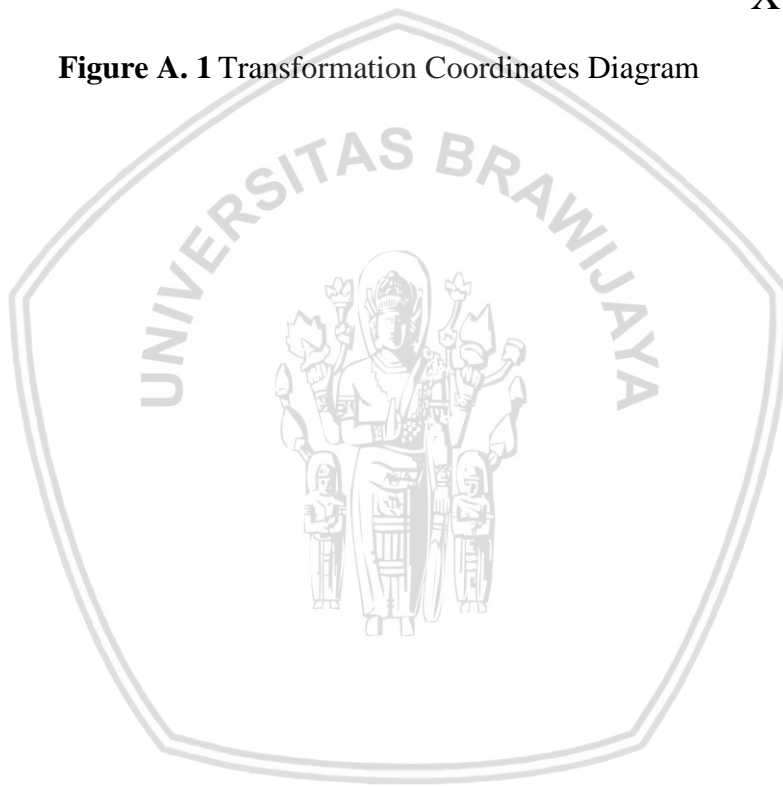


Figure A. 1 Transformation Coordinates Diagram



APPENDIX B

This appendix derives the state space equation of continuous time system into the equation of discrete time system to analyze the behavior of PRB in irregular bridges.

The continuous time system is as follows:

$$\dot{\mathbf{Z}}(t) = \mathbf{AZ}(t) + \mathbf{E}\ddot{\mathbf{x}}_g(t) + \mathbf{BU}(t) \quad (\text{B.1})$$

$\mathbf{E}\ddot{\mathbf{x}}_g(t)$ is the seismic force, $\mathbf{BU}(t)$ is the bearing horizontal force. Both are external forces.

Let the continuous time system $\mathbf{Z}(t)$ is equal to free vibration transient solution $\mathbf{Z}_h(t)$ and steady state solution of forced vibration with external force $\mathbf{Z}_p(t)$ as shown is following equation:

$$\mathbf{Z}(t) = \mathbf{Z}_h(t) + \mathbf{Z}_p(t) \quad (\text{B.2})$$

Solving the free vibration transient solution $\mathbf{Z}_h(t)$, assume that the external forces $\mathbf{E}\ddot{\mathbf{x}}_g(t) + \mathbf{BU}(t) = 0$, so equation (B.1) becomes:

$$\dot{\mathbf{Z}}(t) = \mathbf{AZ}(t) = \frac{d\mathbf{Z}(t)}{dt} \quad (\text{B.3})$$

Doing integration for equation (B.3):

$$\int \mathbf{A} dt = \int \frac{d\mathbf{Z}(t)}{dt} = \mathbf{At} + c' = \ln \mathbf{Z}(t) \quad (\text{B.4})$$

Change the equation (B.4):

$$\mathbf{Z}(t) = e^{\ln \mathbf{Z}(t)} = e^{\mathbf{At} + c'} = e^{\mathbf{At}} e^{c'} = c e^{\mathbf{At}} = e^{\mathbf{At}} \mathbf{Z}(0) \quad (\text{B.5})$$

If $\mathbf{Z}(0)$ is the initial condition of the structure, $e^{\mathbf{At}}$ in equation (B.5) can be expressed as:

$$e^{\mathbf{At}} = \mathbf{I} + t\mathbf{A} + \frac{t^2}{2!}\mathbf{A}^2 + \frac{t^3}{3!}\mathbf{A}^3 + \dots + \frac{t^i}{i!}\mathbf{A}^i = \sum_{i=0}^{\infty} \frac{t^i}{i!}\mathbf{A}^i \quad (\text{B.6})$$

If $e^{\mathbf{At}} = \phi(t)$, from equations (B.5) and (B.6), $\mathbf{Z}(t)$ also can be obtained as:

$$\mathbf{Z}_h(t) = \mathbf{Z}(0)e^{\mathbf{At}} = \mathbf{Z}(0) \sum_{i=0}^{\infty} \frac{t^i}{i!}\mathbf{A}^i = \mathbf{Z}(0)\phi(t) \quad (\text{B.7})$$

Solving $\mathbf{Z}_p(t)$, set the external force is equal to zero, using undetermined coefficient method:

$$\mathbf{Z}_p(t) = \phi(t)\bar{\mathbf{Z}}(t) \quad (\text{B.8})$$

Doing the first differential for $\mathbf{Z}_p(t)$:

$$\dot{\mathbf{Z}}_p(t) = \dot{\phi}(t)\bar{\mathbf{Z}}(t) + \phi(t)\dot{\bar{\mathbf{Z}}}(t) \quad (\text{B.9})$$

Substituting equations (B.8) and (B.9) into equation (B.1):

$$\dot{\phi}(t)\bar{\mathbf{Z}}(t) + \phi(t)\dot{\bar{\mathbf{Z}}}(t) - \mathbf{A}\phi(t)\bar{\mathbf{Z}}(t) = \mathbf{E}\ddot{\mathbf{x}}_g(t) + \mathbf{B}\mathbf{U}(t) \quad (\text{B.10})$$

Since:

$$\dot{\phi}(t) = \mathbf{A}e^{\mathbf{A}t} = \mathbf{A}\phi(t) \quad (\text{B.11})$$

Substituting equation (B.11) to equation (B.10):

$$\phi(t)\dot{\bar{\mathbf{Z}}}(t) = \mathbf{E}\ddot{\mathbf{x}}_g(t) + \mathbf{B}\mathbf{U}(t) \quad (\text{B.12})$$

The equation (B.12) above can be changed into:

$$\dot{\bar{\mathbf{Z}}}(t) = \frac{1}{\phi(t)} [\mathbf{E}\ddot{\mathbf{x}}_g(t) + \mathbf{B}\mathbf{U}(t)] \quad (\text{B.13})$$

Doing the integration for equation (B.13):

$$\bar{\mathbf{Z}}(t) = \int_{\tau} \frac{1}{\phi(\tau)} [\mathbf{E}\ddot{\mathbf{x}}_g(\tau) + \mathbf{B}\mathbf{U}(\tau)] d\tau \quad (\text{B.14})$$

If $\frac{1}{\phi(\tau)} = e^{-\mathbf{A}\tau} = \phi(-\tau)$, equation (B.14) can be further rewritten as:

$$\bar{\mathbf{Z}}(t) = \int_{\tau} \phi(-\tau) [\mathbf{E}\ddot{\mathbf{x}}_g(\tau) + \mathbf{B}\mathbf{U}(\tau)] d\tau \quad (\text{B.15})$$

Substituting equation (B.15) into equation (B.8):

$$\mathbf{Z}_p(t) = \phi(t) \int_{\tau} \phi(-\tau) [\mathbf{E}\ddot{\mathbf{x}}_g(\tau) + \mathbf{B}\mathbf{U}(\tau)] d\tau = \int_{\tau} \phi(t - \tau) [\mathbf{E}\ddot{\mathbf{x}}_g(\tau) + \mathbf{B}\mathbf{U}(\tau)] d\tau \quad (\text{B.16})$$

Substituting equations (B.7) and (B.16) into equation (B.2):

$$\mathbf{Z}(t) = \mathbf{Z}_h(t) + \mathbf{Z}_p(t) = \mathbf{Z}(0)\phi(t) + \int_0^t \phi(t - \tau) [\mathbf{E}\ddot{\mathbf{x}}_g(\tau) + \mathbf{B}\mathbf{U}(\tau)] d\tau \quad (\text{B.17})$$

Assume the time step is Δt , then the time of step k can be expressed as $k\Delta t$, the equation at step k is:

$$\mathbf{Z}_k(k\Delta t) = \mathbf{Z}(0)\phi(k\Delta t) + \int_0^{k\Delta t} \phi(k\Delta t - \tau)[\mathbf{E}\ddot{\mathbf{x}}_g(\tau) + \mathbf{B}\mathbf{U}(\tau)]d\tau \quad (\text{B.18})$$

The time of step $k + 1$ can be expressed as $(k\Delta t + \Delta t)$, the equation for $k + 1$ is:

$$\begin{aligned} \mathbf{Z}_{k+1}(k\Delta t + \Delta t) &= \mathbf{Z}(0)\phi(k\Delta t + \Delta t) + \int_0^{k\Delta t + \Delta t} \phi(k\Delta t + \Delta t - \tau)[\mathbf{E}\ddot{\mathbf{x}}_g(\tau) + \mathbf{B}\mathbf{U}(\tau)]d\tau \\ &= \mathbf{Z}(0)\phi(k\Delta t + \Delta t) + \int_0^{k\Delta t} \phi(k\Delta t + \Delta t - \tau)[\mathbf{E}\ddot{\mathbf{x}}_g(\tau) + \mathbf{B}\mathbf{U}(\tau)]d\tau \\ &\quad + \int_{k\Delta t}^{k\Delta t + \Delta t} \phi(k\Delta t + \Delta t - \tau)[\mathbf{E}\ddot{\mathbf{x}}_g(\tau) + \mathbf{B}\mathbf{U}(\tau)]d\tau \\ &= \mathbf{Z}(0)\phi(k\Delta t)\phi(\Delta t) + \phi(\Delta t) \int_0^{k\Delta t} \phi(k\Delta t - \tau)[\mathbf{E}\ddot{\mathbf{x}}_g(\tau) + \mathbf{B}\mathbf{U}(\tau)]d\tau \\ &\quad + \int_{k\Delta t}^{k\Delta t + \Delta t} \phi(k\Delta t + \Delta t - \tau)[\mathbf{E}\ddot{\mathbf{x}}_g(\tau) + \mathbf{B}\mathbf{U}(\tau)]d\tau \end{aligned} \quad (\text{B.19})$$

Substituting equations (B.18) into (B.19):

$$\begin{aligned} \mathbf{Z}_{k+1}(k\Delta t + \Delta t) &= \phi(\Delta t)\{\mathbf{Z}(0)\phi(k\Delta t) + \int_0^{k\Delta t} \phi(k\Delta t - \tau)[\mathbf{E}\ddot{\mathbf{x}}_g(\tau) + \mathbf{B}\mathbf{U}(\tau)]d\tau\} \\ &\quad + \int_{k\Delta t}^{k\Delta t + \Delta t} \phi(k\Delta t + \Delta t - \tau)[\mathbf{E}\ddot{\mathbf{x}}_g(\tau) + \mathbf{B}\mathbf{U}(\tau)]d\tau = \phi(\Delta t)\mathbf{Z}_k(k\Delta t) \\ &\quad + \int_{k\Delta t}^{k\Delta t + \Delta t} \phi(k\Delta t + \Delta t - \tau)[\mathbf{E}\ddot{\mathbf{x}}_g(\tau) + \mathbf{B}\mathbf{U}(\tau)]d\tau \end{aligned} \quad (\text{B.20})$$

By $\phi(\Delta t) = e^{A\Delta t}$ and $e^{A\Delta t} = A_d$, equation (B.20) can be expressed as:

$$\mathbf{Z}(k + 1) = A_d\mathbf{Z}[k] + \int_{k\Delta t}^{k\Delta t + \Delta t} \phi(k\Delta t + \Delta t - \tau)[\mathbf{E}\ddot{\mathbf{x}}_g(\tau) + \mathbf{B}\mathbf{U}(\tau)]d\tau \quad (\text{B.21})$$

Assuming that the external force is linearly changed at each step, so the external force between k and $k + 1$ steps can be obtained by interpolation:

$$\ddot{\mathbf{x}}_g(t) = \ddot{\mathbf{x}}_g[k] + \left[\frac{\ddot{\mathbf{x}}_g[k+1] - \ddot{\mathbf{x}}_g[k]}{\Delta t} \right] (t - k\Delta t) \quad (\text{B.22})$$

$$\mathbf{U}(t) = \mathbf{U}[k] + \left[\frac{\mathbf{U}[k+1] - \mathbf{U}[k]}{\Delta t} \right] (t - k\Delta t) \quad (\text{B.23})$$

By $\tau' = k\Delta t + \Delta t - \tau$, the integral equation (B.21) is obtained:

$$\mathbf{Z}(k+1) = A_d \mathbf{Z}[k] + \int_0^{\Delta t} \phi(\tau') [\mathbf{E} \ddot{x}_g(\tau') + \mathbf{B} \mathbf{U}(\tau')] d\tau' \quad (\text{B.24})$$

$\ddot{x}_g(\tau')$ and $\mathbf{U}(\tau')$ can be expressed as:

$$\begin{aligned} \ddot{x}_g(\tau') &= \ddot{x}_g[k] + \left[\frac{\ddot{x}_g[k+1] - \ddot{x}_g[k]}{\Delta t} \right] (\Delta t - \tau') = \ddot{x}_g[k+1] - \frac{\ddot{x}_g[k+1]\tau' - \ddot{x}_g[k]\tau'}{\Delta t} \\ &= \ddot{x}_g[k] \left(\frac{\tau'}{\Delta t} \right) + \ddot{x}_g[k+1] \left(\frac{\Delta t - \tau'}{\Delta t} \right) \end{aligned} \quad (\text{B.25})$$

$$\begin{aligned} \mathbf{U}(\tau') &= \mathbf{U}[k] + \left[\frac{\mathbf{U}[k+1] - \mathbf{U}[k]}{\Delta t} \right] (\Delta t - \tau') = \mathbf{U}[k+1] - \frac{\mathbf{U}[k+1]\tau' - \mathbf{U}[k]\tau'}{\Delta t} \\ &= \mathbf{U}[k] \left(\frac{\tau'}{\Delta t} \right) + \mathbf{U}[k+1] \left(\frac{\Delta t - \tau'}{\Delta t} \right) \end{aligned} \quad (\text{B.26})$$

Rearrange the equation (B.24):

$$\begin{aligned} \mathbf{Z}(k+1) &= A_d \mathbf{Z}[k] + \int_0^{\Delta t} \phi(\tau') \left\{ \mathbf{E} \left[\ddot{x}_g[k] \left(\frac{\tau'}{\Delta t} \right) + \ddot{x}_g[k+1] \left(\frac{\Delta t - \tau'}{\Delta t} \right) \right] \right. \\ &\quad \left. + \mathbf{B} \left[\mathbf{U}[k] \left(\frac{\tau'}{\Delta t} \right) + \mathbf{U}[k+1] \left(\frac{\Delta t - \tau'}{\Delta t} \right) \right] \right\} d\tau' \\ &= A_d \mathbf{Z}[k] + \int_0^{\Delta t} \phi(\tau') \left[\mathbf{E} \ddot{x}_g[k] \left(\frac{\tau'}{\Delta t} \right) + \mathbf{B} \mathbf{U}[k] \left(\frac{\tau'}{\Delta t} \right) \right] d\tau' \\ &\quad + \int_0^{\Delta t} \phi(\tau') \left[\mathbf{E} \ddot{x}_g[k+1] \left(\frac{\Delta t - \tau'}{\Delta t} \right) + \mathbf{B} \mathbf{U}[k+1] \left(\frac{\Delta t - \tau'}{\Delta t} \right) \right] d\tau' \\ &= A_d \mathbf{Z}[k] + \int_0^{\Delta t} \phi(\tau') \left(\frac{\tau'}{\Delta t} \right) \left[\mathbf{E} \ddot{x}_g[k] + \mathbf{B} \mathbf{U}[k] \right] d\tau' \\ &\quad + \int_0^{\Delta t} \phi(\tau') \left(\frac{\Delta t - \tau'}{\Delta t} \right) \left[\mathbf{E} \ddot{x}_g[k+1] + \mathbf{B} \mathbf{U}[k+1] \right] d\tau' \\ &= A_d \mathbf{Z}[k] + a + b \end{aligned} \quad (\text{B.27})$$

Based on equation (B.27), it has 2 variables need to be obtained (a and b). a can be derived as:

$$\begin{aligned}
 a &= \int_0^{\Delta t} \phi(\tau') \left[\mathbf{E}\ddot{x}_g[k] \left(\frac{\tau'}{\Delta t} \right) + \mathbf{BU}[k] \left(\frac{\tau'}{\Delta t} \right) \right] d\tau' = \int_0^{\Delta t} e^{A\tau'} \left(\frac{\tau'}{\Delta t} \right) \left[\mathbf{E}\ddot{x}_g[k] + \mathbf{BU}[k] \right] d\tau' \\
 &= \int_0^{\Delta t} \sum_{i=0}^{\infty} \frac{\tau'^i}{i!} \mathbf{A}^i \left(\frac{\tau'}{\Delta t} \right) \left[\mathbf{E}\ddot{x}_g[k] + \mathbf{BU}[k] \right] d\tau' \\
 &= \int_0^{\Delta t} \sum_{i=0}^{\infty} \frac{\tau'^{(i+1)}}{i!} \mathbf{A}^i \left(\frac{1}{\Delta t} \right) \left[\mathbf{E}\ddot{x}_g[k] + \mathbf{BU}[k] \right] d\tau' \\
 &= \left(\frac{1}{\Delta t} \right) \sum_{i=1}^{\infty} \frac{\tau'^{(i+2)}}{(i+2)!} \mathbf{A}^i \left[\mathbf{E}\ddot{x}_g[k] + \mathbf{BU}[k] \right] \Bigg|_0^{\Delta t} \\
 &= \sum_{i=1}^{\infty} \frac{\tau'^{(i+1)}}{(i+2)!} \mathbf{A}^i \left[\mathbf{E}\ddot{x}_g[k] + \mathbf{BU}[k] \right]
 \end{aligned} \tag{B.28}$$

Based on equation (B.27), b can be derived as:

$$\begin{aligned}
 b &= \int_0^{\Delta t} \phi(\tau') \left(\frac{\Delta t - \tau'}{\Delta t} \right) \left[\mathbf{E}\ddot{x}_g[k+1] + \mathbf{BU}[k+1] \right] d\tau' \\
 &= \int_0^{\Delta t} e^{A\tau'} \left(\frac{\Delta t - \tau'}{\Delta t} \right) \left[\mathbf{E}\ddot{x}_g[k+1] + \mathbf{BU}[k+1] \right] d\tau' \\
 &= \int_0^{\Delta t} \sum_{i=0}^{\infty} \frac{\tau'^i}{i!} \mathbf{A}^i \left(1 - \frac{\tau'}{\Delta t} \right) \left[\mathbf{E}\ddot{x}_g[k+1] + \mathbf{BU}[k+1] \right] d\tau' \\
 &= \int_0^{\Delta t} \left[\sum_{i=0}^{\infty} \frac{\tau'^i}{i!} \mathbf{A}^i - \left(\frac{1}{\Delta t} \right) \sum_{i=0}^{\infty} \frac{\tau'^{(i+1)}}{i!} \mathbf{A}^i \right] \left[\mathbf{E}\ddot{x}_g[k+1] + \mathbf{BU}[k+1] \right] d\tau' \\
 &= \left[\sum_{i=0}^{\infty} \frac{\tau'^{(i+1)}}{(i+1)!} \mathbf{A}^i - \left(\frac{1}{\Delta t} \right) \sum_{i=0}^{\infty} \frac{\tau'^{(i+2)}}{(i+2)!} \mathbf{A}^i \right] \left[\mathbf{E}\ddot{x}_g[k+1] + \mathbf{BU}[k+1] \right] \Bigg|_0^{\Delta t} \\
 &= \left[\sum_{i=0}^{\infty} \mathbf{A}^i \left(\frac{\tau'^{(i+1)}}{(i+1)!} - \frac{\tau'^{(i+1)}}{(i+2)!} \right) \right] \left[\mathbf{E}\ddot{x}_g[k+1] + \mathbf{BU}[k+1] \right]
 \end{aligned} \tag{B.29}$$

Since $\sum_{i=0}^{\infty} \frac{\tau'^{(i+1)}}{(i+2)!} \mathbf{A}^i = \mathbf{A}_d^*$, equation (B.28) can be written as:

$$a = \sum_{i=1}^{\infty} \frac{\tau'^{(i+1)}}{(i+2)!} \mathbf{A}^i \left[\mathbf{E}\ddot{x}_g[k] + \mathbf{BU}[k] \right] = \mathbf{A}_d^* \left[\mathbf{E}\ddot{x}_g[k] + \mathbf{BU}[k] \right] \tag{B.30}$$

Since $\sum_{i=0}^{\infty} \frac{\tau'^{(i+1)}}{(i+1)!} \mathbf{A}^i = \widehat{\mathbf{A}}_d$, equation (B.29) can be written as:

$$b = \left[\sum_{i=0}^{\infty} \mathbf{A}^i \left(\frac{\tau'^{(i+1)}}{(i+1)!} - \frac{\tau'^{(i+1)}}{(i+2)!} \right) \right] \left[\mathbf{E}\ddot{x}_g[k+1] + \mathbf{BU}[k+1] \right] = (\widehat{\mathbf{A}}_d - \mathbf{A}_d^*) \left[\mathbf{E}\ddot{x}_g[k+1] + \mathbf{BU}[k+1] \right] \tag{B.31}$$

Substituting equation (B.30) and (B.31) to equation (B.27) can get the equation as follows:

$$\mathbf{Z}[k + 1] = \mathbf{A}_d \mathbf{Z}[k] + \mathbf{A}_d^* (\mathbf{E}_0 \dot{\mathbf{x}}_g[k] + \mathbf{E}_1 \dot{\mathbf{x}}_g[k + 1]) + (\hat{\mathbf{A}}_d - \mathbf{A}_d^*) (\mathbf{B}_0 \mathbf{U}[k] + \mathbf{B}_1 \mathbf{U}[k + 1]) \quad (\mathbf{B.32})$$

$$\mathbf{A}_d^* \mathbf{E} = \mathbf{E}_0$$

$$\mathbf{A}_d^* \mathbf{B} = \mathbf{B}_0 \quad (\mathbf{B.33})$$

$$(\hat{\mathbf{A}}_d - \mathbf{A}_d^*) \mathbf{E} = \mathbf{E}_1$$

$$(\hat{\mathbf{A}}_d - \mathbf{A}_d^*) \mathbf{B} = \mathbf{B}_1$$

From equation (B.32) and (B.33), the discrete time state space equation can be expressed as:

$$\mathbf{Z}[k + 1] = \mathbf{A}_d \mathbf{Z}[k] + \mathbf{E}_0 \dot{\mathbf{x}}_g[k] + \mathbf{E}_1 \dot{\mathbf{x}}_g[k + 1] + \mathbf{B}_0 \mathbf{U}[k] + \mathbf{B}_1 \mathbf{U}[k + 1] \quad (\mathbf{B.34})$$



APPENDIX C

This appendix shows the unclear figure of hysteretic loop in fourth chapter. Not all of the hysteretic loop figures will show here, just some unclear figures at some ground motions sample.

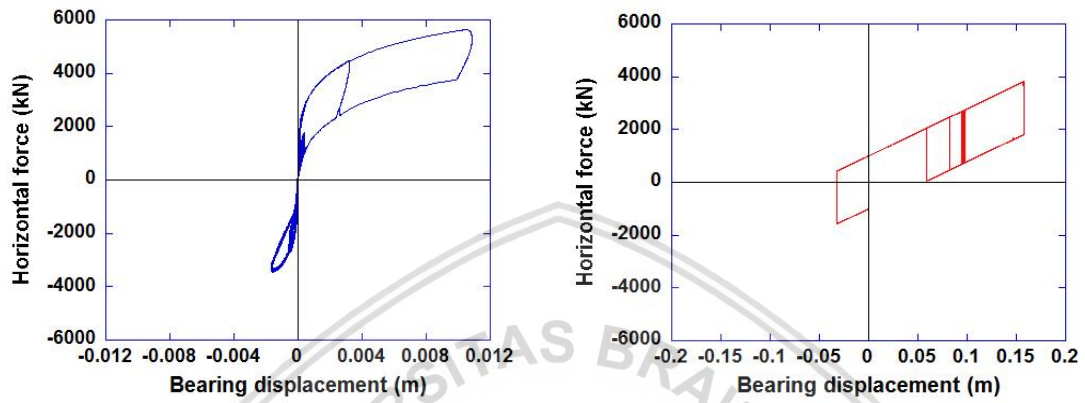


Figure C. 1 Bridge's Hysteretic Loop Subjected to Imperial Earthquake in Short Column

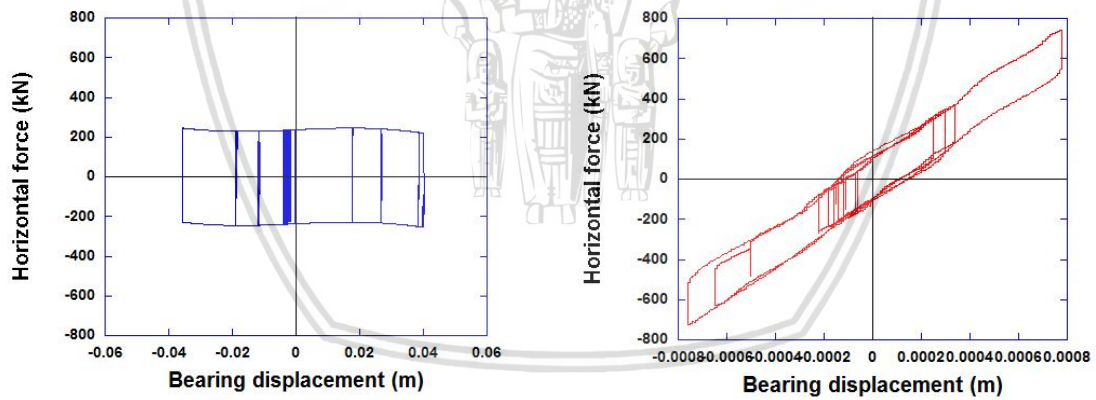
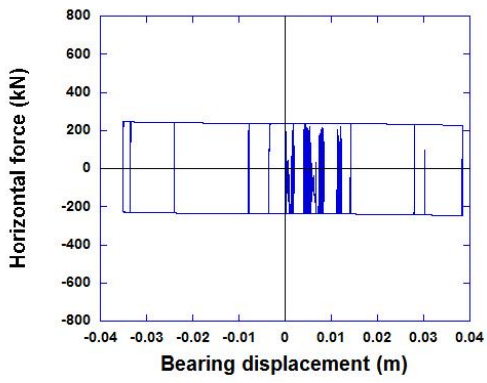
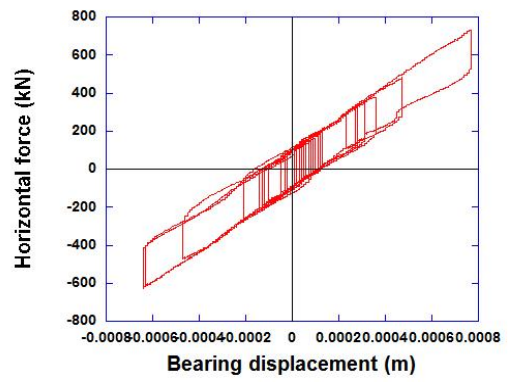


Figure C. 2 Bridge's Hysteretic Loop Subjected to JMA Kobe Earthquake in Long Column

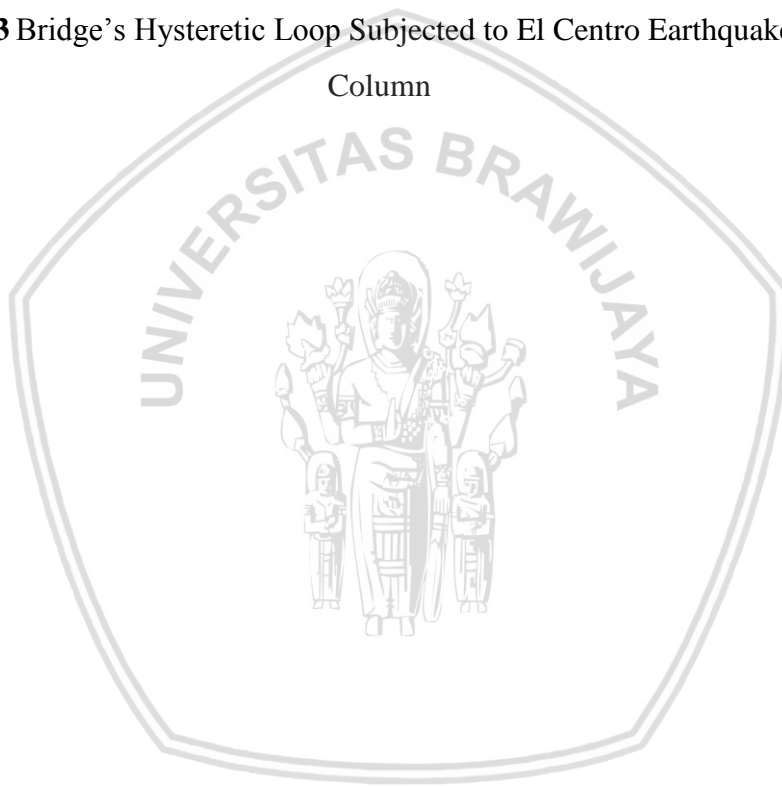


(a) Hysteretic Loop of PRB



(b) Hysteretic Loop of FPS

Figure C. 3 Bridge's Hysteretic Loop Subjected to El Centro Earthquake in Long Column





National Central University Library Letter of Authorization for Electronic Theses and Dissertations

(The latest version since Sep. 2012)

This license authorizes my complete electronic thesis (**not in paper format, see footnote 1**) be archived and read in the "National Central University Library Electronic Theses & Dissertations System".

- Agree (available immediately)
 Agree (available in ____ / ____ / ____ (yyyy/mm/dd) , because _____
 Disagree, because: _____

and be archived and read in NDLTD (National Digital Library of Theses and Dissertations in Taiwan)

- Agree (available immediately)
 Agree (available in ____ / ____ / ____ (yyyy/mm/dd) , because _____
 Disagree, because: _____

I undertake to submit my thesis, to National Central University Library and NDLTD (National Digital Library of Theses and Dissertations in Taiwan), non-exclusively and voluntarily. Based on the concept of sharing sources and mutually benefitted cooperation and in aims to repay the society and for the academic usage, I hereby grant a non-exclusive, for the full term of copy right protection, license to National Central University Library and NDLTD (National Digital Library of Theses and Dissertations in Taiwan), (a) to reproduce, publish, archive, preserve, conserve, communicate to the public by telecommunication or on the internet and distribute my thesis, in microform, paper, electronic and/or any other formats, regardless of place, time, and frequency; (b) to authorize, sub-license, sub-contract or procure any of the acts mentioned in paragraph (a). And grant the reader the right to read, download and print out non-profitably.

Signature of the Author: Krisna Febrian

Student Number: 103322608

Thesis Title: Dynamic Analysis of Irregular Bridges with Polynomial Rocking Bearings

Supervisor: Prof. Lee Tzu-Ying

Faculty, Department, School: Civil Engineering Department, National Central University PH. D Master

Date: 2017/10/05

Footnote :

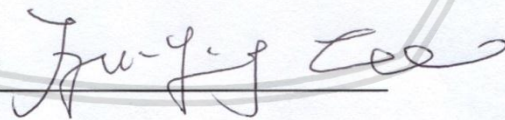
1. The license is limited to only electronic files. In terms of Regulation of Copyright No 15, article 3, theses in paper can be published by the library. If you have patent or submitting concerns and do not want to publish your theses in paper, please fill out the Proclamation form.
2. This form requires the author's own signature, and it should be attached to a page after the paper theses' cover. (type-up signature is allowed for full electronic theses)
3. Readers should observe the Regulation of copyright while searching, reading, downloading and printing theses online non-profitably.

National Central University

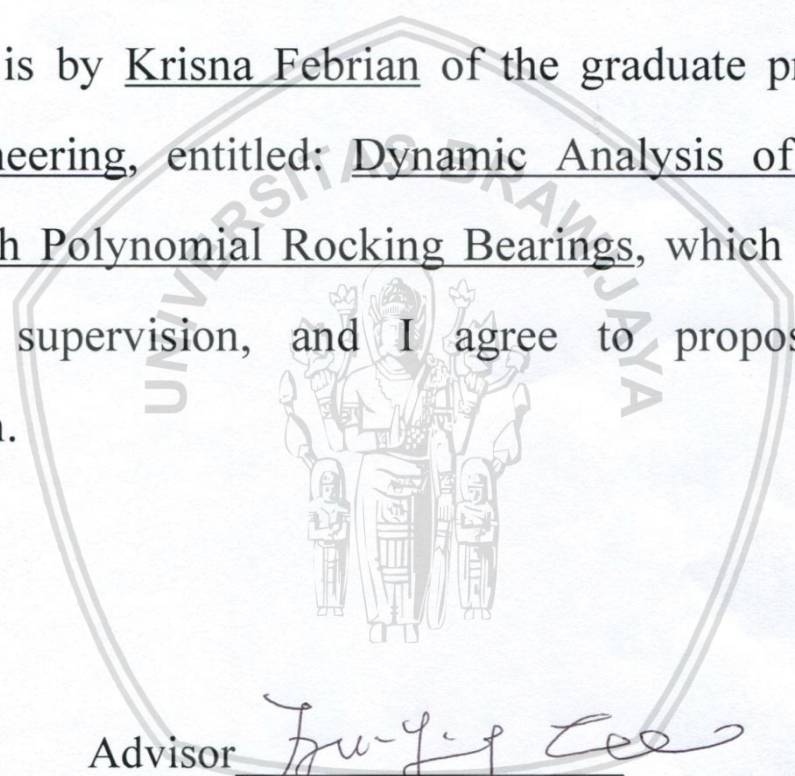
Advisor's Recommendation for Graduate Students

This thesis is by Krisna Febrian of the graduate program in Civil Engineering, entitled: Dynamic Analysis of Irregular Bridges with Polynomial Rocking Bearings, which is written under my supervision, and I agree to propose it for examination.

Advisor



2019/10/5 (YYYY/MM/DD)



National Central University

Verification Letter from the Oral Examination Committee for Graduate Students

This thesis is by Krisna Febrian of the graduate program in Civil Engineering, entitled: Dynamic Analysis of Irregular Bridges with Polynomial Rocking Bearings who is qualified for master degree through the verification of the committee.

Convener of the degree examination committee

Deci Alim Tanjung

Members

Ari Wibowo

Philip Han

Ju-yj Lee

Date: 2017/09/21

(YYYY/MM/DD)

